THE UNIVERSITY OF MICHIGAN
COLLEGE OF ENGINEERING
Department of Mechanical Engineering

PERFORMANCE COEFFICIENTS FOR POWERED WHEELS IN MICHIGAN FARM SOIL

E. Oktar
H. Mat
E. T. Vincent

ORA Project 05600

under contract with:

U. S. ARMY
DETROIT PROCUREMENT DISTRICT
CONTRACT NO. DA-20-018-AMC-0935T
DETROIT, MICHIGAN

administered through:

OFFICE OF RESEARCH ADMINISTRATION ANN ARBOR

October 1964

TABLE OF CONTENTS

LIST OF ILLUSTRATIONS

LIST OF ILLUSTRATIONS (Continued)

LIST OF ILLUSTRATIONS (Continued)

LIST OF ILLUSTRATIONS (Continued)

LIST OF ILLUSTRATIONS (Continued)

LIST OF ILLUSTRATIONS (Continued)

LIST OF ILLUSTRATIONS (Concluded)

LIST OF SYMBOLS AND TERMS

GENERAL

D = soil bed depth, in.
R = rolling resistance of wheel, lb
w = wheel load, lb
w' = actual load on wheel, lb
b = wheel width, in. (characteristic dimension of plate)
d = wheel diameter, in.
P = pressure, lb/in.^{2}
t = time, sec.
Z = sinkage, in. (axle sinkage relative to undisturbed surface)
T = torque, lb/in.
ρ = density, lb/ft^3

BEKKER SOIL VALUES

k_ϕ = sinkage parameter (frictional), lb/in.$^{n+2}$
k_c = sinkage parameter (cohesive), lb/in.$^{n+1}$
n = nondimensional sinkage parameter or index

COEFFICIENT

R/w' = nondimensional drag coefficient
Z/d = nondimensional sinkage coefficient
i = nondimensional slip coefficient
α = nondimensional shape coefficient (aspect ratio = b/d)
μ = nondimensional frictional coefficient (soil to wheel surface)
D/d = nondimensional depth parameter

OBJECTIVE

The object of studies reported herein is the experimental verification of the dimensionless parameters developed in Ref. 1 when applied to powered model wheels of different diameter and aspect ratio operating in a typical Michigan farm soil.

In addition work is reported on the development of a combined radial and shear load transducer capable of operation in the model wheels employed in the above dimensionless work and possessing the desired degree of accuracy for the scale models employed.

ABSTRACT

This report covers experimental results obtained in an attempt to verify the usefulness of similitude studies for soil-vehicle analysis work when employing rigid powered wheels in a typical Michigan farm soil possessing both cohesion and friction.

A range of wheel diameters and aspect ratios was tested with wheel slip from -50 to +100% approximately.

It was impossible with present knowledge to control all parameters involved to a sufficient degree to keep the dimensionless expressions constant, hence complete similarity was not obtained.

However, the results obtained for some of the coefficients appear to be sufficiently close, when plotted in the dimensionless manner, to indicate that, given complete control of the factors, the similitude relationships will prove a very useful tool.

Some factors appear to be relatively insensitive to the parameter which could not be controlled, in which case the tests grouped in a satisfactory manner. Others were spread sufficiently that a definite conclusion could not be drawn.

The tests also showed that the soil properties themselves need some further clarification when the ratio of the depth of soil to bevameter footing falls below a certain value. In this range soil properties appear to vary with soil depth, moreso when using a farm soil than when sand was the medium being tested. This raises the point as to what soil values should be employed in calculating the results.

The measurement of radial and shear loads on a very small surface of a rigid wheel are also reported. The first results indicate that a successful piece of equipment could be produced for this purpose given additional time and money to construct a second version of the model reported upon here.

PART I

A. INTRODUCTION

This report is one of a series (Refs. 1,2,3,4) covering the application of dimensional analysis and similitude testing to a soil-vehicle system.

The present report covers a series of tests employing the same range of wheel sizes used previously, in the same typical Michigan farm soil; the difference in this case is in the application of power to the wheel to cause varying degrees of slip under a range of loads and sinkages. The farm soil was maintained at a constant moisture content of approximately 10% throughout the tests. Under these conditions the soil had both friction and cohesive properties; the average values of k_c, k_ϕ, and n for soil in the tank were 1.09, 1.33, and 1.20 respectively. There is still considerable variation in the soil constants between tests (Ref. 4).

In addition to constant moisture content, the ratio of soil depth to wheel diameter was held constant at 1.56 (Ref. 2) to maintain the depth previously determined as satisfactory for operating conditions in sand. Further tests are needed to determine if this same ratio applies to typical Michigan farm soil.

For convenience, the relationships employed between the model and prototype are repeated below and remain as developed in Ref. 1.

$$\left(\frac{w}{d^{n+2}k_\phi}\right)_p = \left(\frac{w}{d^{n+2}k_\phi}\right)_m \tag{1}$$

$$\left(\frac{k_c}{d\ k_\phi}\right)_p = \left(\frac{k_c}{d\ k_\phi}\right)_m \tag{2}$$

$$\left(\frac{d}{D}\right)_p = \left(\frac{d}{D}\right)_m \tag{3}$$

$$(d)_p = (d)_m \tag{4}$$

$$(\mu)_p = (\mu)_m \tag{5}$$

$$(n)_p = (n)_m \tag{6}$$

$$(i)_p = (i)_m \tag{7}$$

The functional relationships between dependent and independent dimensionless variables are:

$$\frac{R}{W} = f\left\{\left(\frac{w}{d^{n+2}k_\phi}\right), \left(\frac{k_c}{d\,k_\phi}\right), \left(\frac{D}{d}\right), (d), (\mu), (n), (i)\right\} \tag{8}$$

$$\frac{T}{Wd} = f\left\{\left(\frac{w}{d^{n+2}\,k_\phi}\right), \left(\frac{kc}{d\,k_\phi}\right), \left(\frac{D}{d}\right), (\gamma), (\mu), (n), (i)\right\} \tag{9}$$

$$Z/d = f\left\{\left(\frac{W}{d^{n+2}k_\phi}\right), \left(\frac{k_c}{d\,k_\phi}\right), \left(\frac{D}{d}\right), (\gamma), (\mu), (n), (i)\right\} \tag{10}$$

The following pages record tests aimed at demonstrating the validity of the relations expressed by Eqs. (8, 9, and 10) for powered wheels in a typical farm soil.

B. PROGRAM

The program for the work under review followed these steps:

1. Measure the soil moisture content during each test day.

2. Obtain the Bekker soil values at frequent intervals throughout the tests and during each series of tests.

3. Conduct tests under various loadings for drag, sinkage, torque, slip, etc., with at least two sizes of wheels, viz., 12.5 in. and 8.56 in. diameter, as employed previously, with aspect ratios of 0.27, 0.52, and 0.84 for each diameter.

4. From the results of item 3 calculate the dimensionless parameters, plot and examine results.

In addition, the program was begun for developing a shear measuring instrument combined, if possible, with a radial component as used in Ref. 6. After some preliminary tests, a design was developed combining the radial and shear elements which were believed would permit the determination of the total forces on a small element of the wheel surface during rotation under load at all conditions of slip, sinkage, etc. In addition, provision was made for traversing the pick-up across the face of a large aspect-ratio wheel to ascertain the magnitude of the end effects, if any. This instrument was available for installation and test in the wheel shortly before the end of the present contract.

C. SCOPE OF TESTS AND METHOD OF OPERATION

Equations (1-7) show that if all variables were systematically varied over a reasonable range of values an enormous amount of testing would be involved, because the soil values, also a function of moisture content, should be included.

To approach this problem in the limited time available, we decided to limit the scope to one moisture content as a starting point. A moisture content of 10% was selected because the change of soil properties with moisture was of small magnitude at this point, as can be seen from Fig. 1, which shows the results of soil box tests. This moisture content provided experience with the problem of moisture control of the large mass of soil in the tank, because tests with a reasonable variation of moisture but with little accompanying change in soil values could still fit into this program. Six hours are required to determine the moisture content of the soil; during this time the soil bed is gradually changing its moisture, of course. As a result of some experience, the procedure was to add the estimated amount of water uniformly throughout the bed before tests began, cultivate as necessary to spread this throughout the soil, then sample for the moisture content and proceed with the test runs while the actual moisture content was being determined. Occasionally this method resulted in too high or too low a water content, but tests were considered acceptable if the final water content was between 9-11% approximately. After some experience, we were able to hold moisture to within 9.5 to 11.5% in general. (See Figs. 2a and 2b for the test results taken during runs in the tow tank itself.)

The wheel slip was varied from about -50% to +100%, the slip being calculated from Eq. (11)

$$i = \frac{v_w - v_a}{v_a} \times 100\% \qquad (11)$$

where

i = nondimensional slip coefficient, o/o
v_w = theoretical forward speed of wheel for no slip in fps
= peripheral velocity of surface of wheel in fps, and
v_a = actual forward velocity of wheel axle in fps.

With the above nomenclature a negative slip corresponds to braking the wheel, skidding relative to the ground in the direction to decelerate the

carriage, producing a drag against the motion; while a positive slip corresponds to the wheel skidding to accelerate the carriage, producing a force in the direction of motion. With this system v_w can be any value desired, e.g., three times that of v_a, the axle speed, which results in a slip of +200%, but for a locked wheel $v_w = 0$, and only 100% negative slip is possible without reversing the direction of rotation of the wheel.

Equations (1-7), which must be fulfilled for similitude, show that in the case of Eq. (1), for given values of k_ϕ and n, we have

$$\left(\frac{w}{d^{n+2}k_\phi}\right)_p = \left(\frac{w}{d^{n+2}k_\phi}\right)_m . \qquad (1)$$

Using the same schedule of loads for the 1.04-ft wheel as in Ref. 3, then for the 0.714-ft diameter wheel the equivalent loads should be as follows when n = 1.20 and k_ϕ = 1.25:

1.04 ft-wheel, lbs	100	60	40	20	10
0.714 ft-wheel, lbs	30.0	18.0	12.0	6.0	3.0

Weights were available for the schedule of 33.0, 20.0, 13.0, 6.25, and 3.25 from the work of Ref. 3, and cross plots will be made from which the required readings for the exact load coefficients, drag, etc., can be read for any or all conditions and, if necessary, allowance made for the small variations of k_ϕ and n during the tests.

Considering Eq. (2), then

$$\left(\frac{k_c}{d\,k_\phi}\right)_p = \left(\frac{k_c}{d\,k_\phi}\right)_m . \qquad (2)$$

To fulfill this relation with the 12.5-in. and 8.56-in. wheels k_c/k_ϕ for 12.5 in. wheel = $(1.46\ k_c/k_\phi)$ for the 8.56-in. diameter. Such a change of value for k_c/k_ϕ to maintain this equality does not seem out of order if Refs. 4 and 5 are studied, however the means to effect this change of soil values has not been investigated with soil of the type under consideration. The work of Refs. 4 and 5 was conducted with sand and its modifications, also with a magnetic material, barium ferrite. To establish such a range of values for k_c/k_ϕ as indicated above for the farm soil would involve considerable experiment. We decided to proceed without change of soil properties, in other words neglecting Eq. (2) for the time being, and to establish the degree of variation between the tests without such control. This should at least pin

down the degree of influence that the relation of Eq. (2) has on the results.

One other important factor in this study is that given by Eq. (3), which has been shown to exert considerable influence upon the results (see Ref.2). In the tests being discussed the ratio of wheel diameter to soil depth was held constant at 1.56, the same as that found to give satisfactory correlation in Ref. 2; this however does not necessarily give the same correlation for the present soil because sand was used previously. The effect of variation of d/D should be tested with the Michigan farm soil.

In the tests under review a soil depth of 8 in., giving a d/D = 1.56 for the 12.5-in. wheel, was the greatest that could be employed with the present equipment. Any greater depth resulted in a large amount of soil being thrown out of the tow tank during soil preparation procedures. A change of equipment would therefore be involved if the effects of d/D are to be investigated.

Another factor appears, which is a side effect of the d/D ratio: Which set of measured soil properties are to be employed in any investigation? This question arises directly from the change of soil depth with wheel diameter. For the 12.5-in. wheel, the value of D is 8 in.; for the 8.56-in. wheel, the value becomes 5.5 in. With the soil depths indicated, the same depths used when investigating sand, a distinct change was observed in some of the soil parameters when using farm soil with change of depth which was not observed for the sand. It can be concluded that the farm soil is sensitive to the depth above hardpan of any sort, while the sand continues to flow round the footing more easily in shallow depths than does farm soil. The actual change of these magnitudes is given in Table I for the average moisture conditions employed in these tests.

TABLE I

EFFECT OF SOIL DEPTH UPON THE SOIL PROPERTIES

	8.0 in.	5.5 in.
k_c	1.07	1.27
k_ϕ	1.3	3.4
n	1.2	1.25
k_c/k_ϕ	0.82	0.374

The main change is in the value of k_ϕ which in turn affects k_c/k_ϕ. Using these two sets of values in Eq. (2) yields the following:

$$\frac{k_c}{k\phi}_{12.5"} = 0.82$$

$$1.46\, k_c/k\phi_{8.56"} = 1.46 \times 0.374$$

$$= 0.546$$

$$\frac{k_c}{k\phi}_{12.5"} \neq \left(1.46 \frac{k_c}{k\phi}\right)_{8.56"} .$$

The difference in the ratio for prototype and model is not as great as the ratio of the direct magnitudes shown in Table I, however there is sufficient difference—0.82 to 0.546—that complete similarity and equality of dimensionless coefficients cannot be expected unless the effect of the factor $k_c/dk\phi$ is of small magnitude as far as the dimensionless factors are concerned. If correct conditions are to be obtained, both $k\phi$ and $k_c/k\phi$ should be changed considerably with but small effect upon k_c.

Each of the relations Eqs. (4-7) can be fulfilled easily: the wheels of varying diameter can be made with the same aspect ratio α; the soil, if unchanged by moisture variations or soil depth, has the same μ and n; while the slip i is capable of variation over the same wide limits in each wheel size.

The result is that the similitude relations Eqs. (1-7) can be fulfilled, with the exception of Eq. (2), plus that extra item of soil depth effect on soil values.

The tests were thus conducted to verify the validity of the similitude parameters, using rigid aluminum wheels operating in typical Michigan farm soil. The wheel diameters, loads, etc., are shown in Table II; the slip was varied from -50% to +100% approximately; and the drag, torque, sinkage, etc., were recorded for a soil moisture content of about 10%.

TABLE II

WHEEL SIZES, ASPECT RATIOS, SOIL DEPTH, AND LOADS USED

Wheel dia., in.	Aspect Ratios	Loads, lbs	Soil Depth, in.
12.5	0.27,0.52,0.84	10,20,40,60,100	8.0
8.56	0.27,0.52,0.84	3.25,6.25,13.0,20.0,33.0	5.5

D. TEST RESULTS

The above program was carried out, and, over the period of testing, the moisture was controlled within the limits of 9.3 to 11.6%, the majority of the readings being in the 9.8 to 11.0% range; periodic checks on the Bekker soil values were also made and the averages used in the calculations.

Figure 3 shows the assigned directions of positive and negative forces and torques exerted by the soil on the wheel, where

V_a = forward velocity of the wheel axle or carriage in fps;
V_w = peripheral velocity of the wheel in fps = $\omega \frac{d}{24}$ fps;
d = diameter of wheel in in.;
ω = angular velocity of wheel, rad/sec
R = resultant horizontal force on wheel due to the earth, -ve as a drag on carriage, +ve as a driving force;
T = torque exerted on wheel ft/lb, -ve when $V_w < V_a$, +ve when $V_w > V_a$.

The nomenclature for Fig. 3 results in a drag such as that provided by a towed load's being negative, a powered wheel giving a drawbar pull becomes positive. A driving torque applied to a wheel is positive, a braking one negative.

The results obtained for each wheel diameter are divided into two groups: Group 1 consists of the fundamental recorded data for the 12.5-in. wheel plotted directly from the test results (Figs. 4-12). Cross plots of this material are shown in Figs. 13-21, plotted on a wheel-load base which permits some correction of observed data and at the same time permits any load condition to be read from the graphs. Observe that the load coefficient $w/d^{n+2}k_\phi$ is, for a given soil and moisture content when n and k_ϕ have fixed values, a function of the load. Then the horizontal axis of Figs. 13-21 can also be an axis of load coefficient. The scale for this coefficient has been added to each of the above diagrams.

Figures 40-45 show the corresponding set of Group 1 observed data for the 8.56-in. wheel; Figs. 46-51 are the corresponding cross plots. As before, load coefficient scales have been added.

Group 2 consists of the results obtained by calculation from the data of Group 1. The calculations for sinkage coefficient, drag coefficient, and torque coefficient are plotted on both slip and load axes, and are shown in Figs. 22-39 for the 12.5-in. diameter wheel and in Figs. 52-63 for the 8.56-in. diameter wheel. Again when the horizontal axis is load, it has also been plotted as load coefficient.

E. DIMENSIONLESS PARAMETERS

A third set of parameters, which are dimensionless, have been plotted with the aid of Figs. 4-63. One can plot various groups of the dimensionless coefficients on an axis of slip coefficient (dimensionless) for constant values of the load coefficient $w/d^{n+2}k_{\phi}$, or similar constant slip curves on an axis of load coefficient.

In Eq. (8), for example, theory states that R/w would be constant if the right-hand side of this equation were also constant. The first term of this right-hand side—the load coefficient—can be maintained constant because R/w can be obtained, from the curves, for any selected value of the load coefficient. The second term has already been discussed, and at present cannot be maintained constant. The remaining items, by adjusting the required conditions, or because they are constants for a given soil, have been maintained at a given value, at least to a first approximation. These items will be considered in turn:

D/d = soil depth to wheel diameter; constant by adjustment of D for each value of wheel diameter employed.

α = aspect ratio; constant by use of the correct wheel dimensions.

μ = coefficient of friction; should vary but little with change of wheel size, provided moisture is constant.

n = sinkage index; changes slightly with soil depth and moisture content (see Table I). No means yet available to keep it exactly constant without also affecting the values of k_c and k_{ϕ}.

i = wheel slip coefficient; can be kept constant by reading the appropriate values from the curves.

From the data, we can thus state that except for the second term, R/w, T/wd, and z/d can be plotted on a dimensionless basis.

Figures 64-85 plot these terms on a slip base for various values of the load coefficient; plots on a load coefficient base for the average drag and torque coefficients for the two sizes, at various slips are given in Figs. 86-88. One exception however is the torque coefficients for $\alpha = 0.27$ for the two wheel sizes, shown in Figs. 78-80; these are so widely separated that no averaging is justified. These results thus throw doubt as to whether Figs. 86-88 represent a true condition. These average diagrams have been plotted

on the assumption that at the same load coefficient the 12.5- and 8.56-in. wheels should have the same drag coefficient, etc., if the other terms are constant; thus the use of the average value of the two sizes. But, as pointed out, in the light of Figs. 78-80 a preferred plot of the data handles the two diameters separately; this approach is shown below.

If all the points of Figs. 78-80 are plotted on one graph (Fig. 89), and one curve can now represent almost all of the data for the 12.5-in. wheel but not the 8.56-in. wheel, the result is that a plot on a base of load coefficient becomes that shown in Fig. 90; i.e., torque coefficient for each given diameter remains constant at some slips for the range of load coefficients covered, but there is a wide variation between the results for the two wheel sizes.

Reexamining Figs. 81-83 in this light indicates that the same results could be obtained with these data for $\alpha = 0.84$ and 8.56-in. and 12.5-in. wheels, in place of Fig. 88. The revised diagrams are shown in Figs. 91 and 92. The results for the two diameters at each slip for this aspect ratio are grouped closer together than in Fig. 90, but can still be shown as two separate sets of curves in place of the theoretical single one. Figure 92 shows up the differences made by the averaging of Fig. 88.

Considering these data for the torque coefficient redirects attention to Figs. 86 and 87, and the question can be asked "Does the average plot for the 12.5-in. and 8.56-in. wheel for each slip represent a single nondimensiona curve or are there two curves, similar to Fig. 90, for the torque coefficient? Admittedly, the data for drag do not change so much as for torque, perhaps because k_c/dk_ϕ has a smaller effect on drag.

For sinkage results, Figs. 93 and 94 plot sinkage coefficient versus load coefficient.

F. DISCUSSION

Examination of the results plotted in the dimensionless manner, i.e., the various coefficients on a slip or load coefficient base, permits certain observations.

From Eqs. (8-10), one would expect the coefficients to plot dimensionless provided the right-hand side of the equations are constant. The inability to keep the second term $k_c/dk\phi$ constant has already been discussed. In addition, the tests were conducted at two values of α, the aspect ratio. Neglecting the first, it follows that two sets of dimensionless curves should result, one for each aspect ratio. Taking the various curves in turn we will examine what has actually happened.

1. SINKAGE COEFFICIENT

The sinkage coefficients of Figs. 70 and 71 on a slip base, and Figs. 93 and 94 on a load coefficient base, show a distinct similarity in as much as two separated sets of curves occur at each aspect ratio. According to Eq. (10), Z/d should be constant when all the factors on the right are constant. The diagrams under discussion show great separation of the points for any given value of the load coefficient. It follows that the effect of $k_c/dk\phi$ is considerable in this case; in addition, perhaps the soil values resulting from depth (shown in Table II) are entering the picture. The change in shape of the curves, straight lines for the 12.5-in. wheel and curves for the 8.56-in. one, could also be caused by the effect of the bottom of the tank, despite d/D being constant. In fact, Z/d will, given sufficient load, reach a limiting value as the load coefficient increases, because the wheel will eventually rest on the tank bottom. The data for the 8.56-in. wheel then may already be reflecting this effect. With lower load coefficients relative to this limiting value, these curves could become straight lines, the same as those for the 12.5 in. wheel. Indications point in this direction.

Regarding dimensionless parameters for the sinkage. The work presented here has not established their existence, not because they are nonexistent, but because of insufficient control of the various factors affecting the results.

2. DRAG COEFFICIENT

The drag coefficients (Figs. 72-77) for $\alpha = 0.27$ and 0.84 for the two wheel sizes plotted for load coefficients of 5, 10, and 15, show considerable

similarity. The two curves on each diagram should, theoretically, be identical. At slips greater than ±30%, reasonable plotting occurs; only in the range of ±10% slip is there serious divergence.

Figures 86 and 87 show the average drag coefficient for the two wheel diameters at each value of slip plotted against load coefficient.

If one could have included the effects of k_c/dk_ϕ in these results, possibly the plotting could have been improved.

Figures 84 and 85 show all of the points for $\alpha = 0.27$ and 0.84. From these plots one could almost say that drag coefficient is independent of load coefficient for each value of the slip, because diagrams similar to Figs. 86 and 87 would now consist of a series of straight lines parallel to the load-coefficient axis. Once again the effects of the missing factor should be obtained before giving a positive result. However, the indications are that reasonable dimensionless data have been obtained under the limited conditions of the test.

3. TORQUE COEFFICIENT

The plots of torque coefficient shown in Figs. 78-80 for $\alpha = 0.84$, show greater differences with respect to aspect ratio than did the plots of drag coefficient; aspect ratio has become a more dominant factor.

The data of Figs. 78-83 have been superimposed on Figs. 89 and 91 for each of the aspect ratios. In Fig. 89 the points for all load coefficients of the 12.5-in. wheel almost coincide except at the large negative slips, while the 8.56-in. data coincide at low slips and separate at positive values.

For Fig. 91, three curves can be drawn for each wheel diameter, though the difference between them for each wheel size is relatively quite small.

In evaluating these diagrams it must be remembered that variations in moisture content of the soil between the tests has some effect on the results. Allowing for these variations, one is inclined to state that torque coefficient is almost independent of load coefficient, but is dependent on the slip, aspect ratio, and wheel size.

Figures 90 and 92 have been plotted from a dimensionless standpoint; if the results were completely dimensionless the lines for the 12.5-in. and 8.56-in. wheels at -50% slips should be identical. Similarly the solid and dotted lines for all other slips should coincide.

In fact, this is far from the truth; the differences are relatively small for $\alpha = 0.84$, but are great when $\alpha = 0.27$. One could conclude that

the factor k_c/dk_ϕ has a greater effect at small aspect ratios.

In the case of the drag coefficients shown in Figs. 84 and 85, there is also a distinct shift with aspect ratio. In this case the drag coefficient increases with the aspect ratio, at least in the positive slips.

G. CONCLUSIONS

The work under review has failed to pin point definitely the dimensionless relationships, but has shown that the differences encountered have, in some cases, been small. When a little license is taken with the observed points and an average used, the gap between the usual two curves for each of the load coefficients is relatively small and a single curve can be drawn. In other cases this difference is great; some factors appear to be affected much more than others by the parameter k_c/dk_ϕ; this of course assumes that Eqs. (8-10) apply.

In some cases, such as the torque coefficient curves of Fig. 89, the value at this coefficient is independent of the load coefficient over a considerable portion of the range, for example, when the slip was from 0% approximately to +100% and the wheel diameter was 12.5 in. But this same torque coefficient factor is not equal for the two wheel sizes for any given load coefficient; the difference is too great for an average value to mean anything. Such cases reflect the absence of control of k_c/dk_ϕ. With such control, plus constant soil values irrespective of soil depth, one could draw some conclusions about the validity of Eqs. (8-10) for the farm soil in question.

This report brings up the problem of the effect of soil depth in the tank relative to wheel size. To eliminate this problem would require a much deeper tow tank, which in turn would involve establishing experimentally the ratio of wheel size to soil depth parameters. From the present tests one can conclude that farm soil behaves quite differently from sand when exposed in given depths over a hard surface and tested for Bekker values with the same size equipment. Apart from increased soil depth, one other solution would be to coordinate the dimensions of the bevameter footing to the depth and type of soil.

If scale model tests in Michigan farm soil are to be carried out successfully, some means must be found of holding constant all the factors of Eqs. (8-10). This is our chief conclusion.

A second but equally important conclusion is that soil values must be investigated to establish values when the depth over hard-pan is relatively small compared to the wheel diameter. Indications are that soil values in Eqs. (8-10) will not be constant without greater soil depths than those presently used. To establish the validity of the dimensionless parameters will probably require a relatively great depth of soil so that the wheel size will in all cases be small relatively, and the method and penetrator for the soil values for various wheel sizes will give the same soil properties irrespective of soil depth.

PART II

A. SHEAR TRANSDUCER

To understand the effects of load, soil, etc., on the performance of a wheel one must know the total resultant forces acting on the surface of the wheel. Measurements were made of the radial load on a small element of a wheel's surface when operating in sand (Ref. 6). These measurements provide only part of the required information; in addition to the radial load a tangential force component relative to the wheel surface must provide the tractive force between the wheel and the ground.

Theoretically the total load-carrying capacity of the wheel can be defined in terms of the combined radial and tangential forces in a manner similar to the resultant lifting force of an airfoil or the resistance of a ship's hull. Any reasonably simple, theoretical relationship between wheel drag, sinkage, load, etc., cannot be determined unless the sum of the total forces on the wheel can be obtained and interpreted in some simple mathematical manner. Thus for a complete analysis, the shear force must be determined as well as the radial one for all points on the surface in contact with the ground.

A number of attempts have been made to determine this shear load; but because in all cases so far seen the load was measured on a relatively large portion of wheel surface, average values only were obtained.

In this case we attempted to reduce to a minimum the surface area on which the measurements were made so that the forces at a point could be approached as closely as possible. The design provided a surface area of 1/16 sq in. on which both radial and shear loads could be determined simultaneously; the mechanism is described below.

B. DESCRIPTION OF APPARATUS

The fundamental element of the apparatus consists of a square element, 1/4 in. x 1/4 in., of the wheel's surface supported so that it can move freely in both radial and tangential directions over extremely small distances (about 0.003 in.) under the influence of the forces of the soil on its surface. These movements are applied to the cores of two differential transformers, one for radial movement and the other for the tangential direction. It follows that signals are developed proportional to these movements, and the forces can be recorded individually.

The apparatus, shown diagrammatically in Fig. 95, consists of a framework, A, fitted into the rolling surface of the wheel and provided with a slot, B, into which the measuring surface, C fits. The measuring surface consists of a rectangular element, 1/4 in. x 1/4 in., which forms part of the wheel surface.

This surface is connected to a rod, D, pivoted at its upper end to a block, E, held by two cantilever springs so that E is compelled to move in a vertical direction only under the influence of the forces applied to the measuring surface. Attached to E is a rod on which the core of a differential transformer is mounted; thus any vertical movement of block E under the control of the measuring surface and springs, F, can be calibrated and recorded in terms of a vertical load applied to the measuring surface. Because the maximum resulting motion is small, about 0.003 in., there is a well-defined linear relationship between force and displacement; thus the radial load can be determined.

The tangential force on the 1/16 sq in. area is opposed by the loads of the two springs, G, and the resulting movement recorded by the differential transformer, H. Again the small movements result in a linear scale; in addition the rod joined to the springs has great flexibility so that radial movement does not disturb the individual results. Location of the measuring element in the slot is affected by two linear ball bearings, shown in Fig. 95.

Two shoes, added to the surface in contact with the ground, are adjustable so that the circumferential clearance between them and the moving element can be set at a minimum value for the exclusion of dirt and still permit the desired movement of the element.

C. CALIBRATION

When complete the instrument was placed in a calibrating stand, and both radial and tangential loads applied to the surface.

The instrument proved quite sensitive, so much so that friction of all parts had to be reduced to a minimum for a sufficiently accurate return to the null position. The movements under calibrating conditions were transferred to a two-channel oscilloscope, and eventually sufficiently satisfactory operation was obtained to permit a test in the wheel.

D. WHEEL TESTS

On assembly in the wheel, various modifications were necessary to provide for ease of adjustment, setting of zero, etc., because outside settings could not be transferred without maladjustments when in place.

On the first runs, the wheel rotated but not in contact with the ground. Under these circumstances the recorder reflected the changing direction of gravity on the rotating mechanism. This was overcome by correcting the balancing mechanism.

Figure 96 shows an early run with a load of 40 lb on the wheel; it shows the wave due to gravity as well as the high peak due to soil contact. The change in the zero as well as the shape of the diagram is apparent. This change was the result of dirt's entering the mechanism. The greatest force on the 1/16 sq in. area indicated by the peak in the diagram, amounts to about 3 oz for the radial load and to 2-3/4 oz for the tangential load. The variation of each rotation caused by the dirt is apparent. During this early test, paper speed was kept at a minimum.

As a result of this preliminary run, modifications were made: the mechanism was correctly balanced, efforts were made to prevent entrance of dirt, etc. Figure 97 shows a second run under a 20 lb load. Dirt remains a problem, zero changes occur, etc., which throw considerable doubt on the accuracy of the diagram.

Further efforts were made to exclude the very fine dust from the close clearances; the best of the diagrams obtained is shown in Fig. 98. This was taken at the first revolution of the run. Again zero change occurred, and subsequent diagrams varied considerably with the entrance of dirt. Figure 98 indicates a maximum radial load of 9.7 oz with a shear of 2.4 oz, equivalent to 9.7 and 2.4 psi, respectively.

Many changes were made in an effort to eliminate the introduction of friction caused by dirt's entering the moving element, all without success. The soil had been cultivated so that it was well powdered, and even the presence of moisture tending to bind it together did not stop some particles entering the clearance on the sides of the moving element even though this clearance was about 0.0003 in. and its width in the radial direction eventually reduced to about 0.010 in.

At this time the contract terminal date was reached and the work was brought to a standstill.

E. CONCLUSIONS

The basic principle of recording both radial and tangential forces on a small element of a rotating wheel has been demonstrated as a possibility.

The present apparatus suffered from the defect that the extremely fine dust associated with the farm soil employed could not be excluded from the mechanism with the design employed.

Judging from the initial early experiments, with sand as the working material, the present design would be suitable for that type of soil.

In order to be successful with the farm soil a redesign would be necessary, a design in which positive exclusion of dirt would be necessary.

REFERENCES

1. Performance Coefficients for Powered Wheels in Sand, Report No. 02860-36-F, ORA, The University of Michigan, Ann Arbor, March 1962.

2. A Similitude Study of the Drag and Sinkage of Wheels Using the Sinkage Parameter System of Soil Values, Report No. 02860-27-P, ORA, The University of Michigan, Ann Arbor, April 1961.

3. Research in Vehicle Mobility, Report No. 2544-31-F, The University of Michigan Research Institute, Ann Arbor, July 1960.

4. Performance Coefficients for Towed Wheels in Farm Soil, Report No. 05020-9-F, ORA, The University of Michigan, Ann Arbor, January 1963.

5. Control of the Properties of Research Soil Systems, Report No. 02860-33-P, ORA, The University of Michigan, Ann Arbor, January 1962.

6. Pressure Distribution On and Flow of Sand Past a Rigid Wheel by E. T. Vincent, Report No. 03026-1-T, University of Michigan Research Institute, Ann Arbor, November 1960.

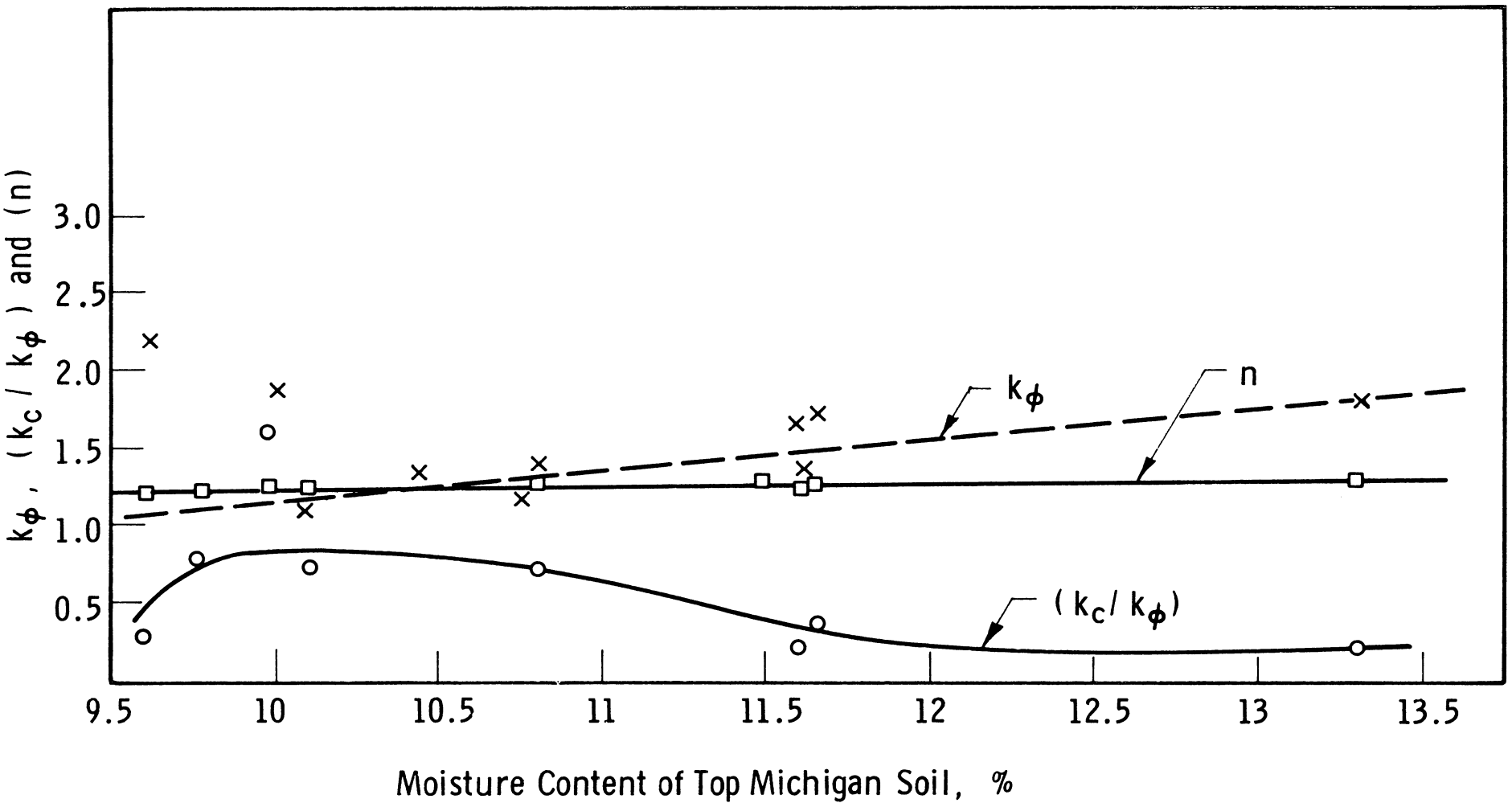

Fig. 1. Soil properties and moisture content.

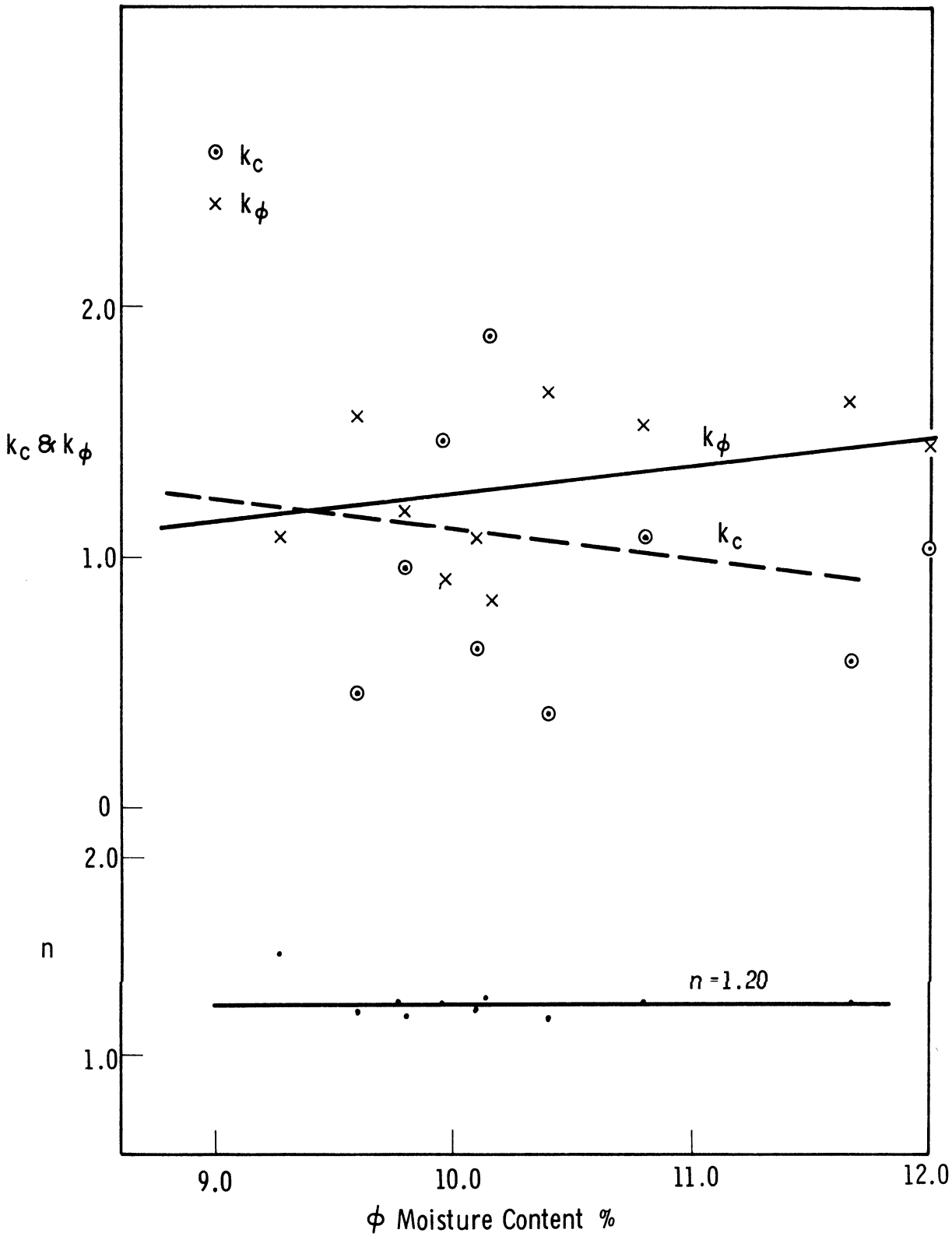

(a) Soil value measurements at various moisture contents during 12.5-in. wheel tests, d/D = 1.56, footings of 2-1/2 in. and 4-1/2 in. dia.

Fig. 2. Soil values determined with soil in tow tank during test.

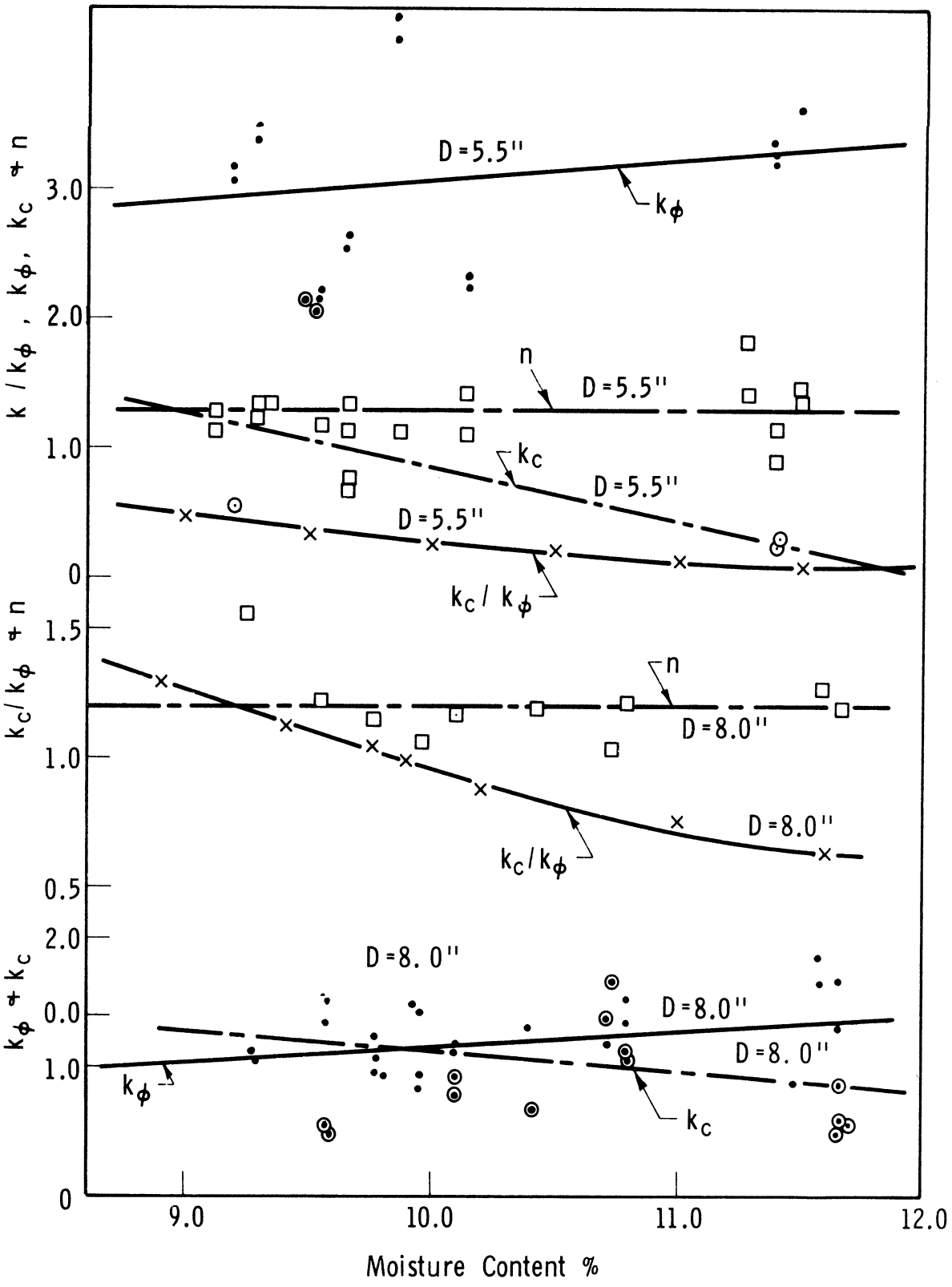

(b) Soil value measurements in tank with 8- and 5.5-in. soil depths, footings of 2-1/2-in. and 4-1/2-in. dia.

Fig. 2. Concluded.

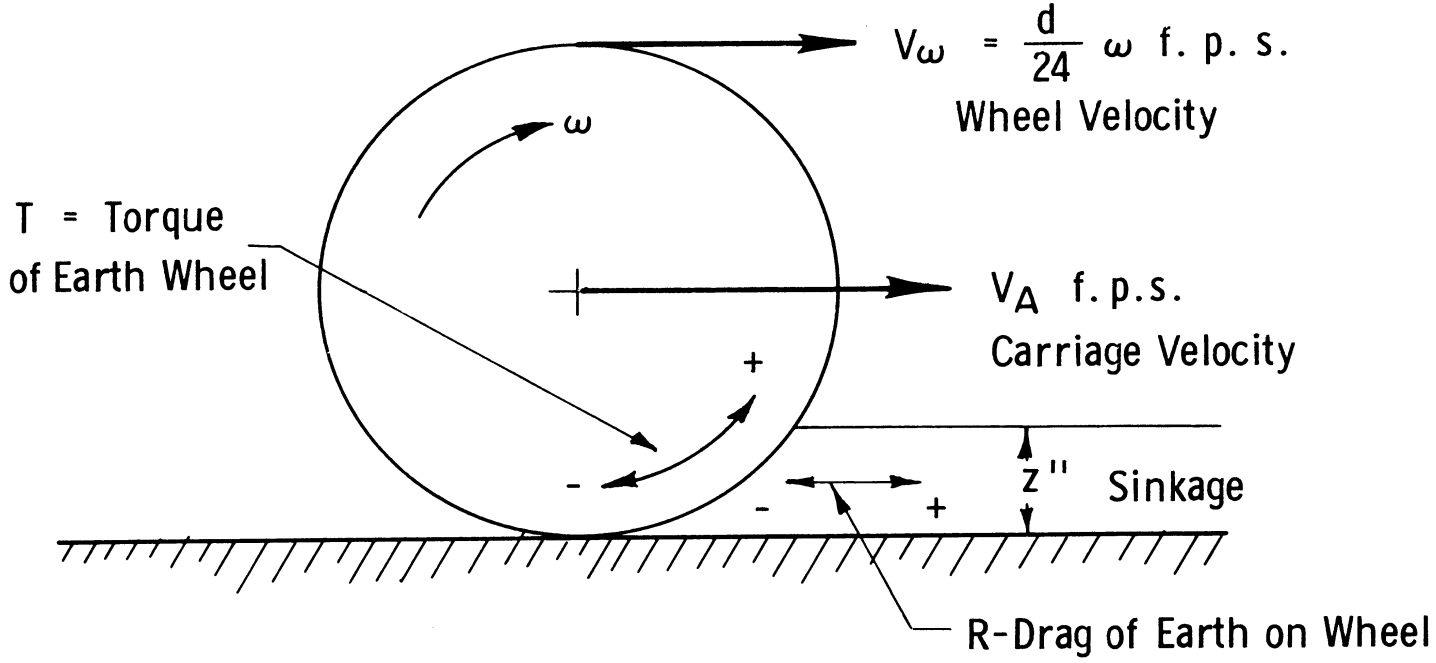

V_a = forward velocity of the wheel axle or carriage f. p. s.
V_w = peripheral velocity of wheel f. p. s.
= ω d/24 f. p. s.
d = diameter of wheel in in.
ω = angular velocity of wheel rad/sec
R = resultant horizontal force on wheel due to the earth. -ve as a drag on carriage, + ve as a driving force
T = torque everted on wheel ft/lbs - ve when $V_w < V_a$
+ ve when $V_w > V_a$

Fig. 3. Nomenclature and direction of forces exerted on wheel.

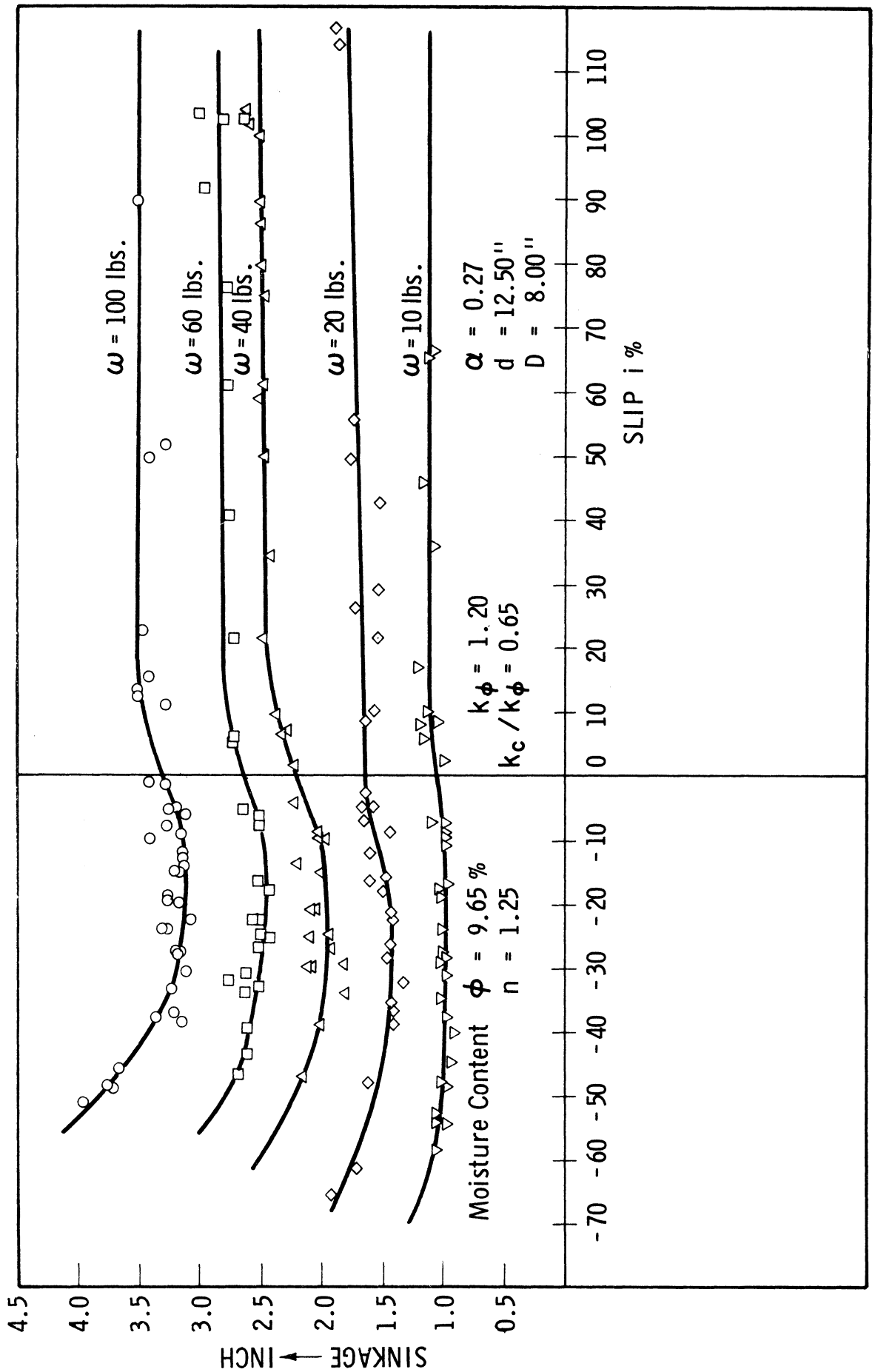

Fig. 4. Sinkage-slip curves for d = 12.5 in., α = 0.27, D = 8.0 in.

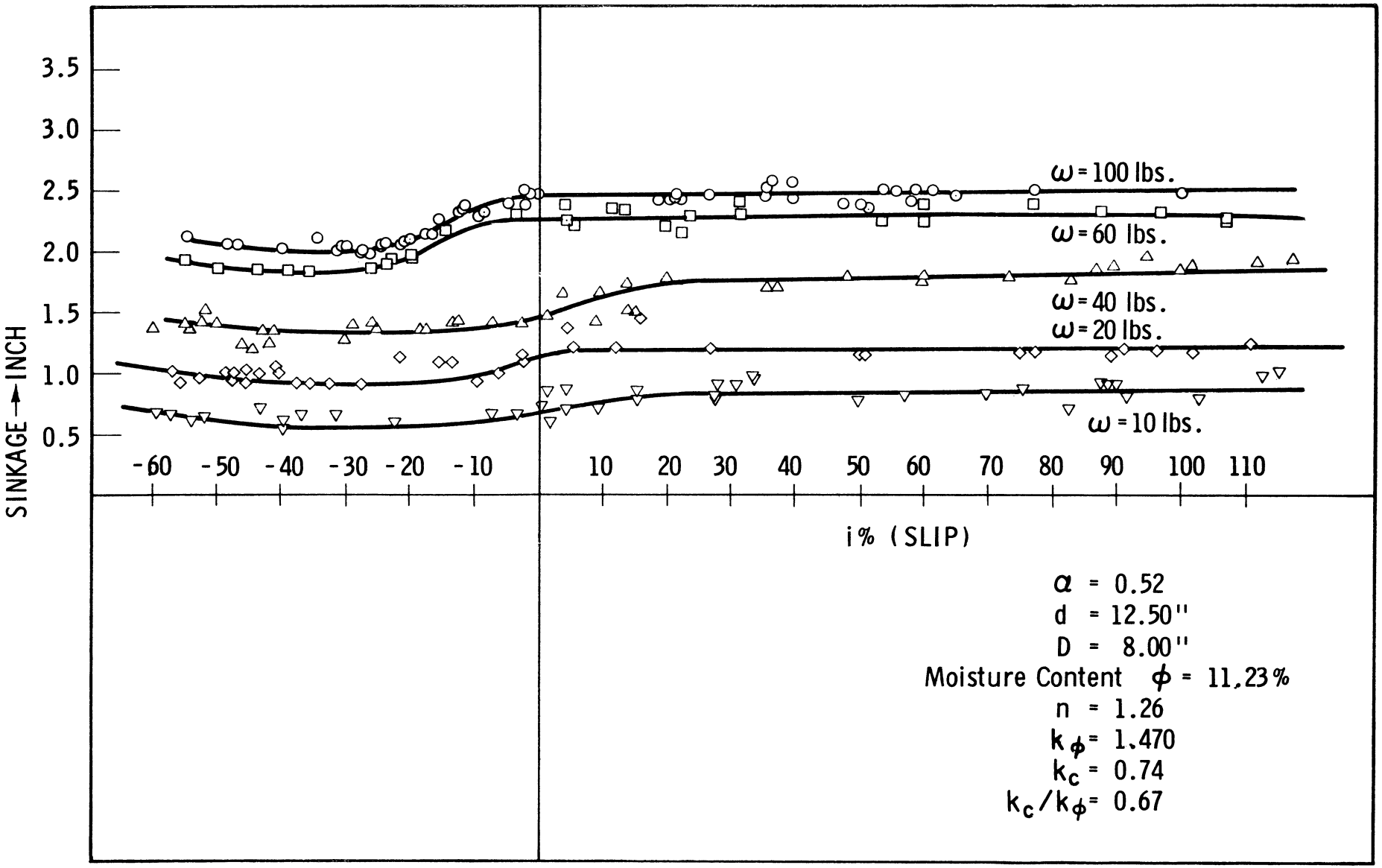

Fig. 5. Sinkage-slip curves for d = 12.5 in., α = 0.52, D = 8.0 in.

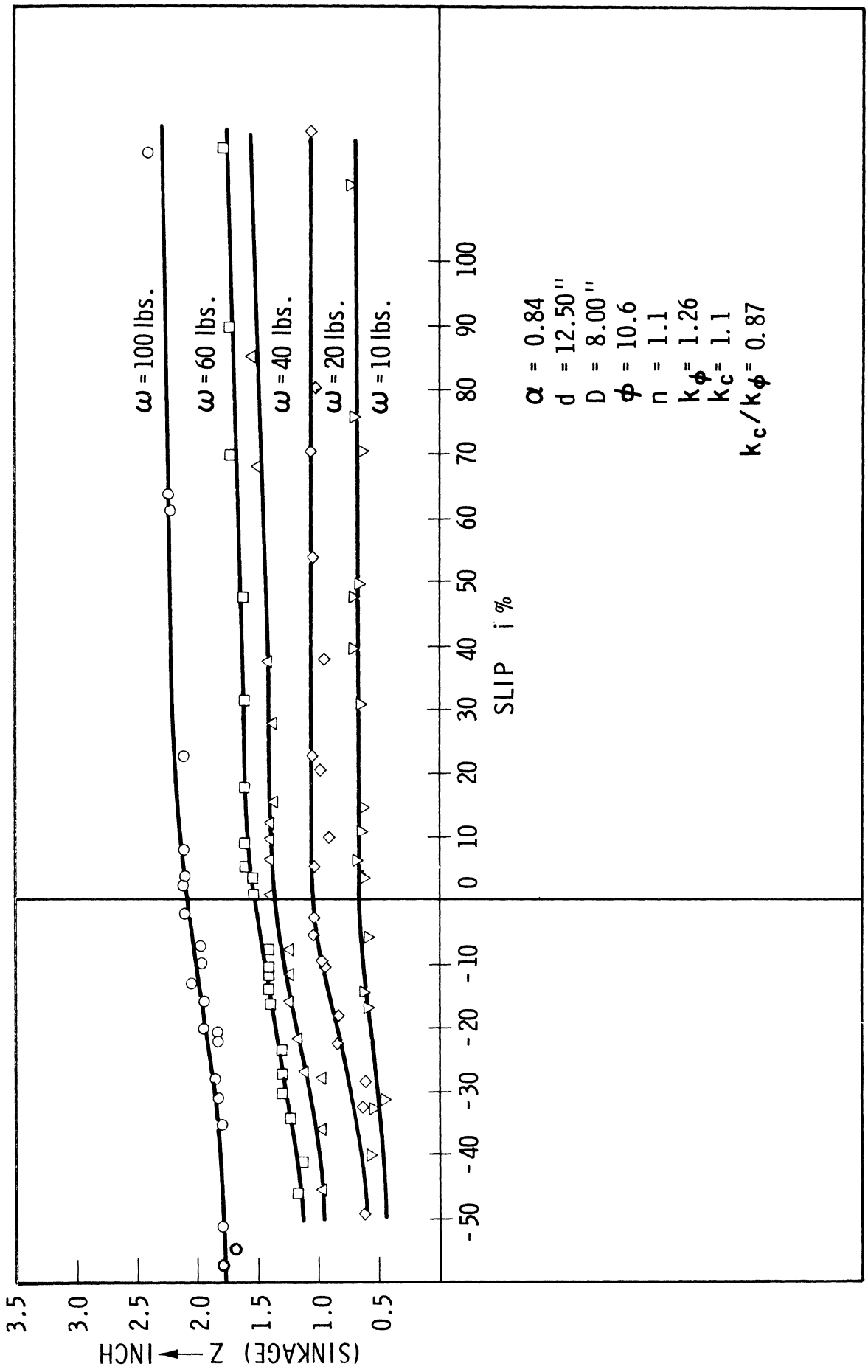

Fig. 6. Sinkage-slip curves for d = 12.5 in., α = 0.84, D = 8.0 in.

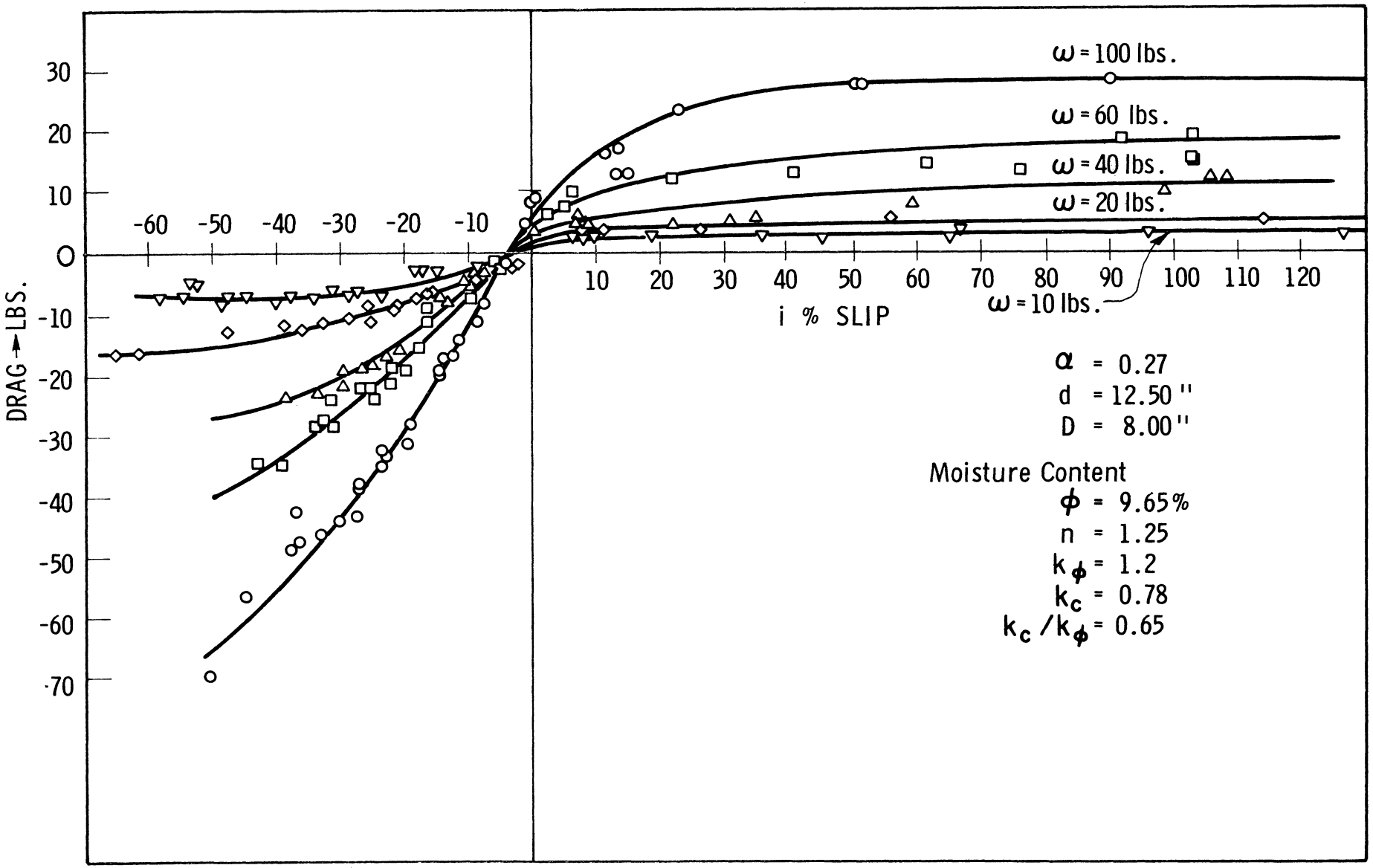

Fig. 7. Drag-slip curves for d = 12.5 in., α = 0.27, D = 8.0 in.

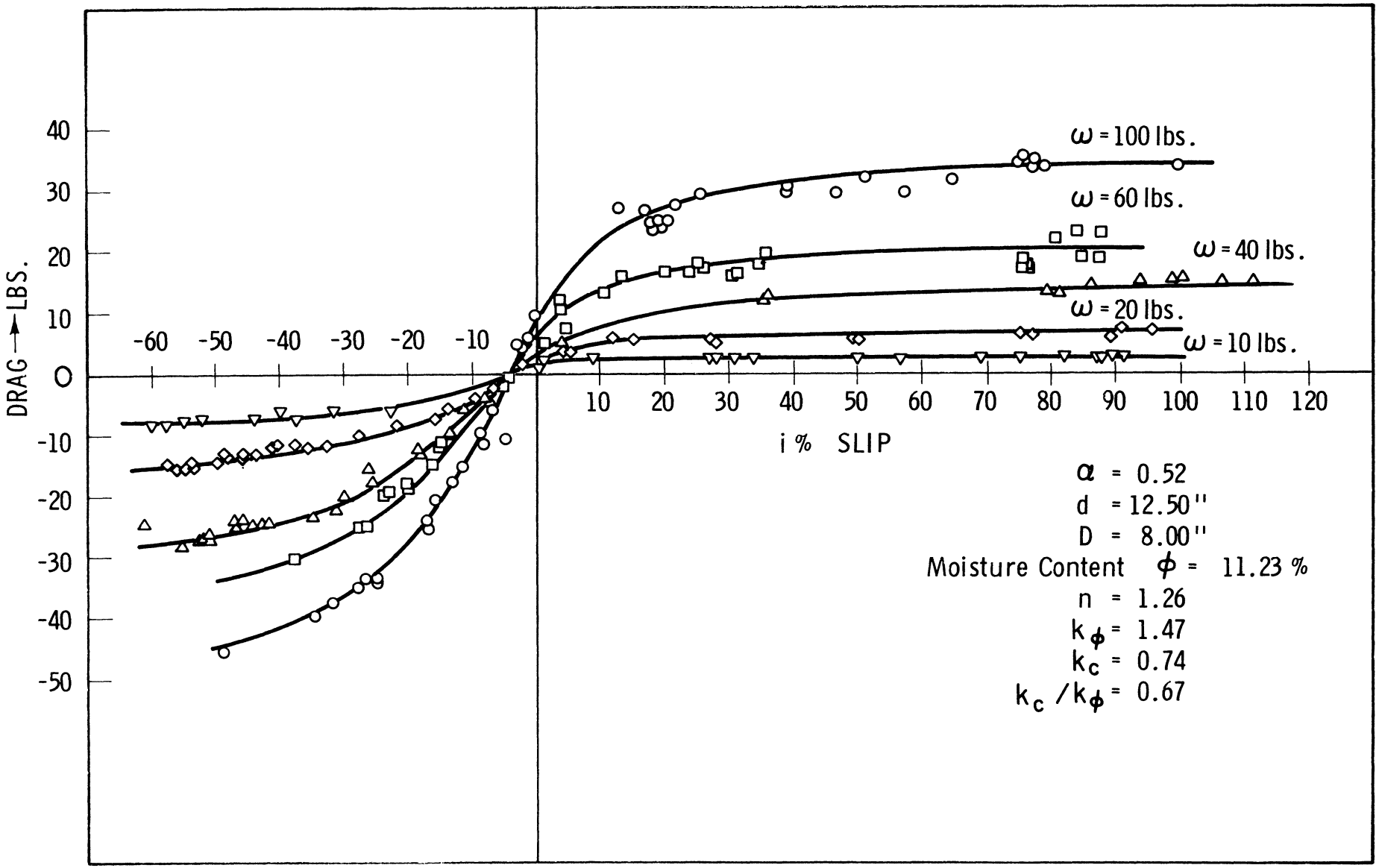

Fig. 8. Drag-slip curves for d = 12.5 in., α = 0.52, D = 8.0 in.

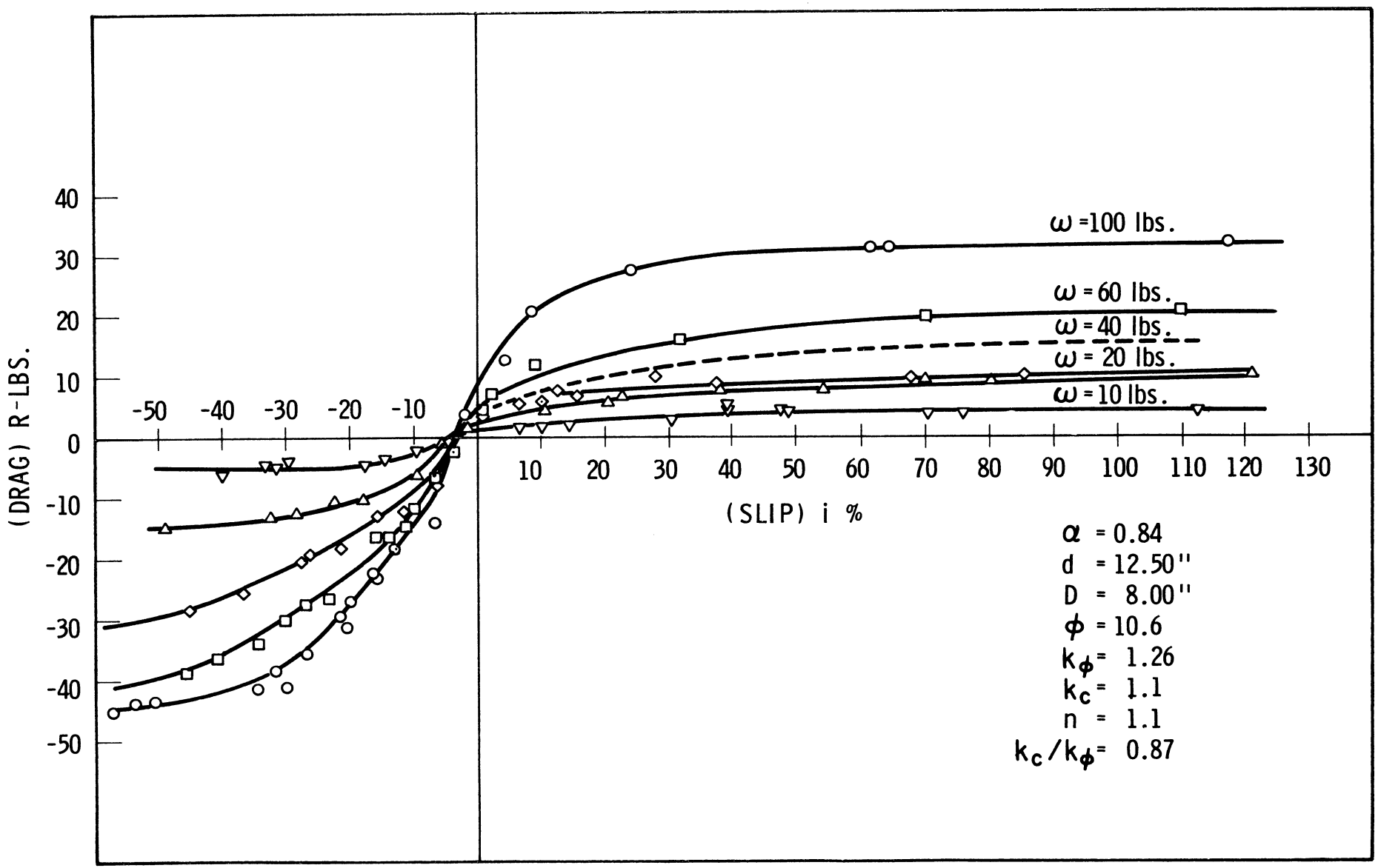

Fig. 9. Drag-slip curves for d = 12.5 in., α = 0.84, D = 8.0 in.

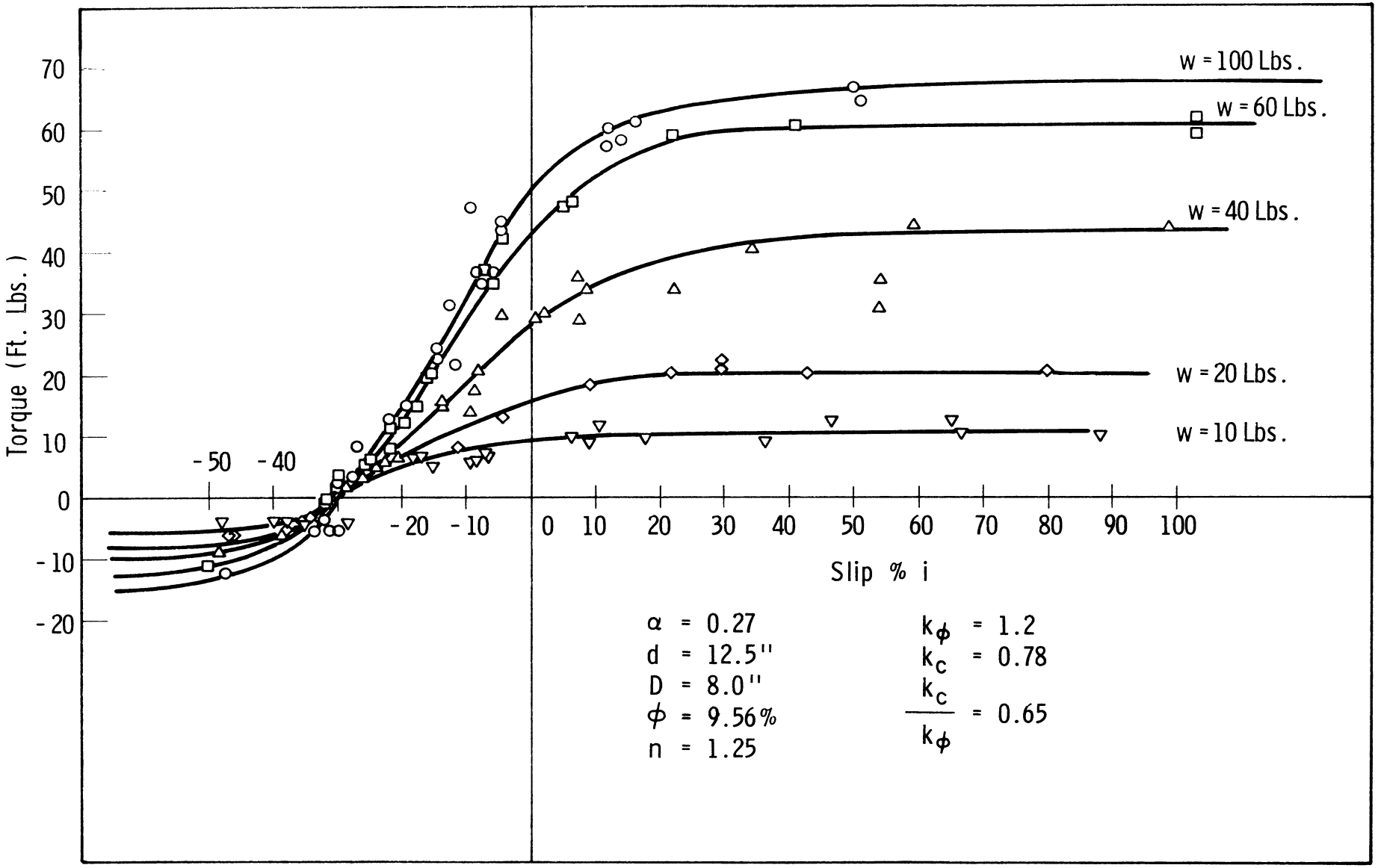

Fig. 10. Torque-slip curves for d = 12.5 in., α = 0.27, D = 8.0 in.

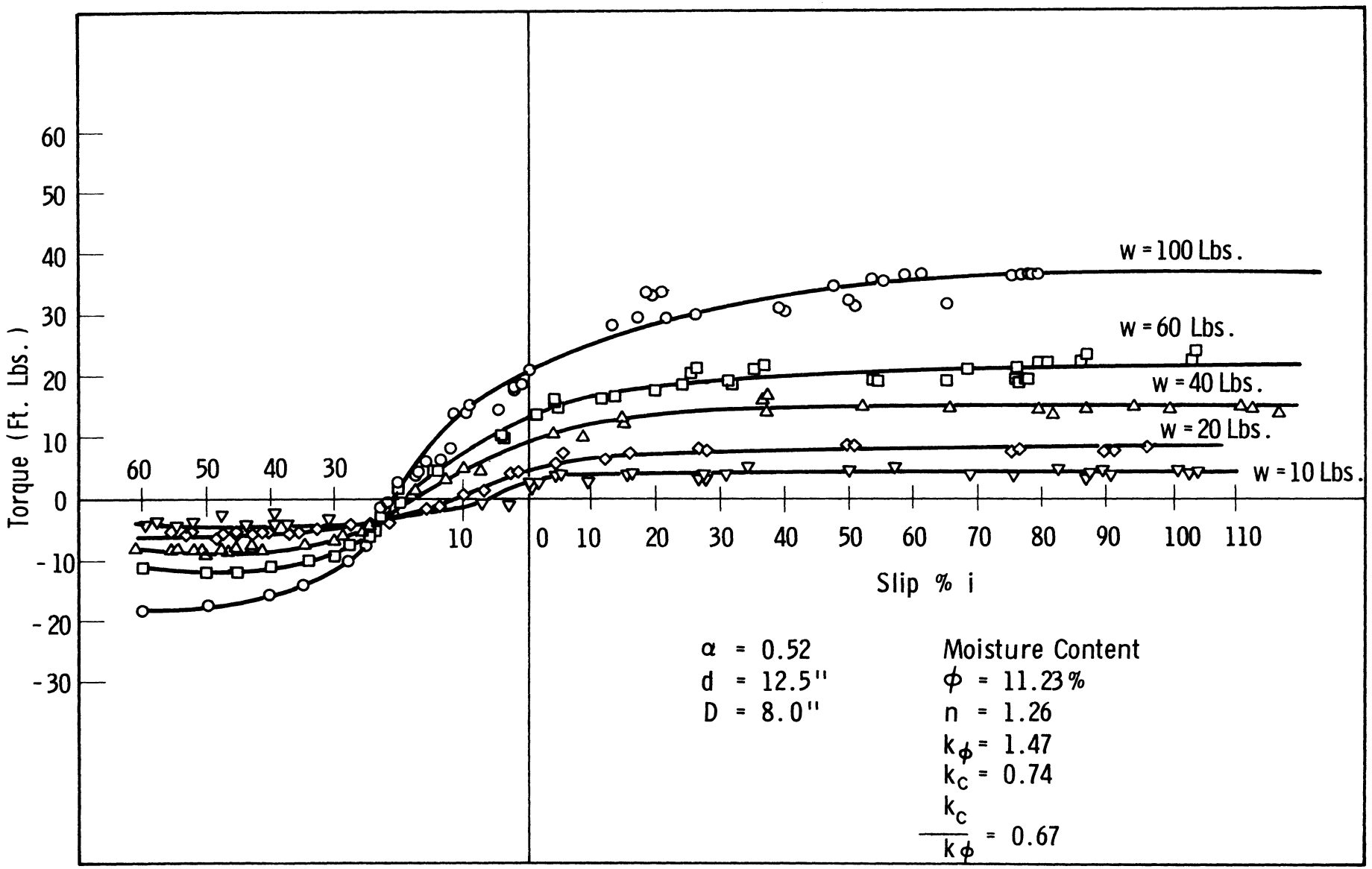

Fig. 11. Torque-slip curves for d = 12.5 in., α = 0.52, D = 8.0 in.

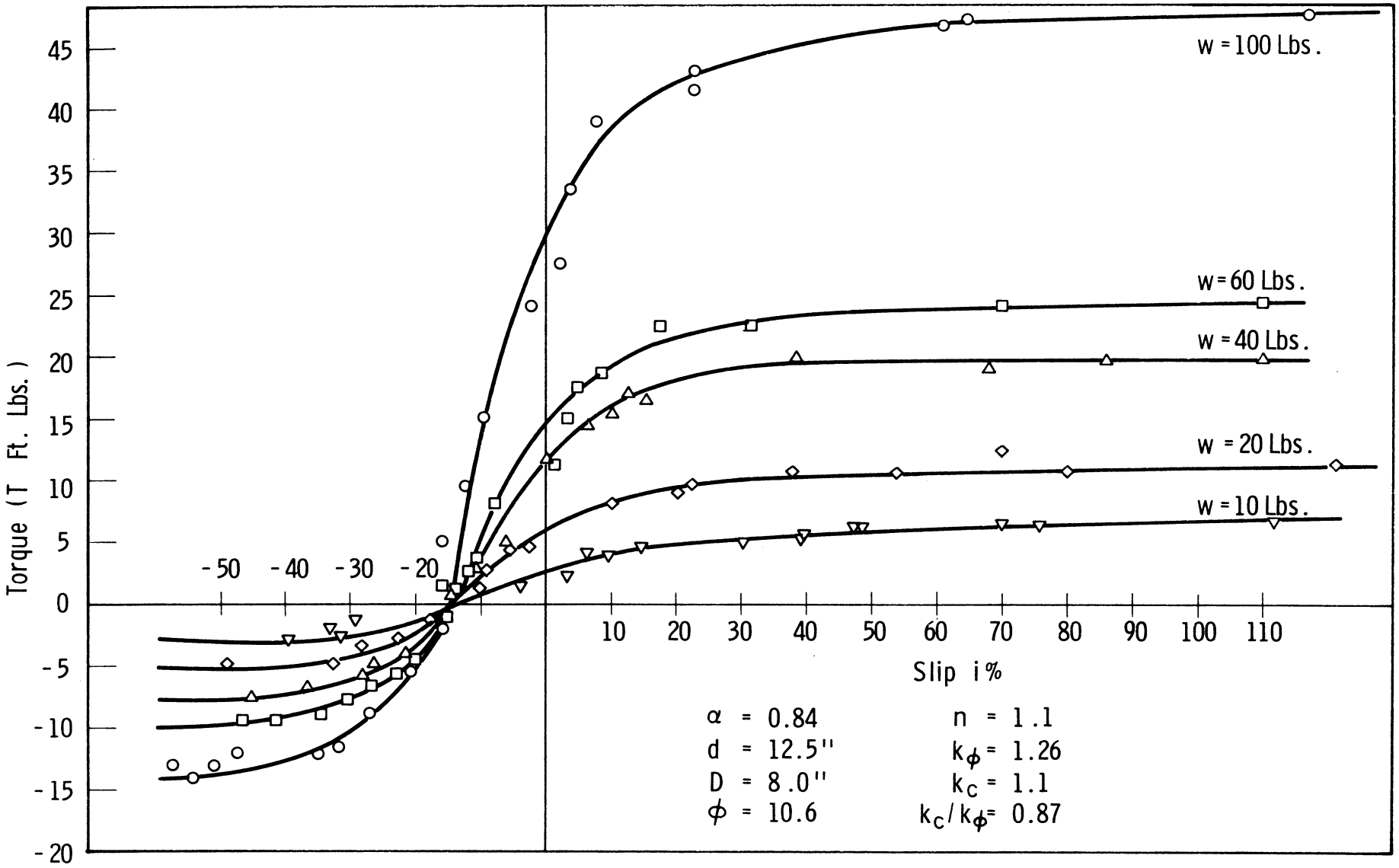

Fig. 12. Torque-slip curves for d = 12.5 in., α = 0.84, D = 8.0 in.

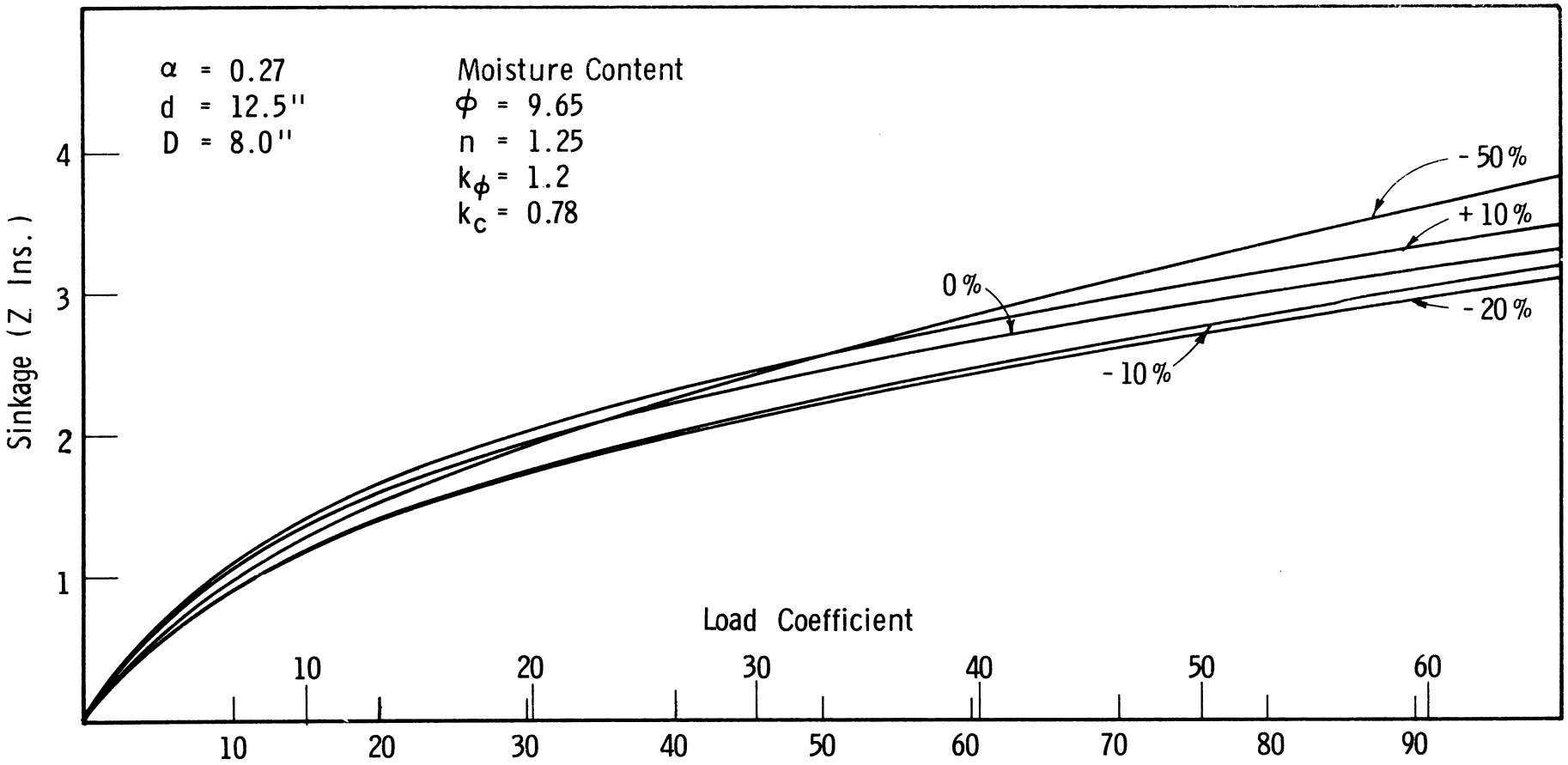

Fig. 13. Sinkage-load curves for d = 12.5 in., α = 0.27, D = 8.0 in.

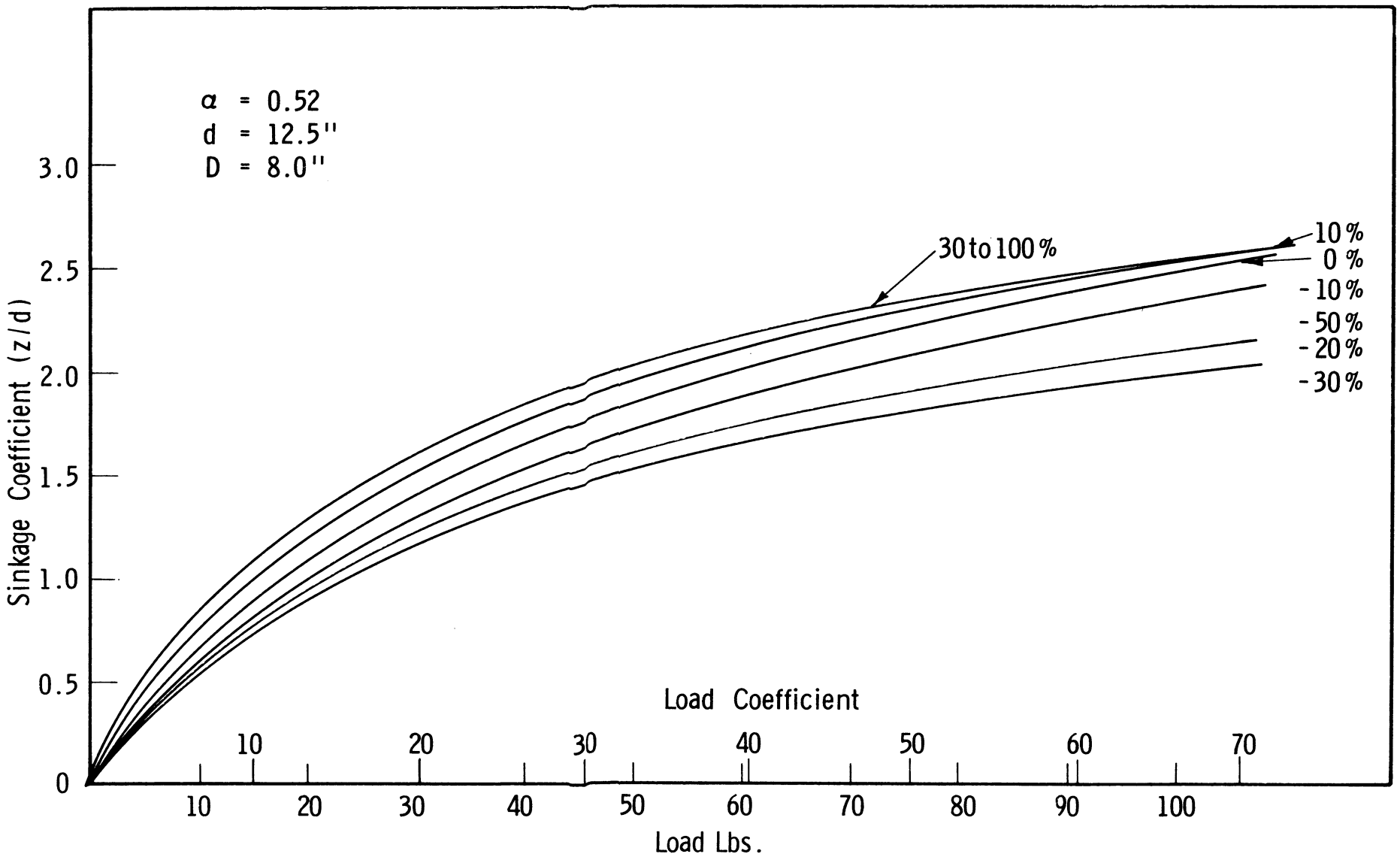

Fig. 14. Sinkage-load curves for d = 12.5 in., α = 0.52, D = 8.0 in.

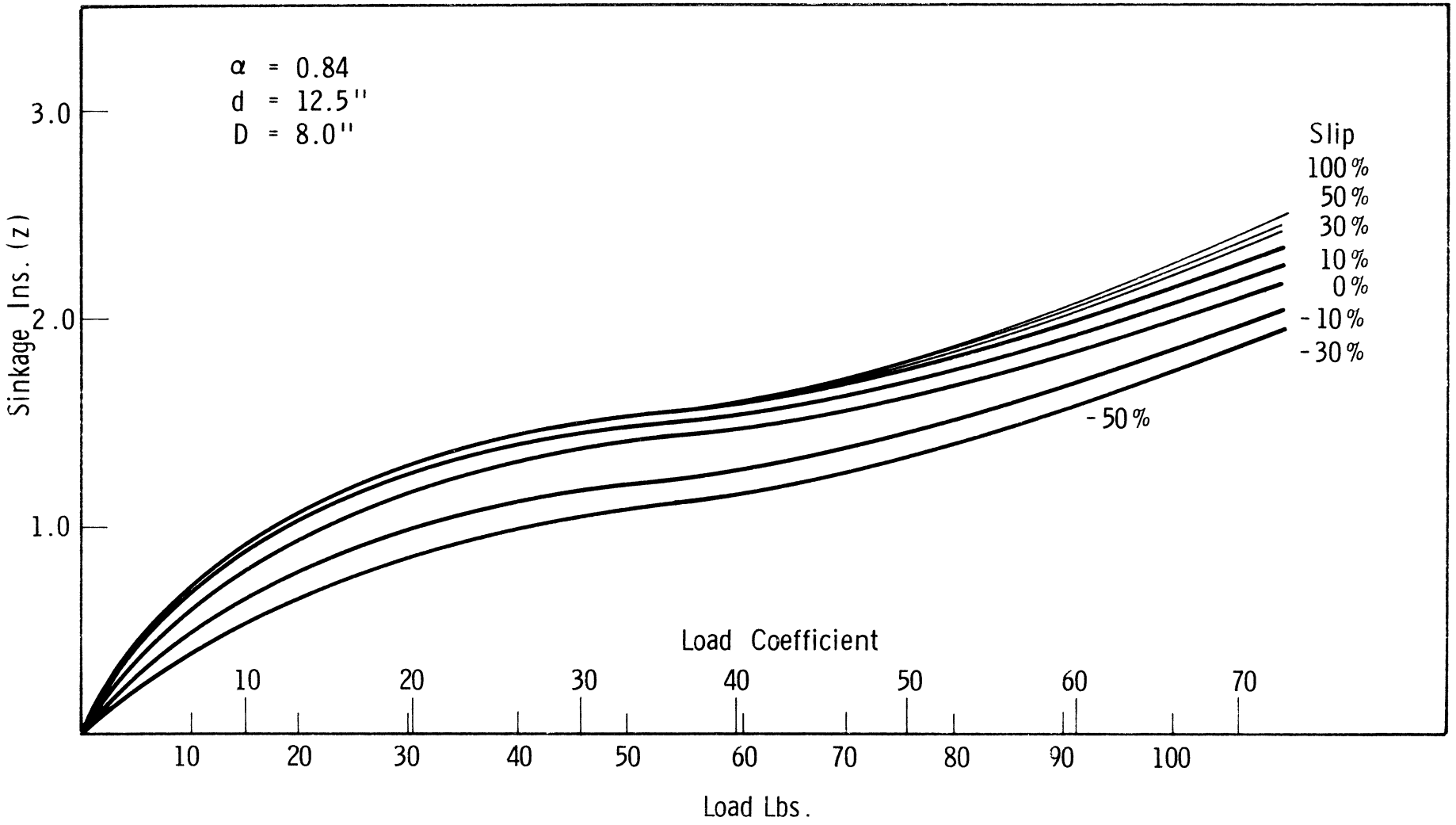

Fig. 15. Sinkage-load curves for d = 12.5 in., α = 0.84, D = 8.0 in.

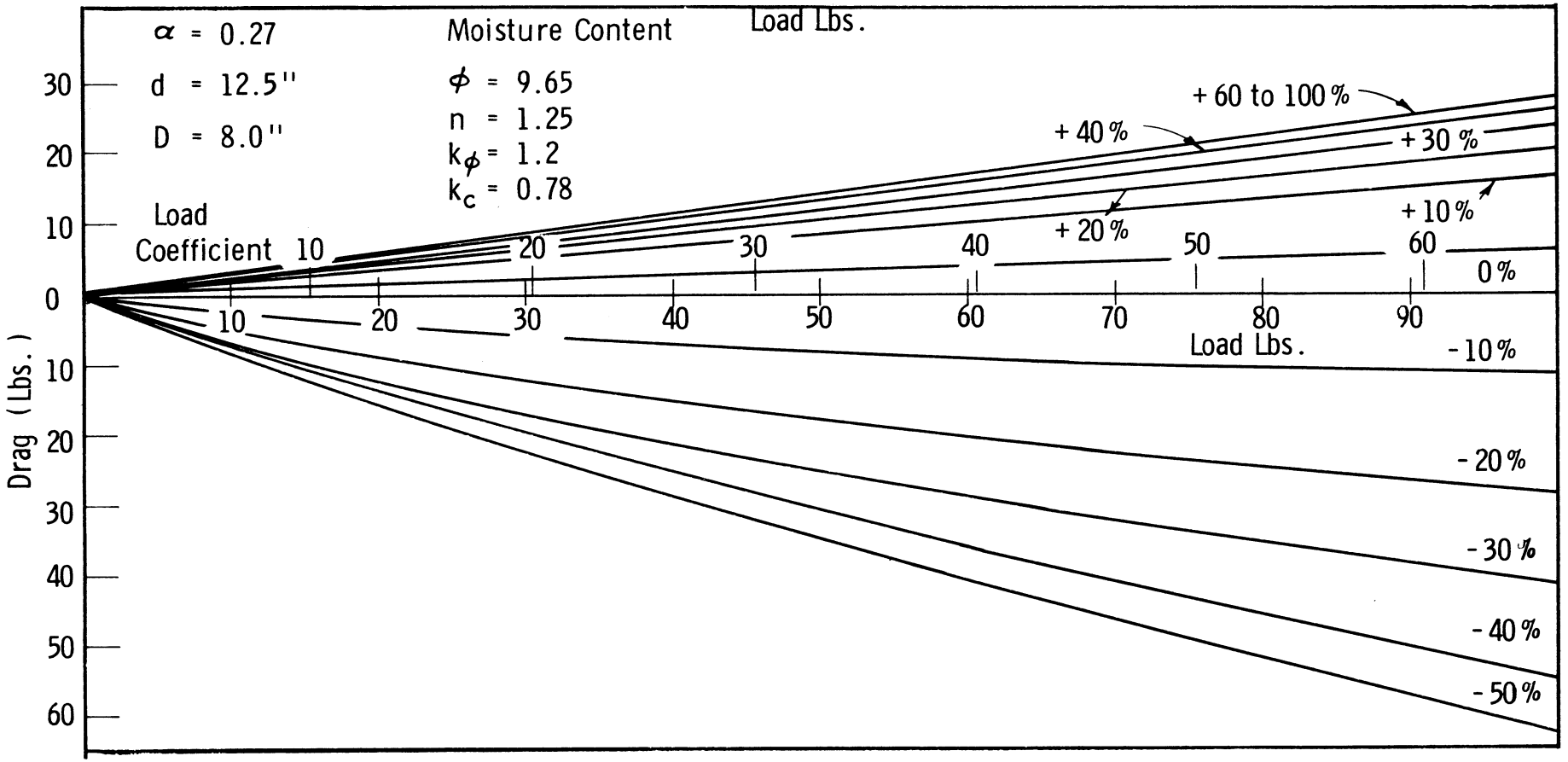

Fig. 16. Drag-load curves for d = 12.5 in., α = 0.27, D = 8.0 in.

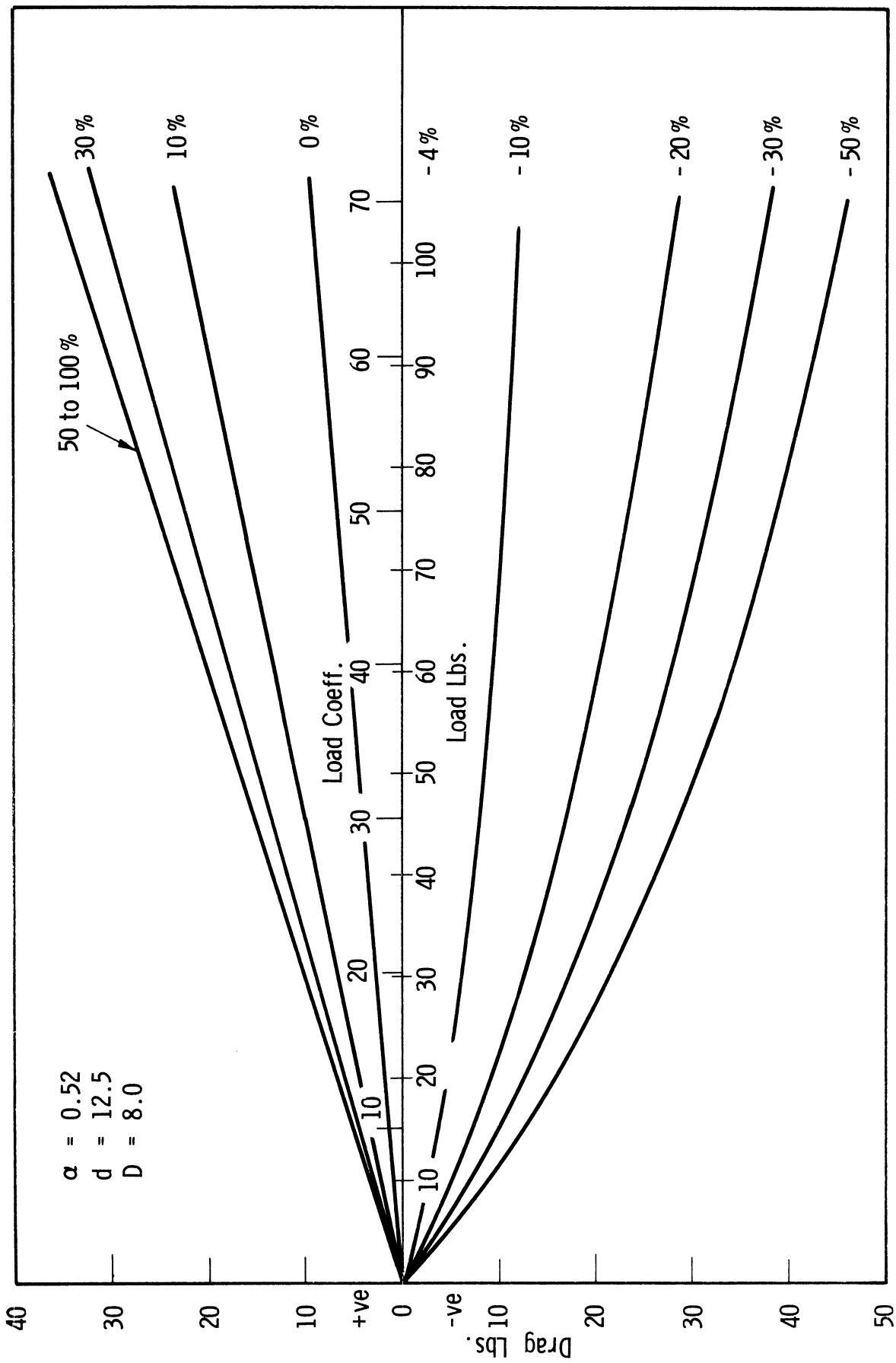

Fig. 17. Drag-load curves for d = 12.5 in., α = 0.52, D = 8.0 in.

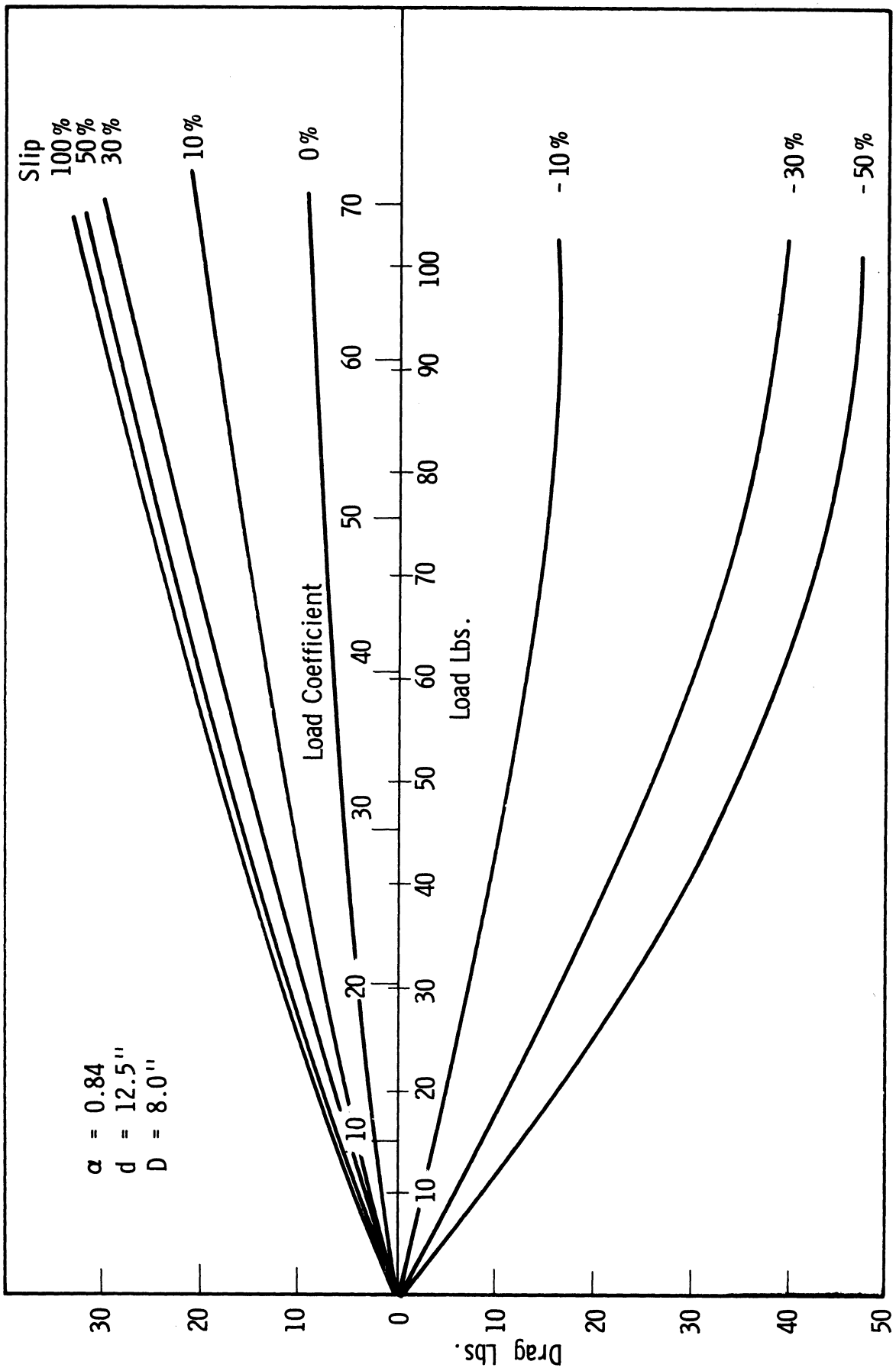

Fig. 18. Drag-load curves for d = 12.5 in., α = 0.84, D = 8.0 in.

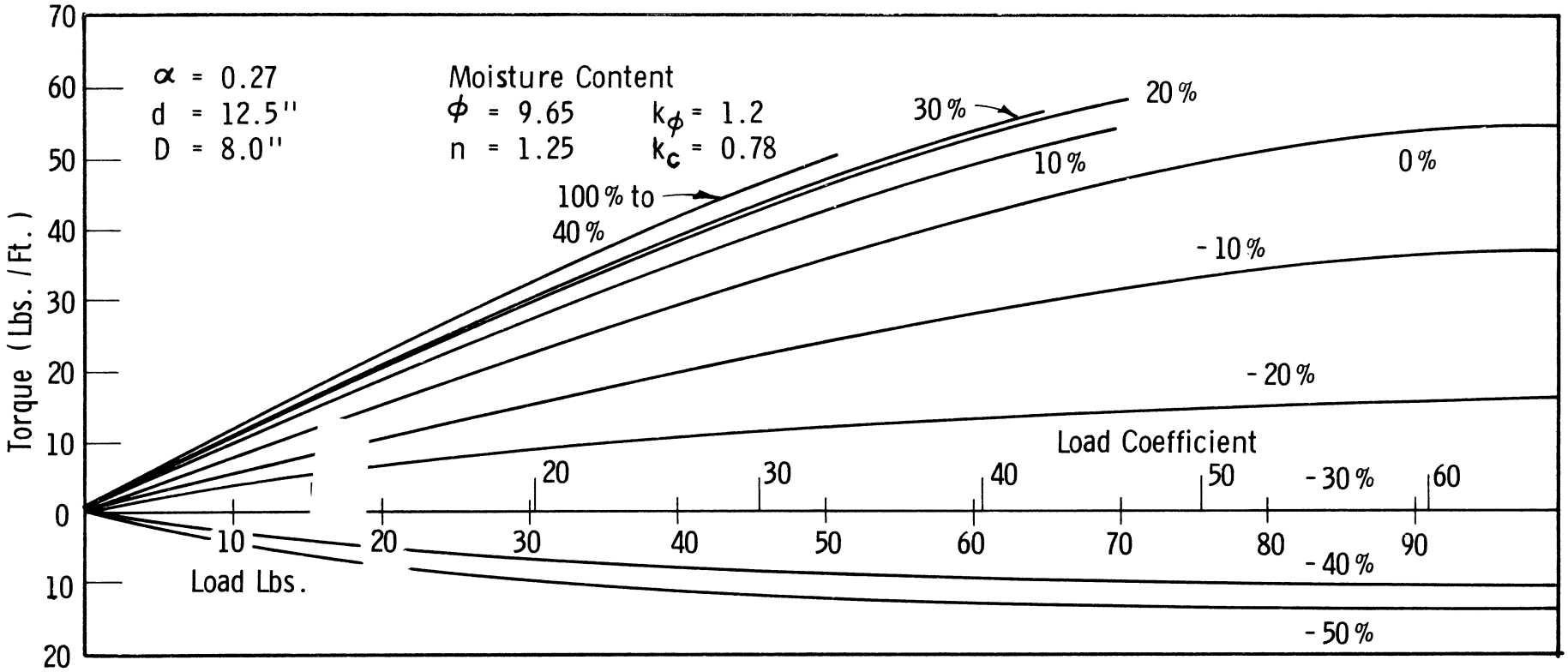

Fig. 19. Torque-load curves for d = 12.5 in., α = 0.27, D = 8.0 in.

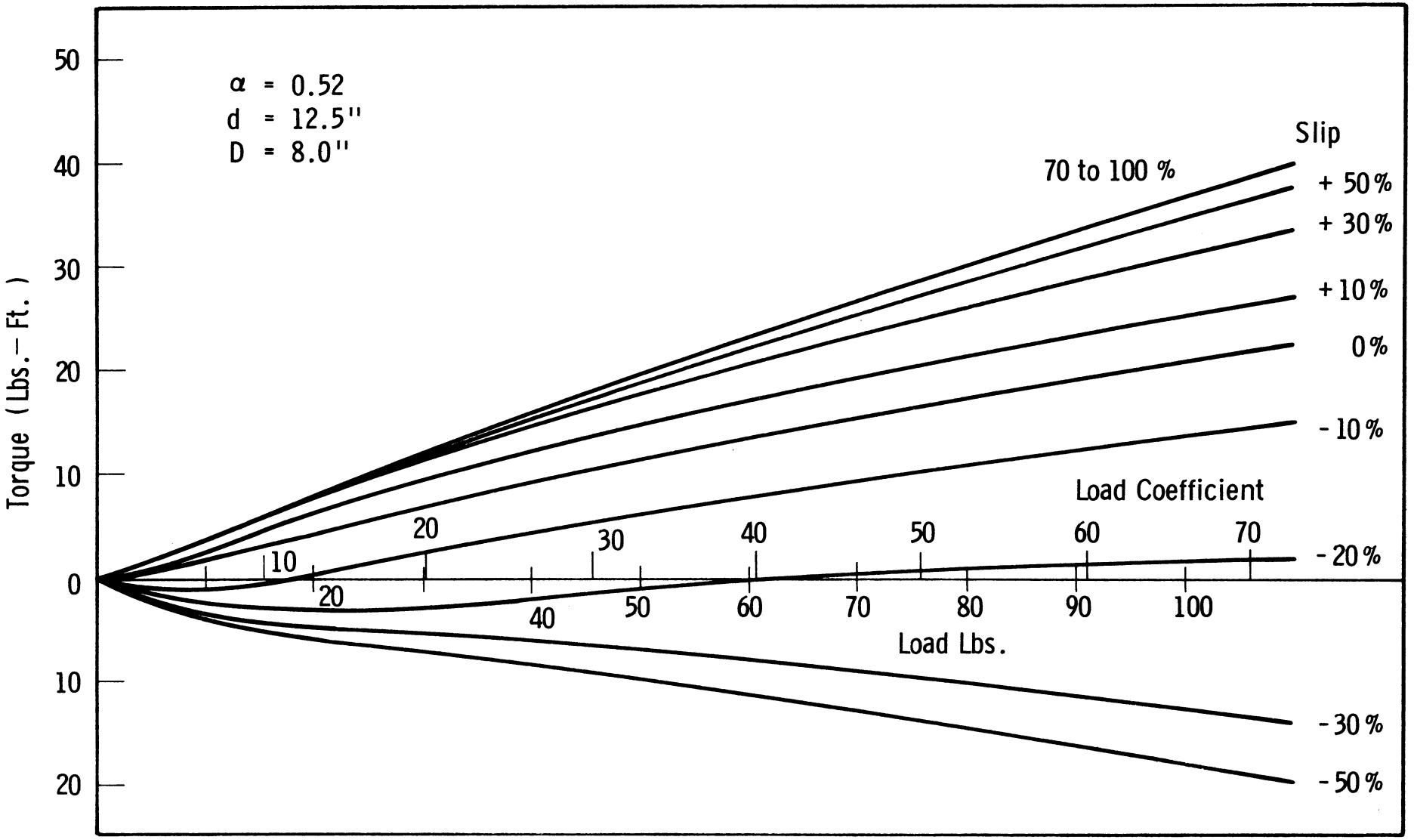

Fig. 20. Torque-load curves for d = 12.5 in., α = 0.52, D = 8.0 in.

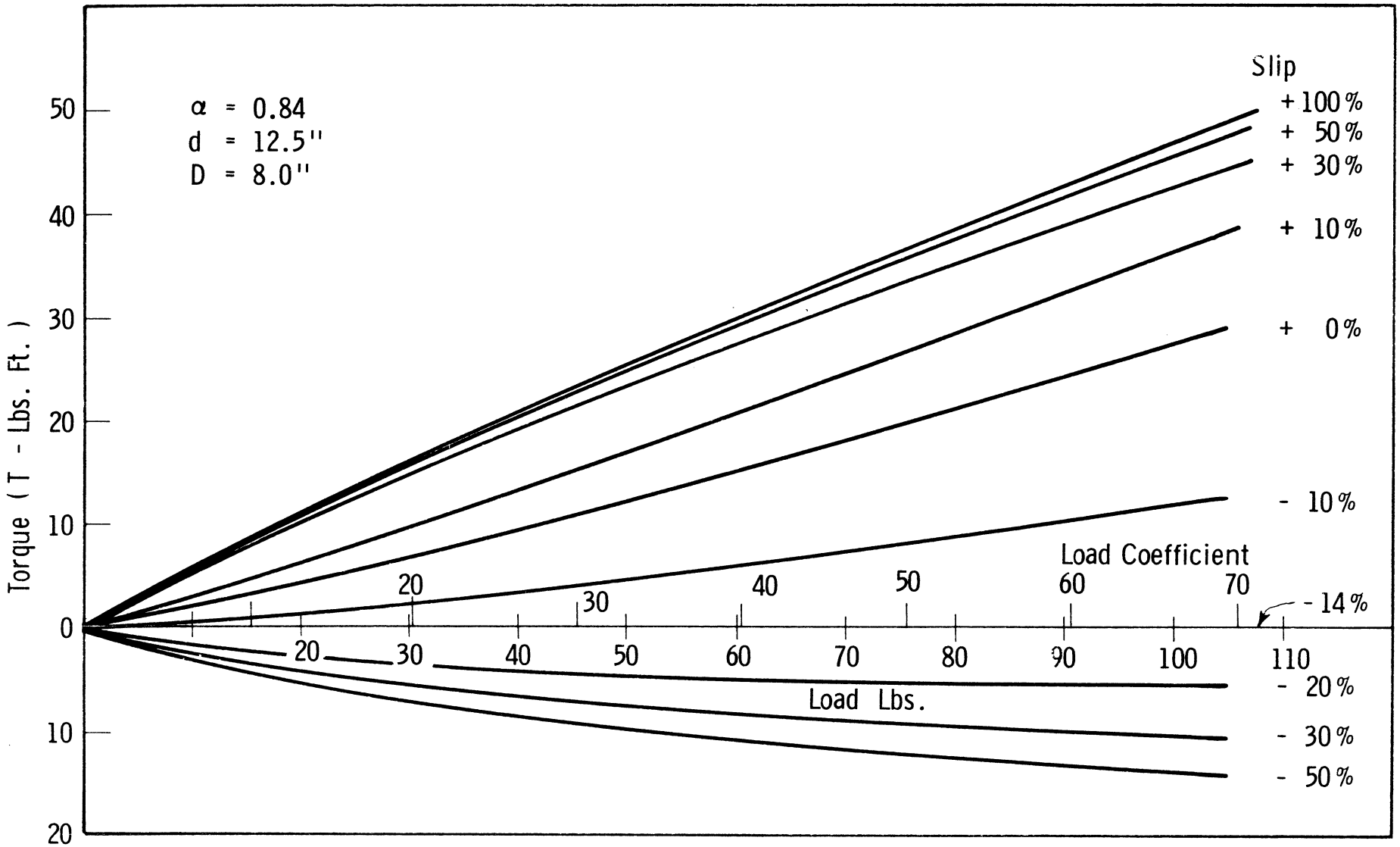

Fig. 21. Torque-load curves for d = 12.5 in., α = 0.84, D = 8.0 in.

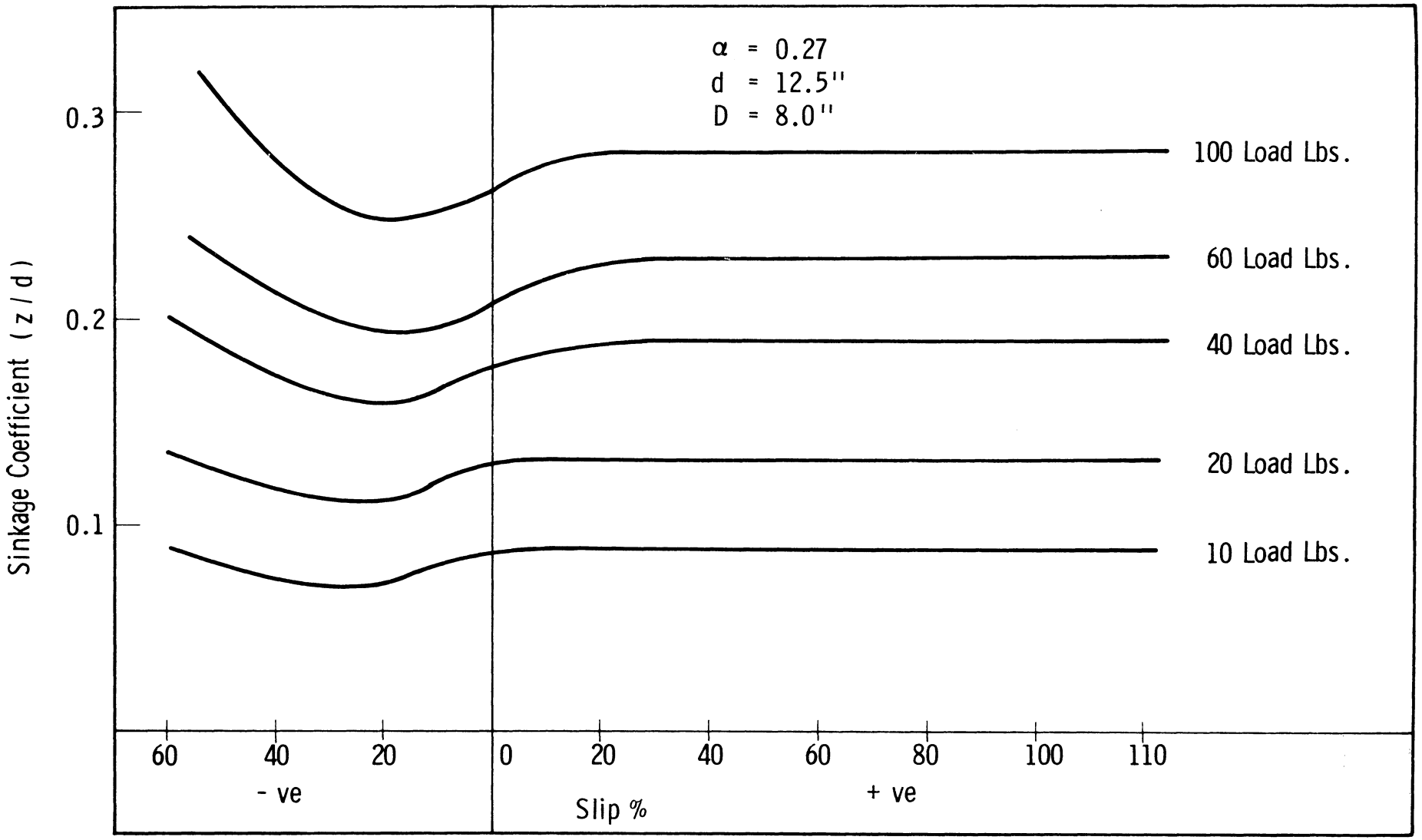

Fig. 22. Sinkage coefficient-slip curves for d = 12.5 in., α = 0.27, D = 8.0 in.

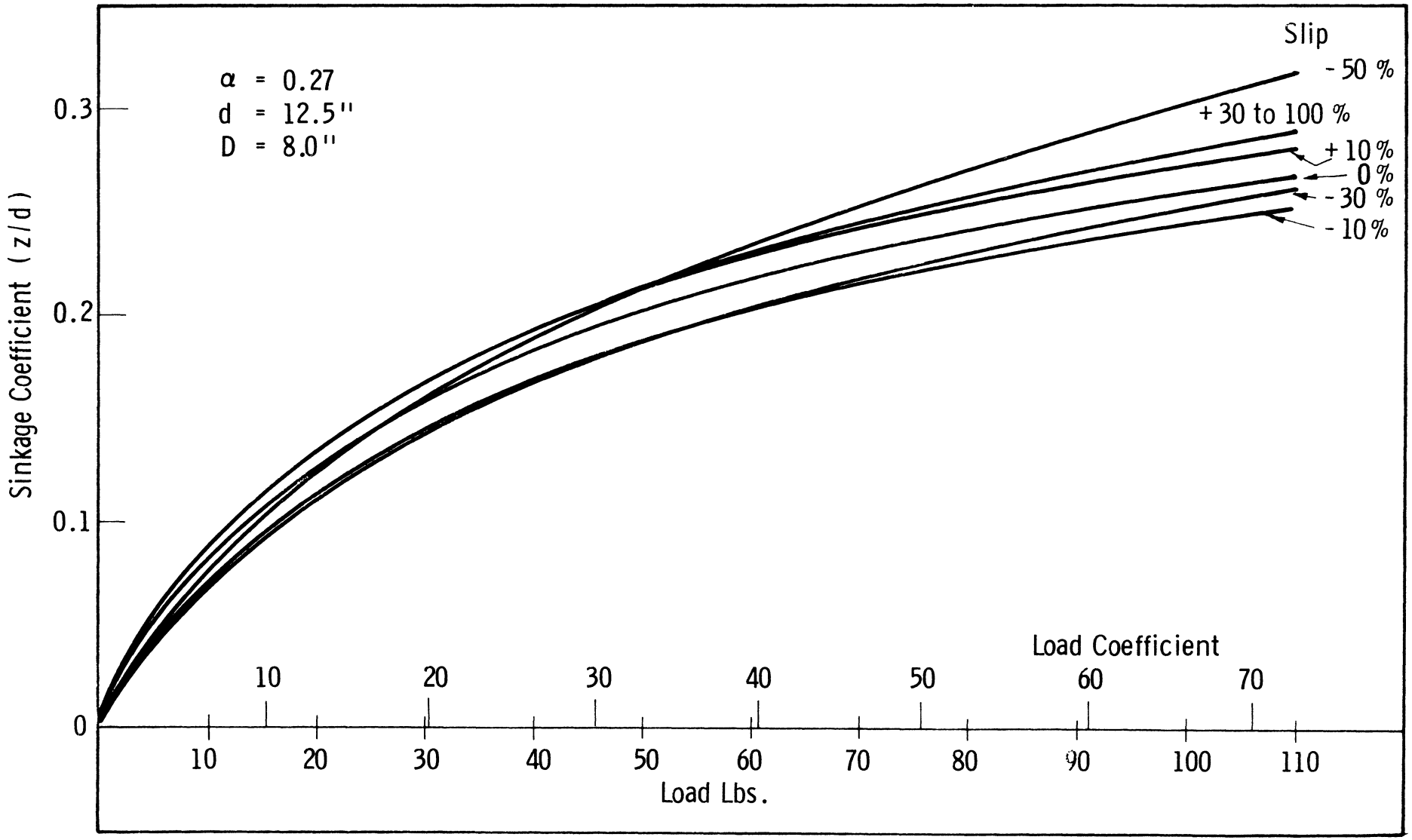

Fig. 23. Sinkage coefficient-load curves for d = 12.5 in., α = 0.27, D = 8.0 in.

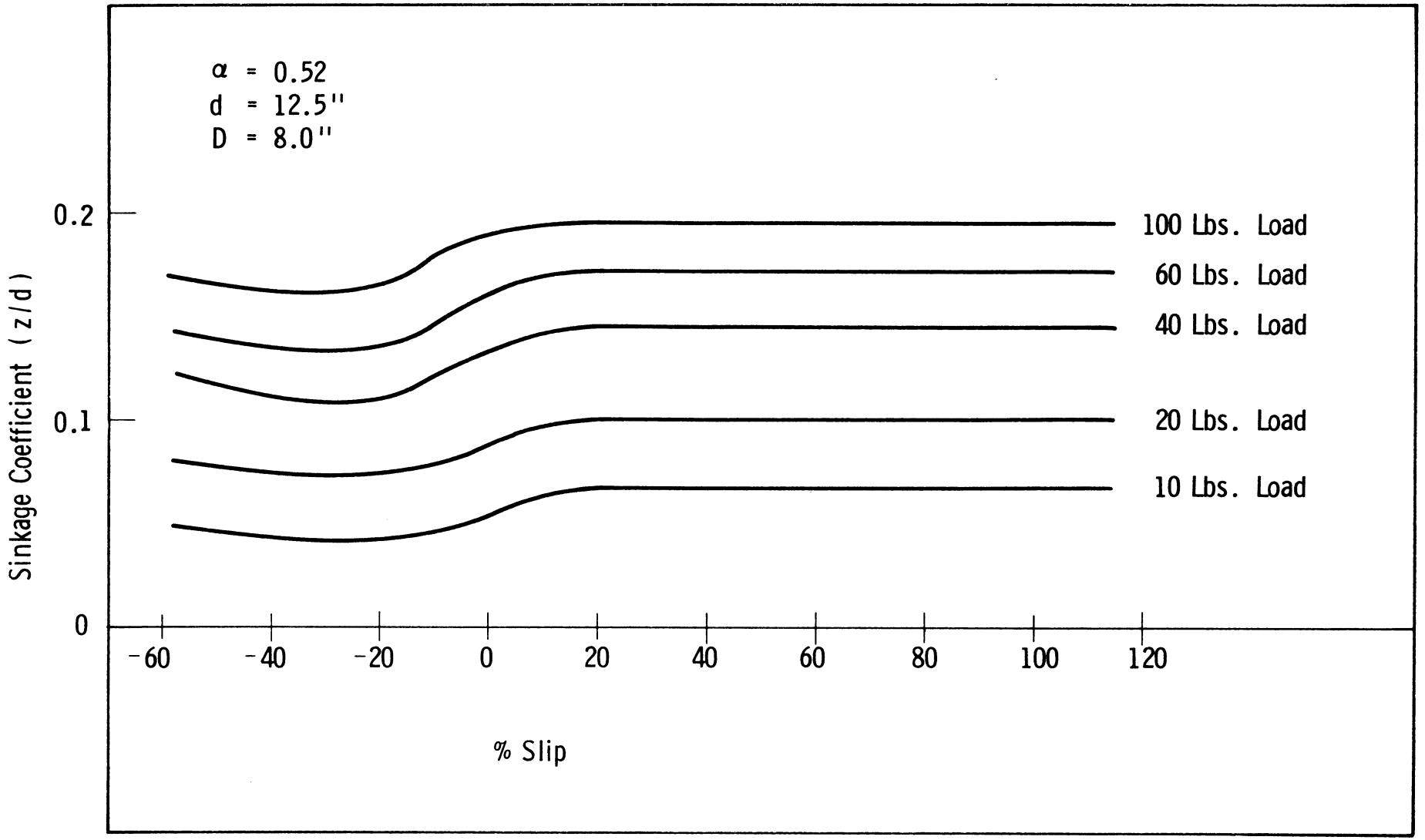

Fig. 24. Sinkage coefficient-slip curves for d = 12.5 in., α = 0.52, D = 8.0 in.

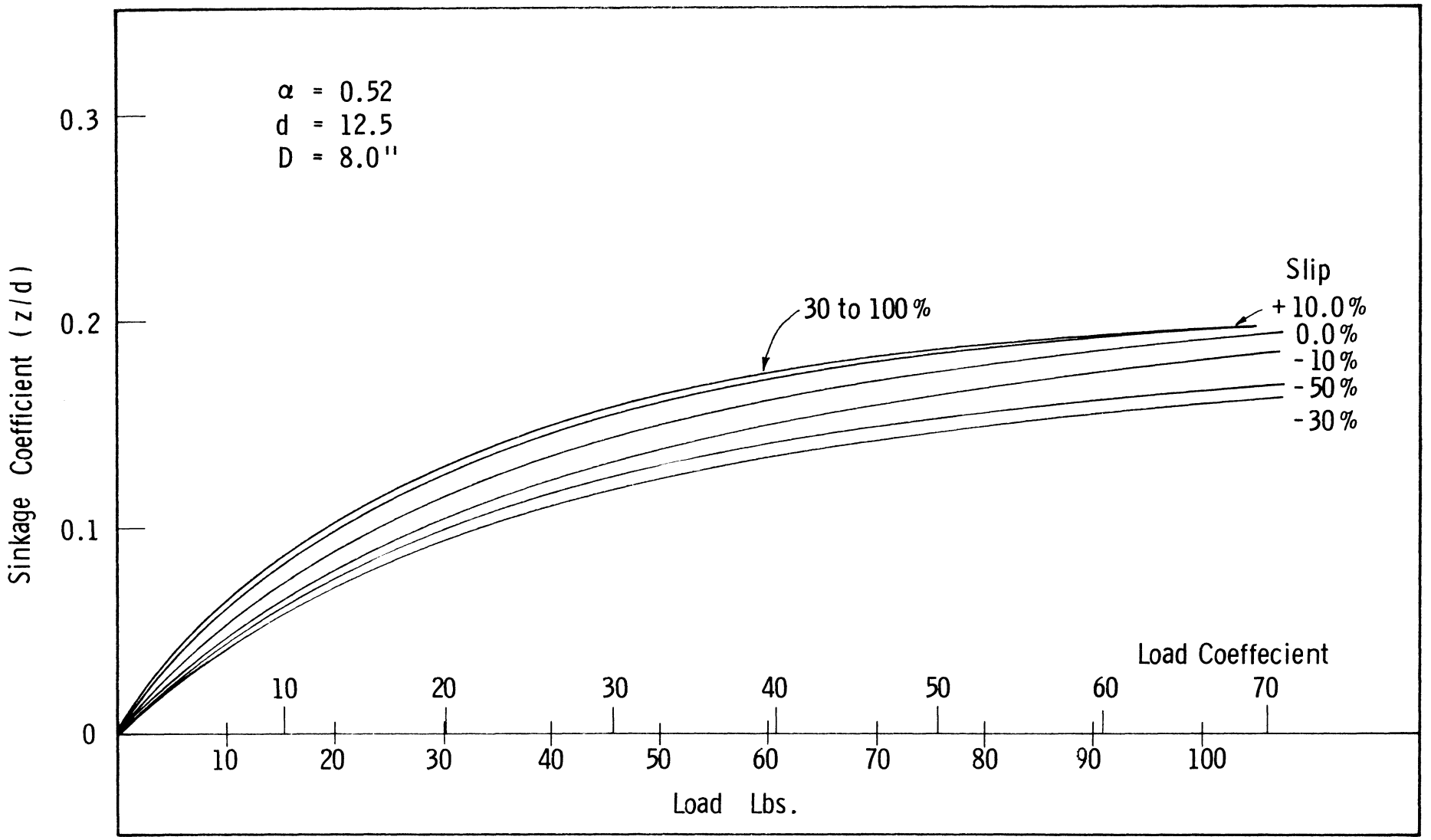

Fig. 25. Sinkage coefficient-load curves for d = 12.5 in., α = 0.52, D = 8.0 in.

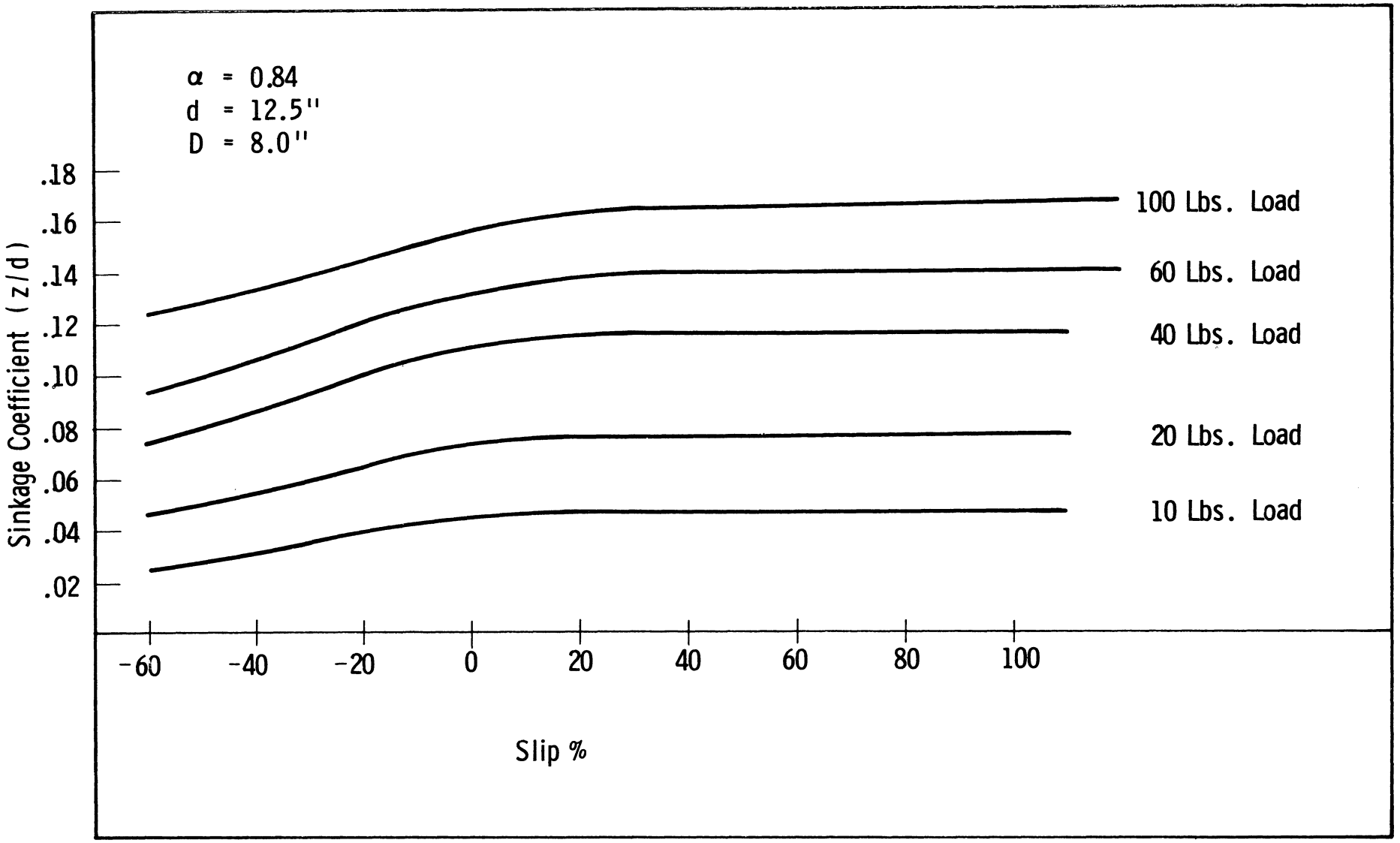

Fig. 26. Sinkage coefficient-slip curves for d = 12.5 in., α = 0.84, D = 8.0 in.

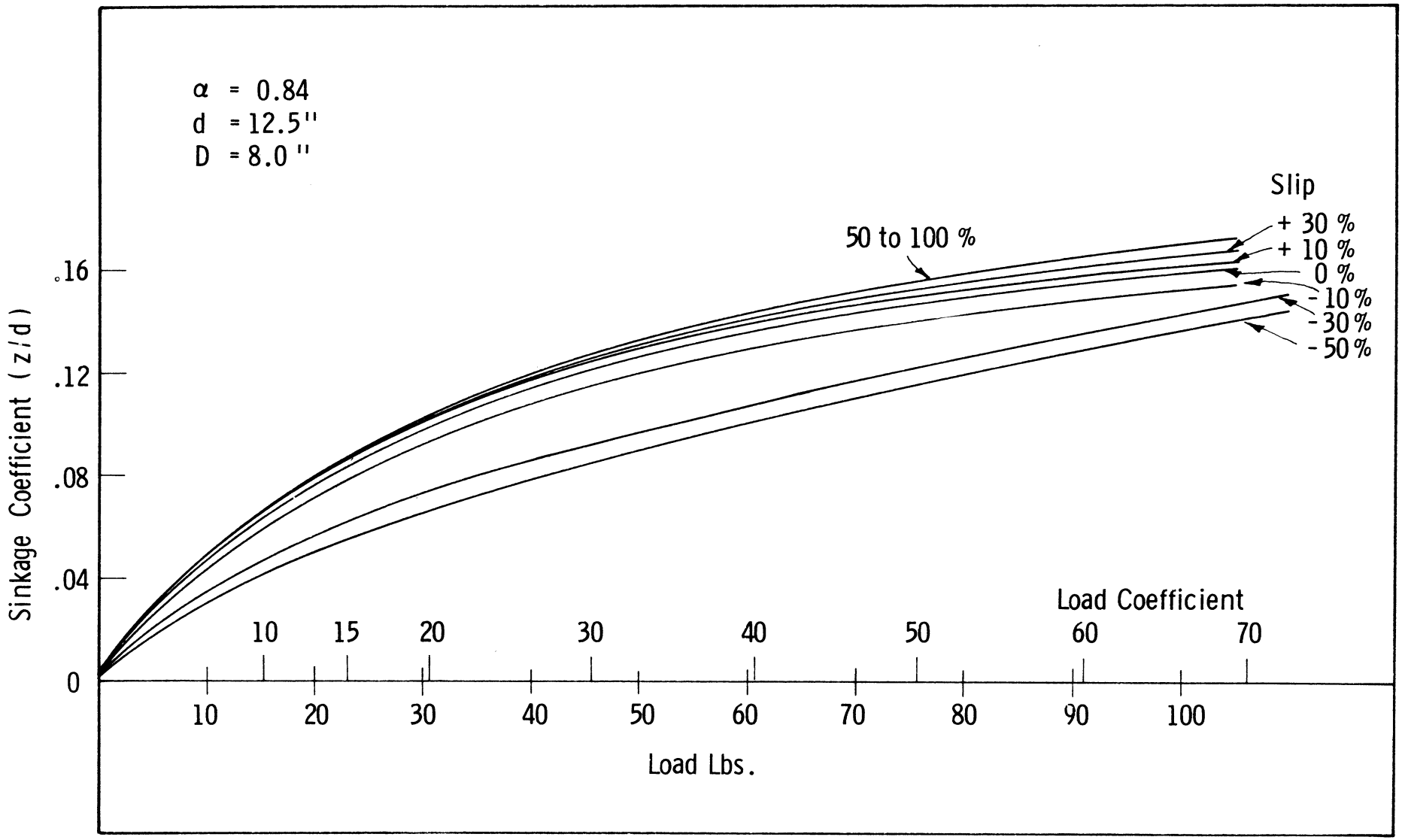

Fig. 27. Sinkage coefficient-load curves for d = 12.5 in., α = 0.84, D = 8.0 in.

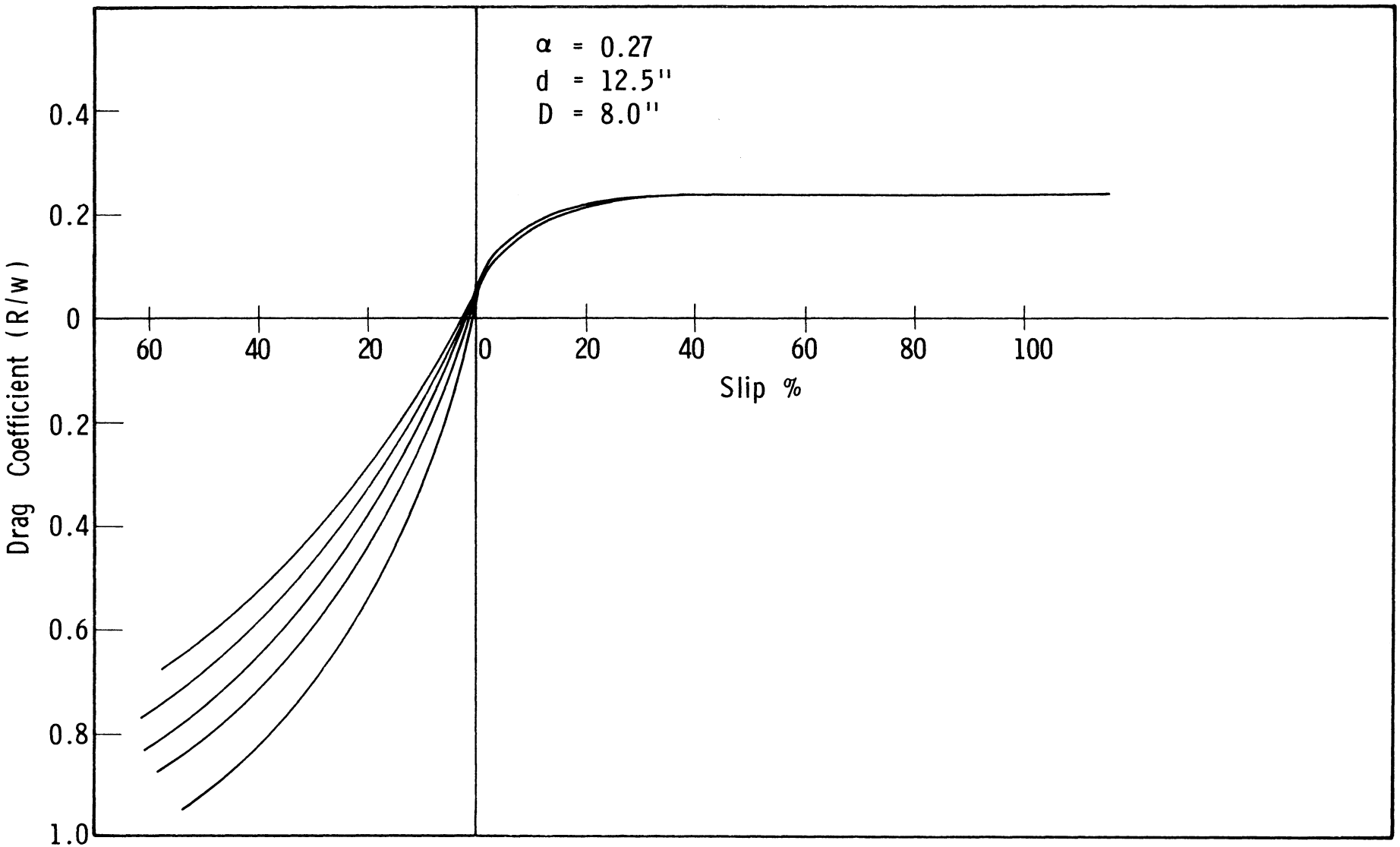

Fig. 28. Drag coefficient-slip curves for d = 12.5 in., α = 0.27, D = 8.0 in.

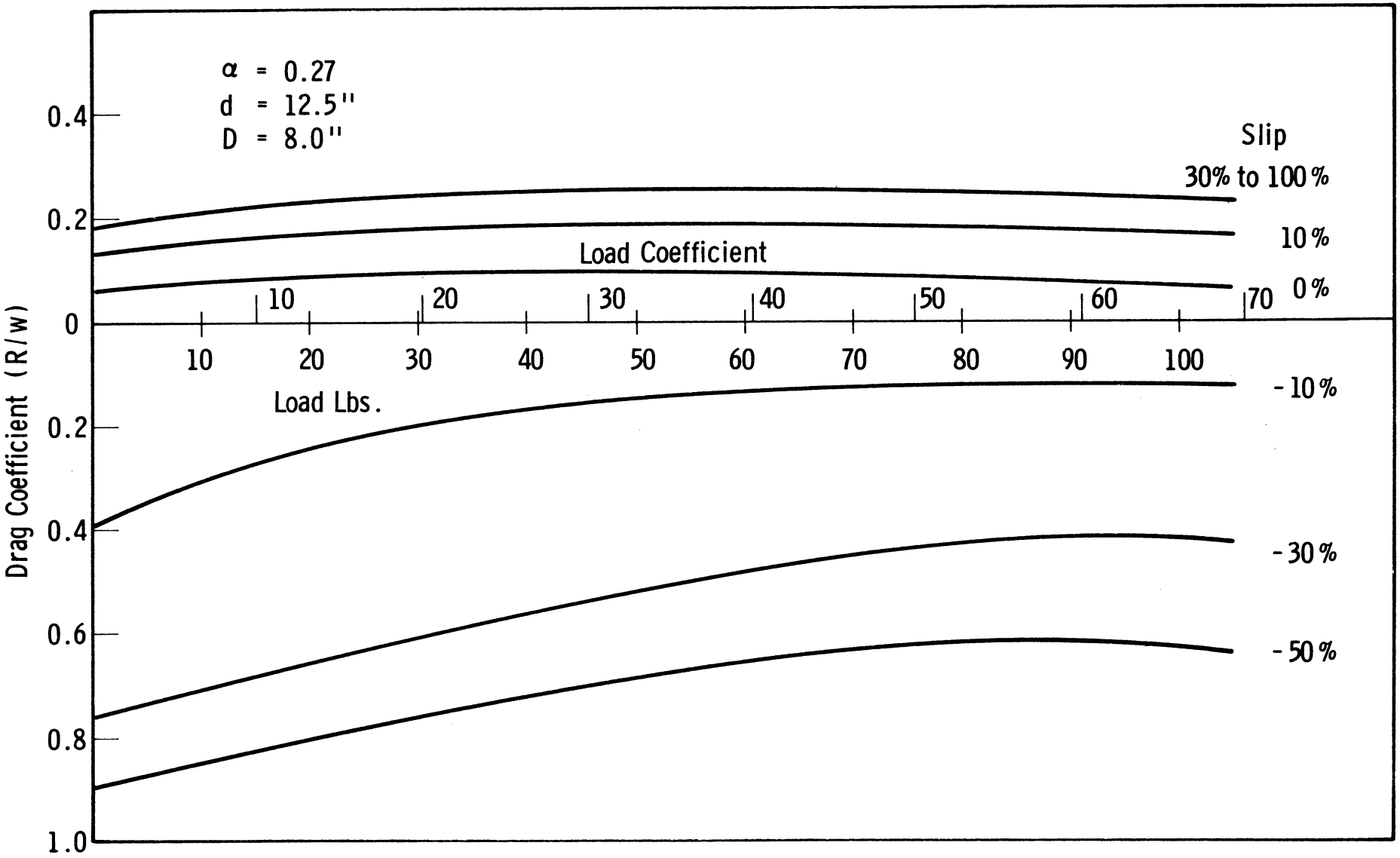

Fig. 29. Drag coefficient-load curves for d = 12.5 in., α = 0.27, D = 8.0 in.

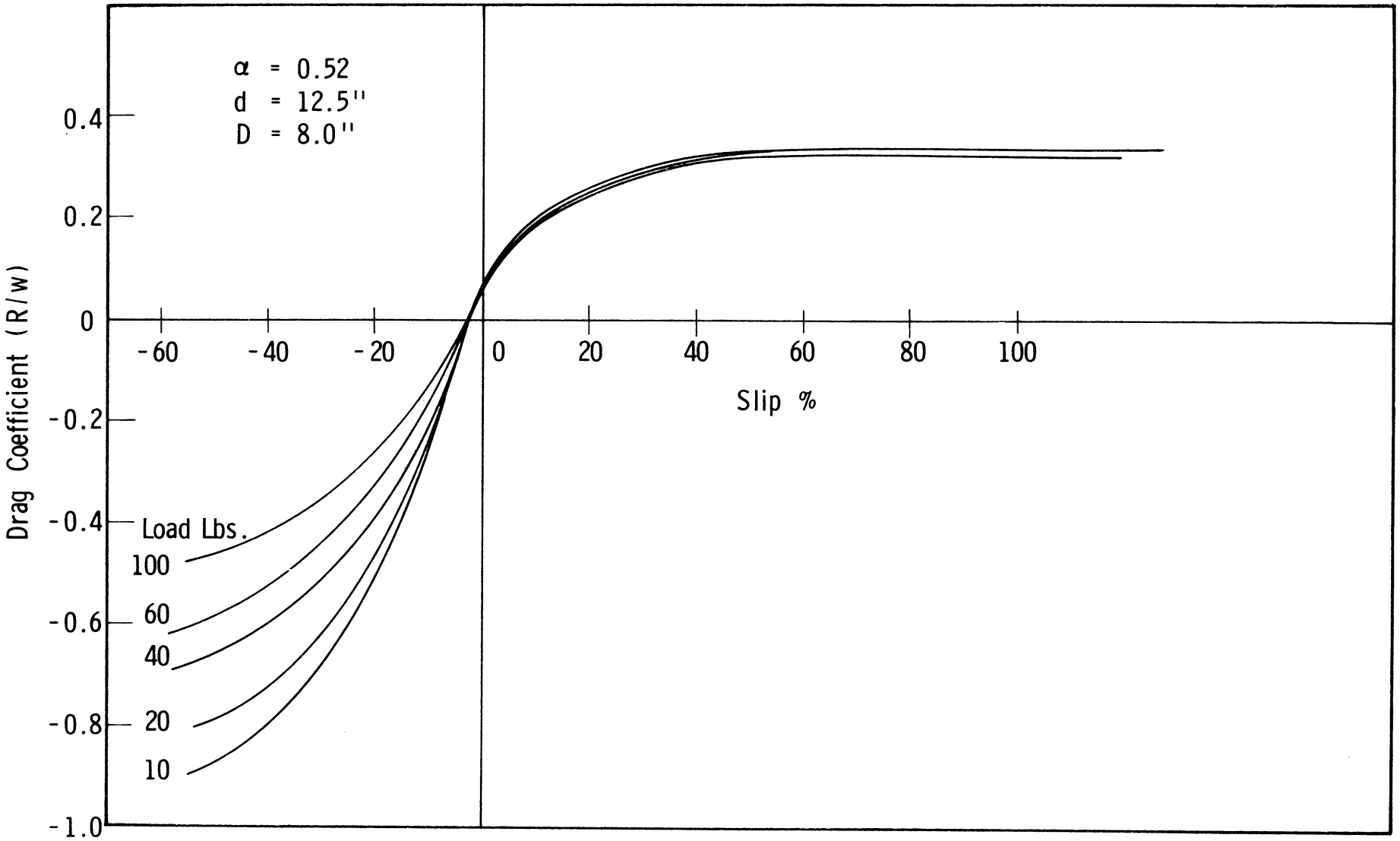

Fig. 30. Drag coefficient-slip curves for d = 12.5 in., α = 0.52, D = 8.0 in.

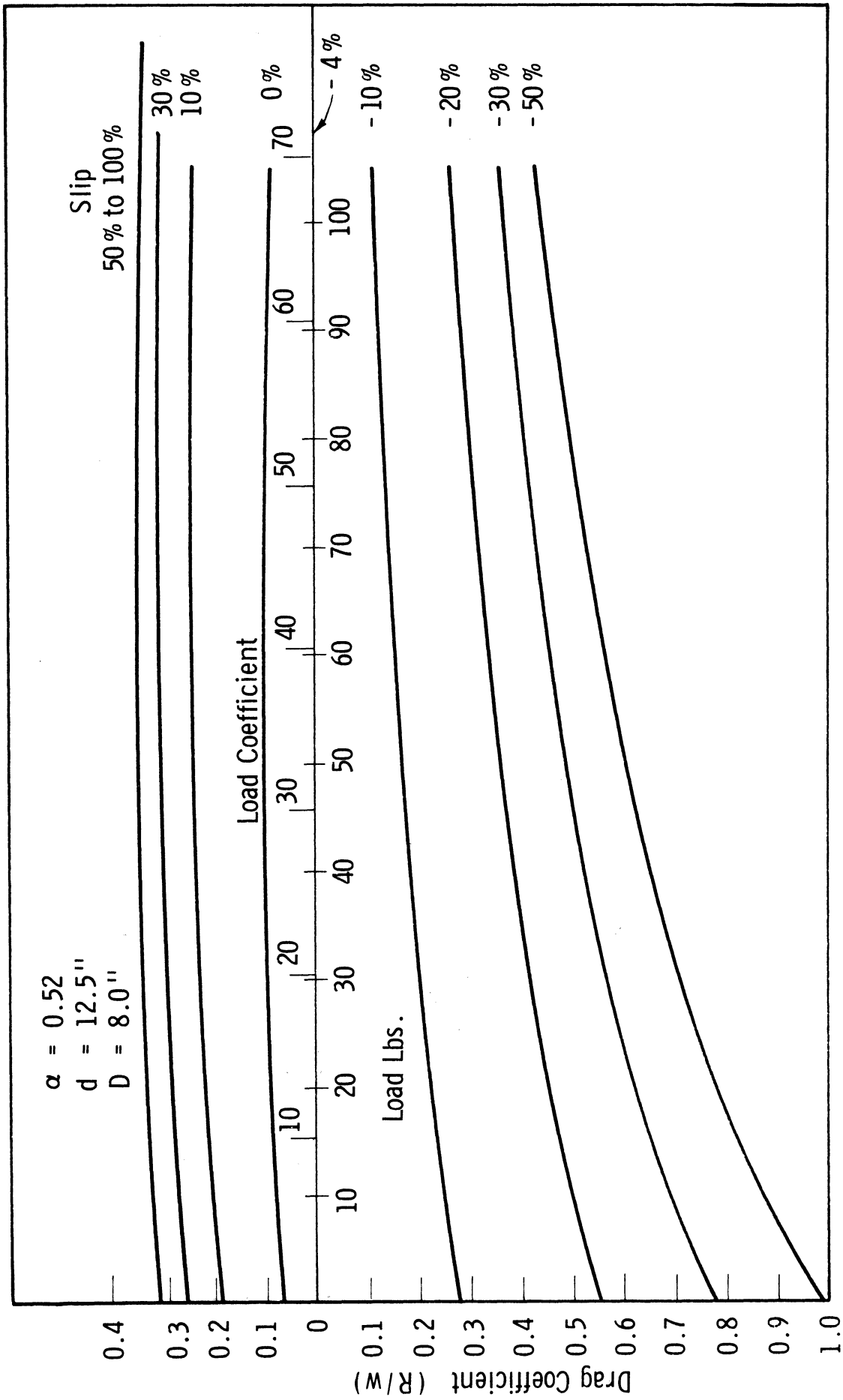

Fig. 31. Drag coefficient-load curves for d = 12.5 in., α = 0.52, D = 8.0 in.

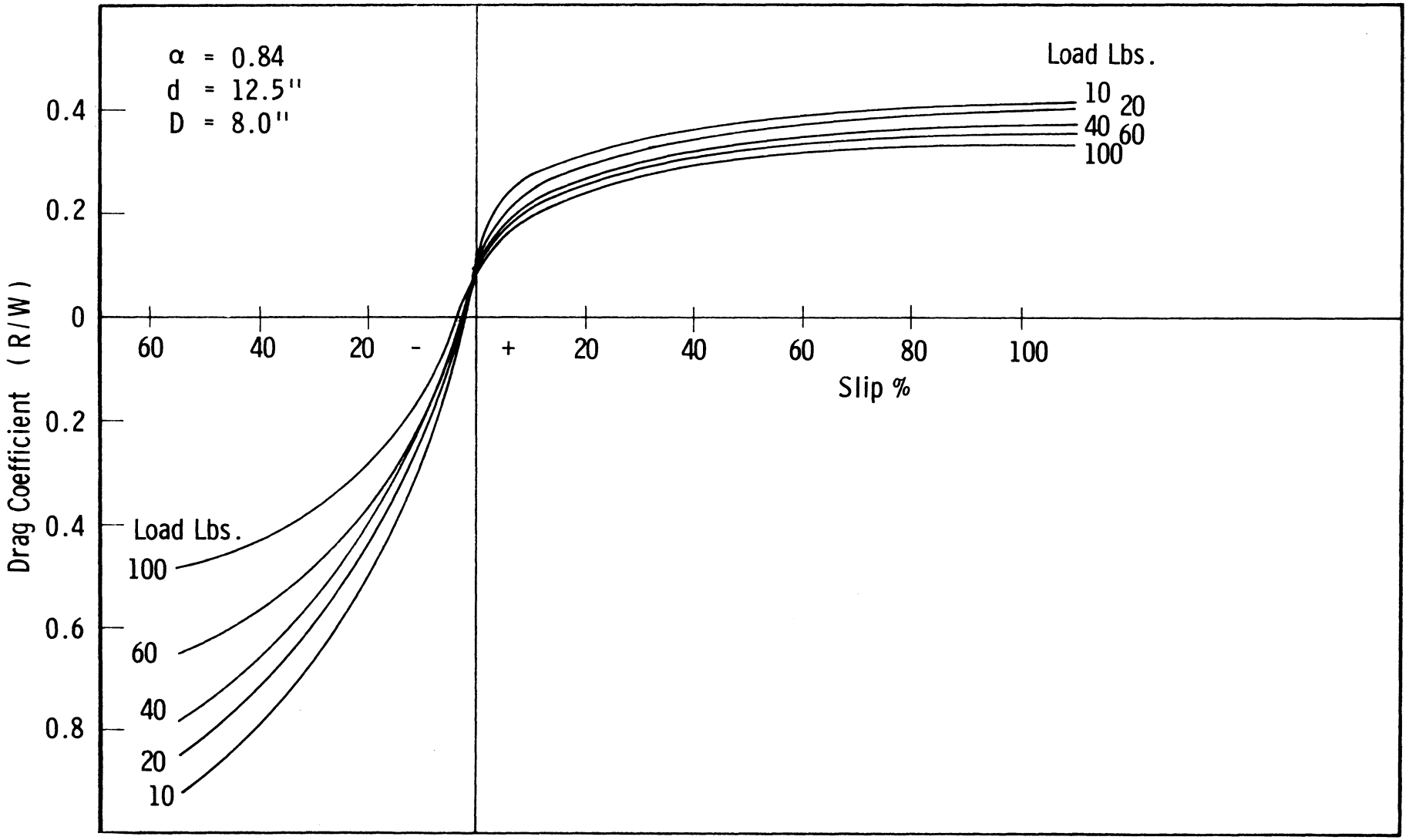

Fig. 32. Drag coefficient-slip curves for d = 12.5 in., α = 0.84, D = 8.0 in.

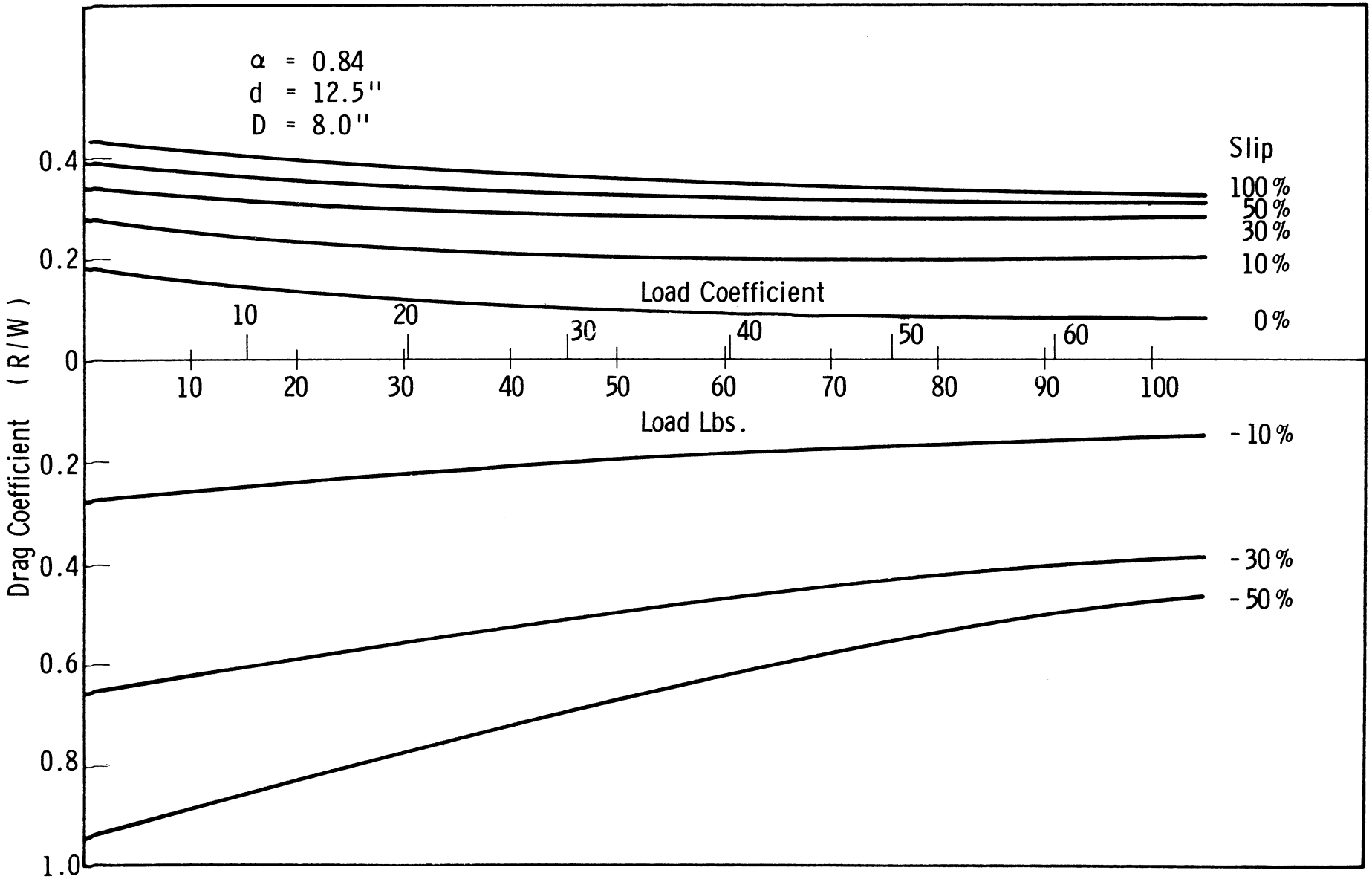

Fig. 33. Drag coefficient-load curves for d = 12.5 in., α = 0.84, D = 8.0 in.

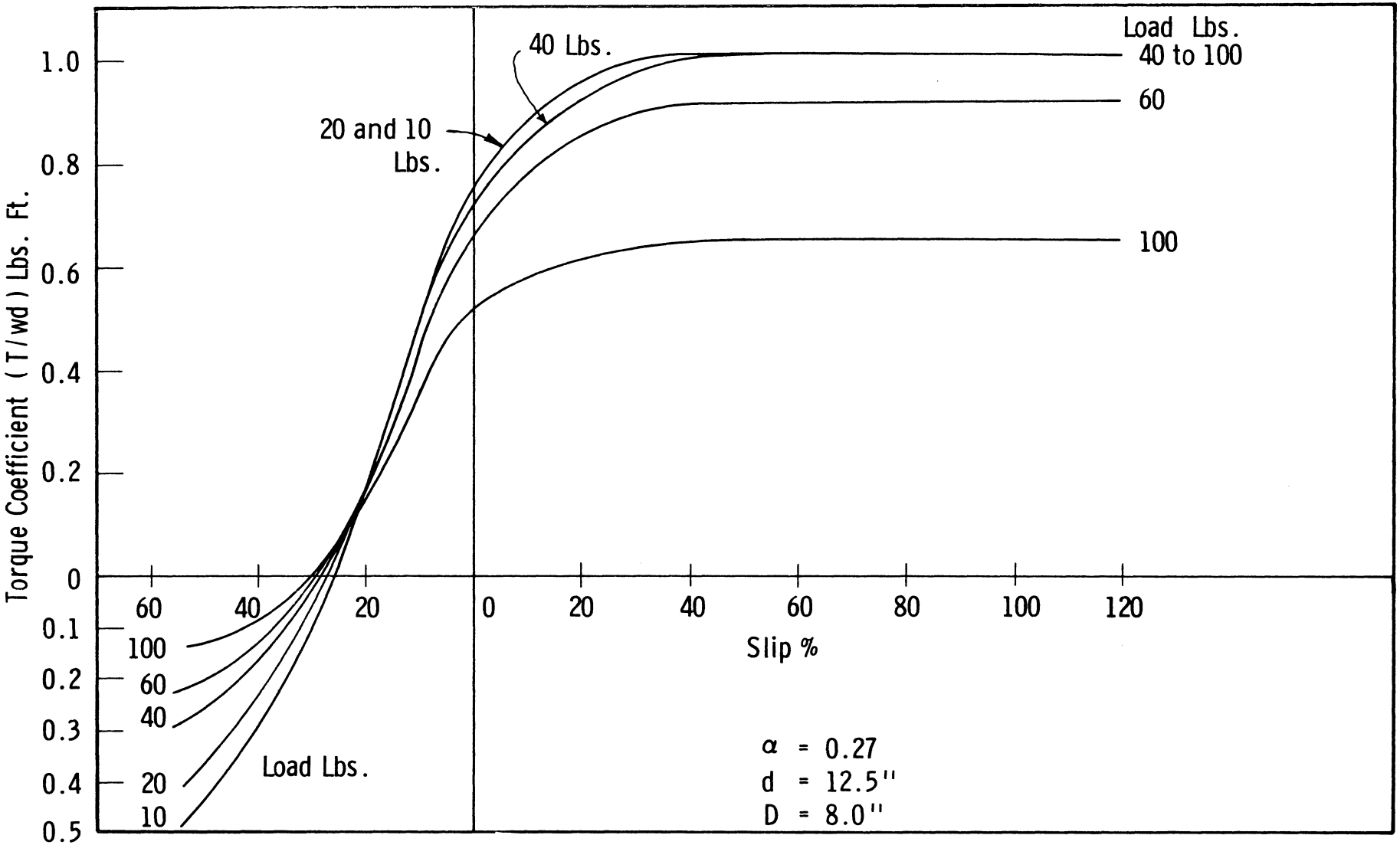

Fig. 34. Torque coefficient-slip curves for d = 12.5 in., α = 0.27, D = 8.0 in.

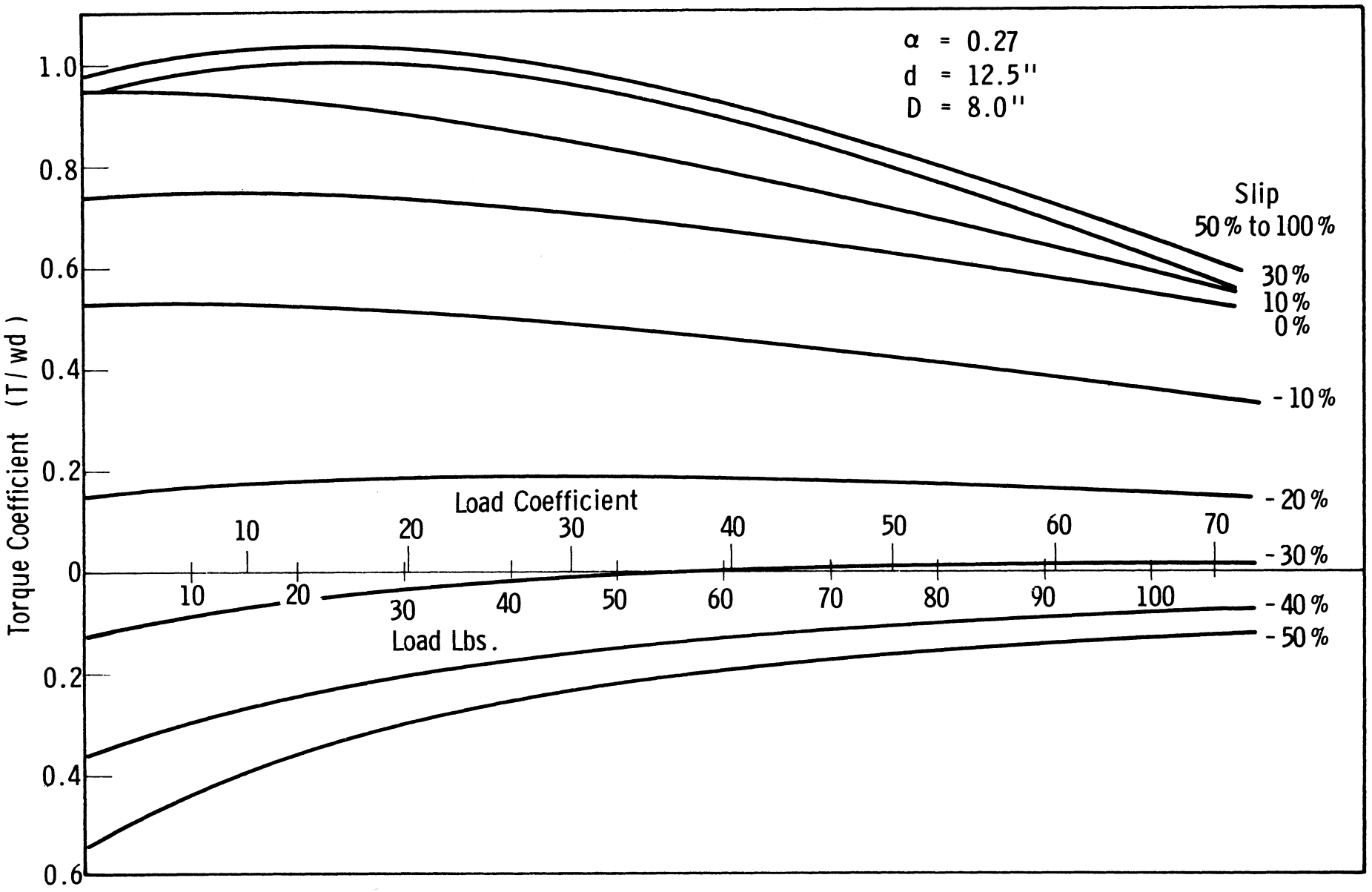

Fig. 35. Torque coefficient-load curves for d = 12.5 in., α = 0.27, D = 8.0 in.

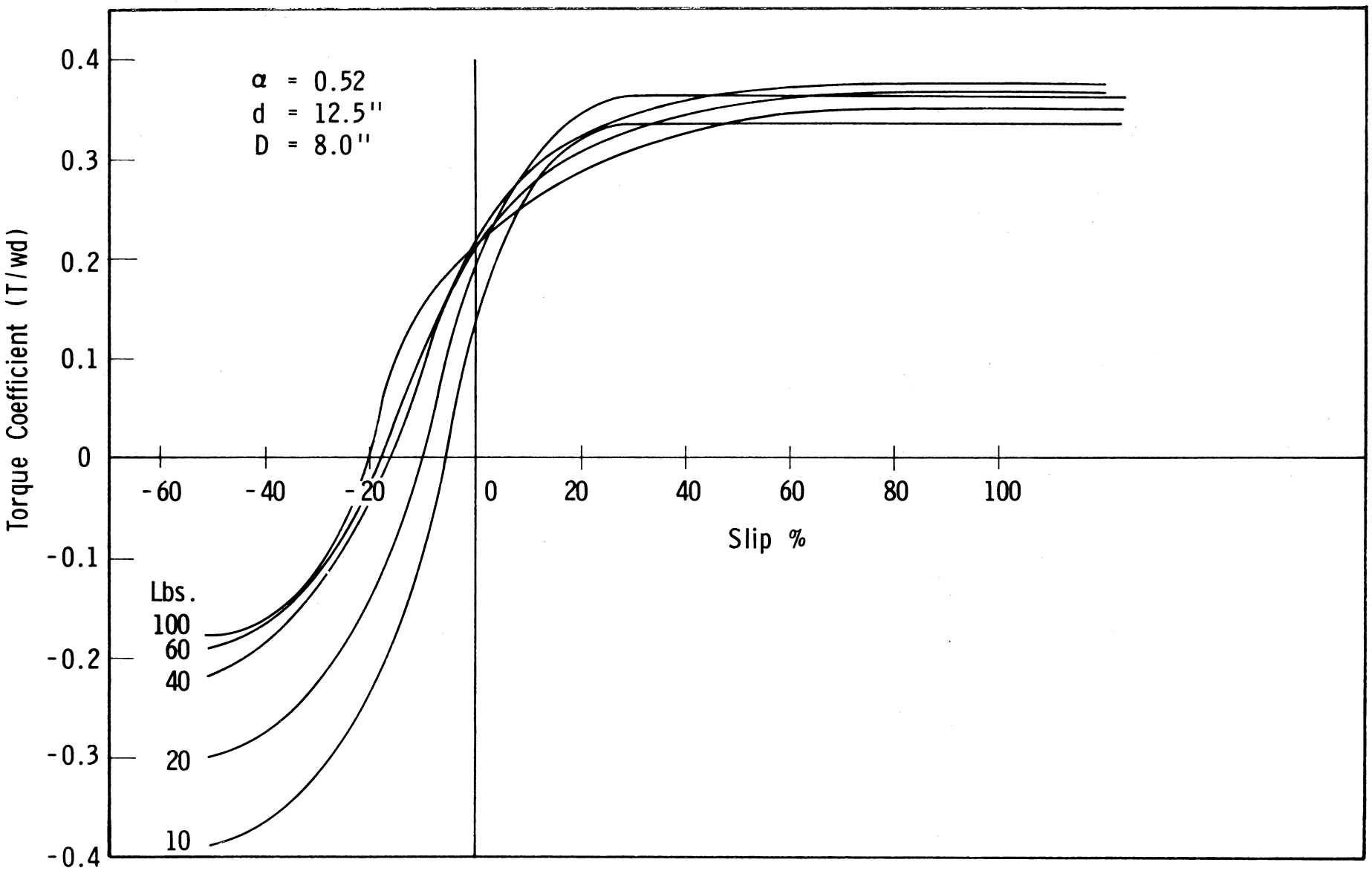

Fig. 36. Torque coefficient-slip curves for d = 12.5 in., α = 0.52, D = 8.0 in.

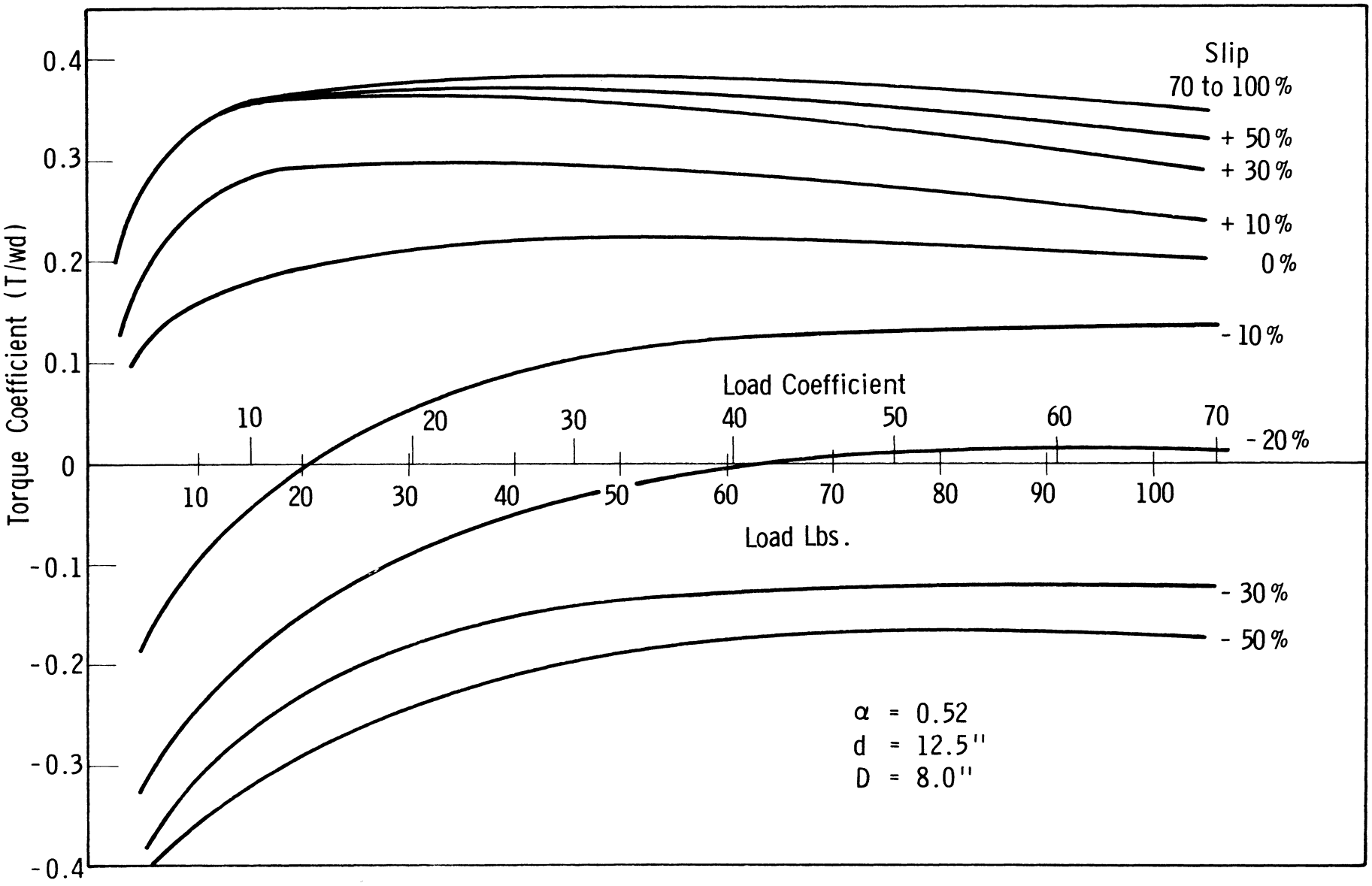

Fig. 37. Torque coefficient-load curves for d = 12.5 in., α = 0.52, D = 8.0 in.

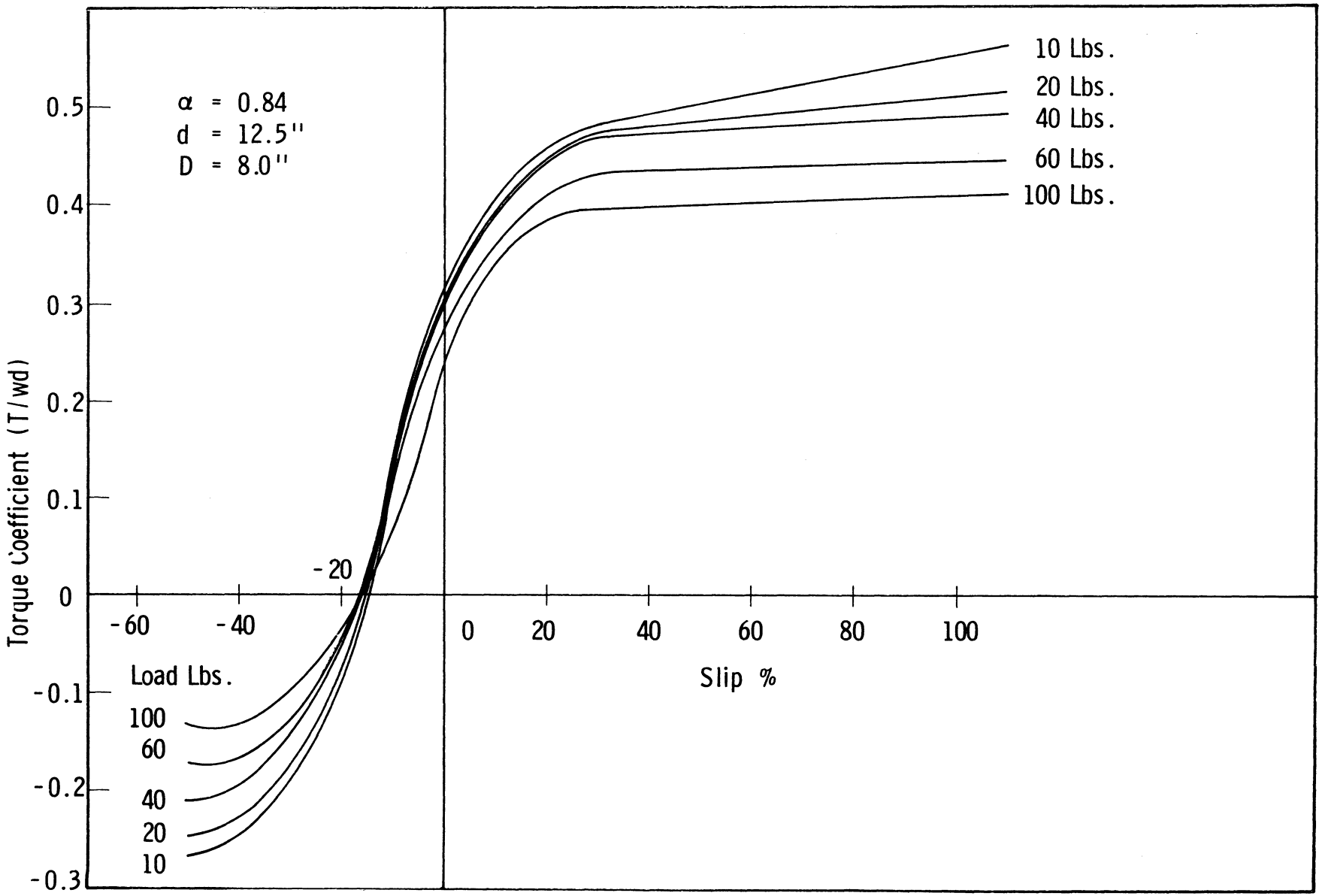

Fig. 38. Torque coefficient-slip curves for d = 12.5 in., α = 0.84, D = 8.0 in.

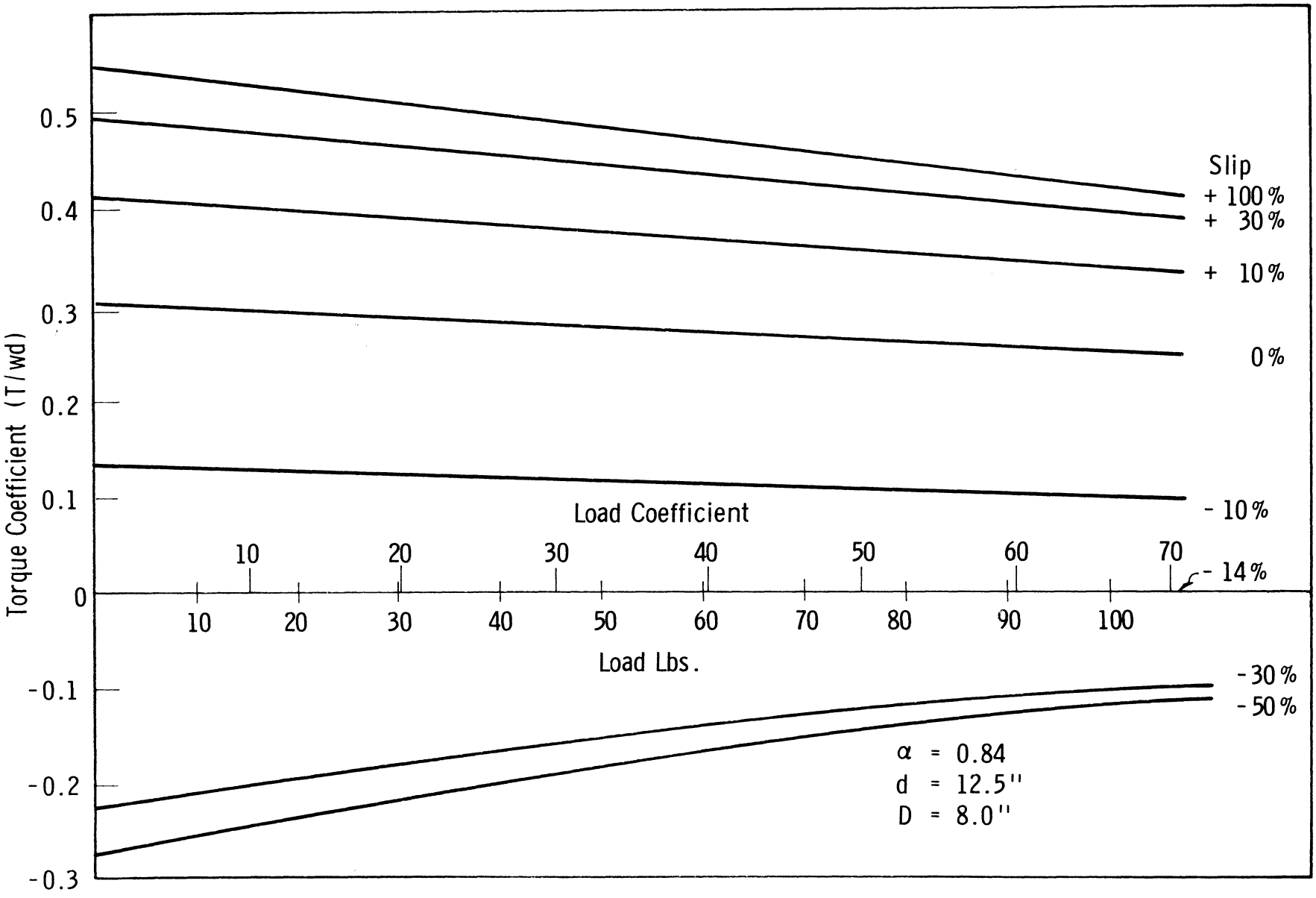

Fig. 39. Torque coefficient-load curves for d = 12.5 in., α = 0.84, D = 8.0 in.

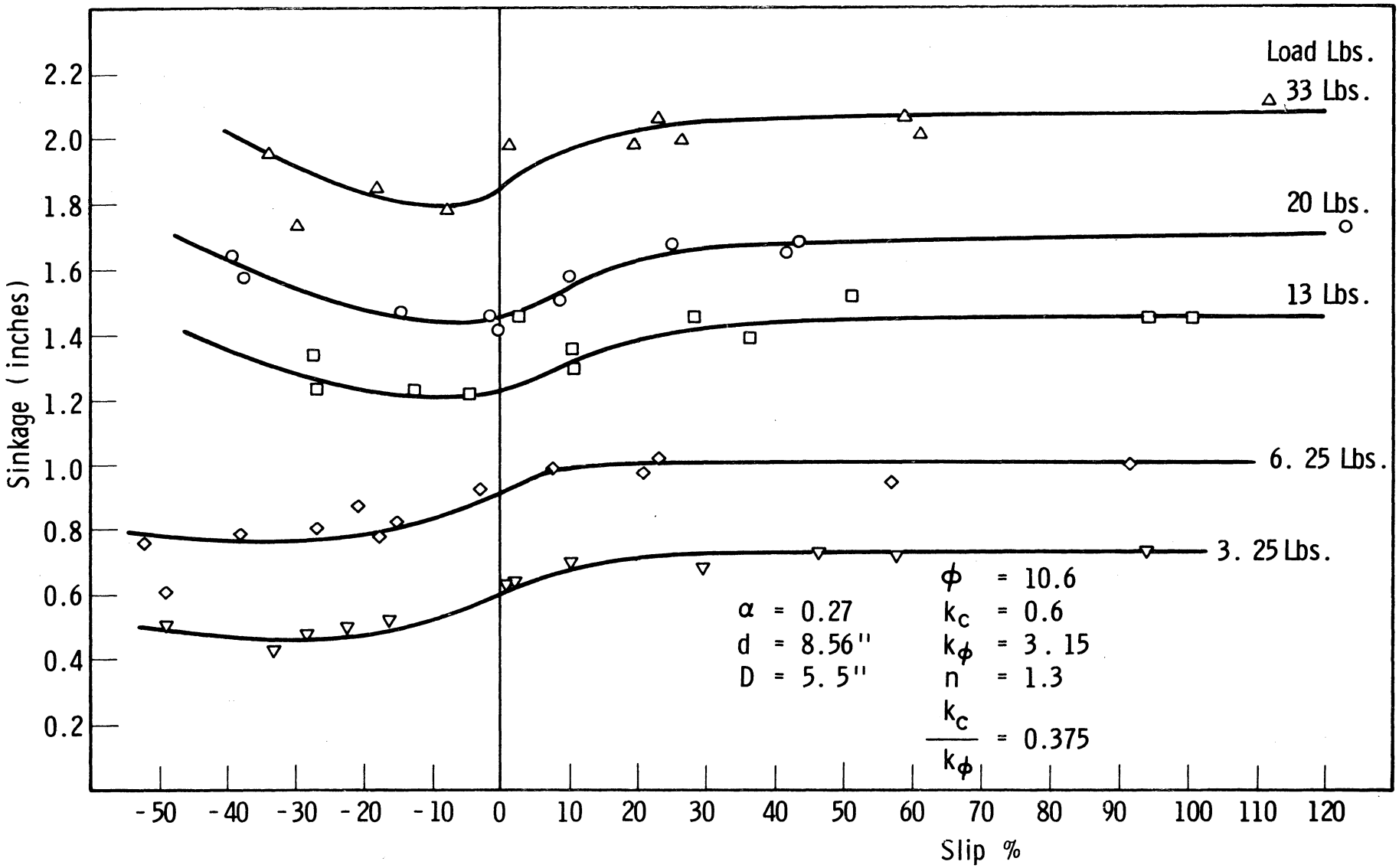

Fig. 40. Sinkage-slip curves for d = 8.56 in., α = 0.27, D = 5.5 in.

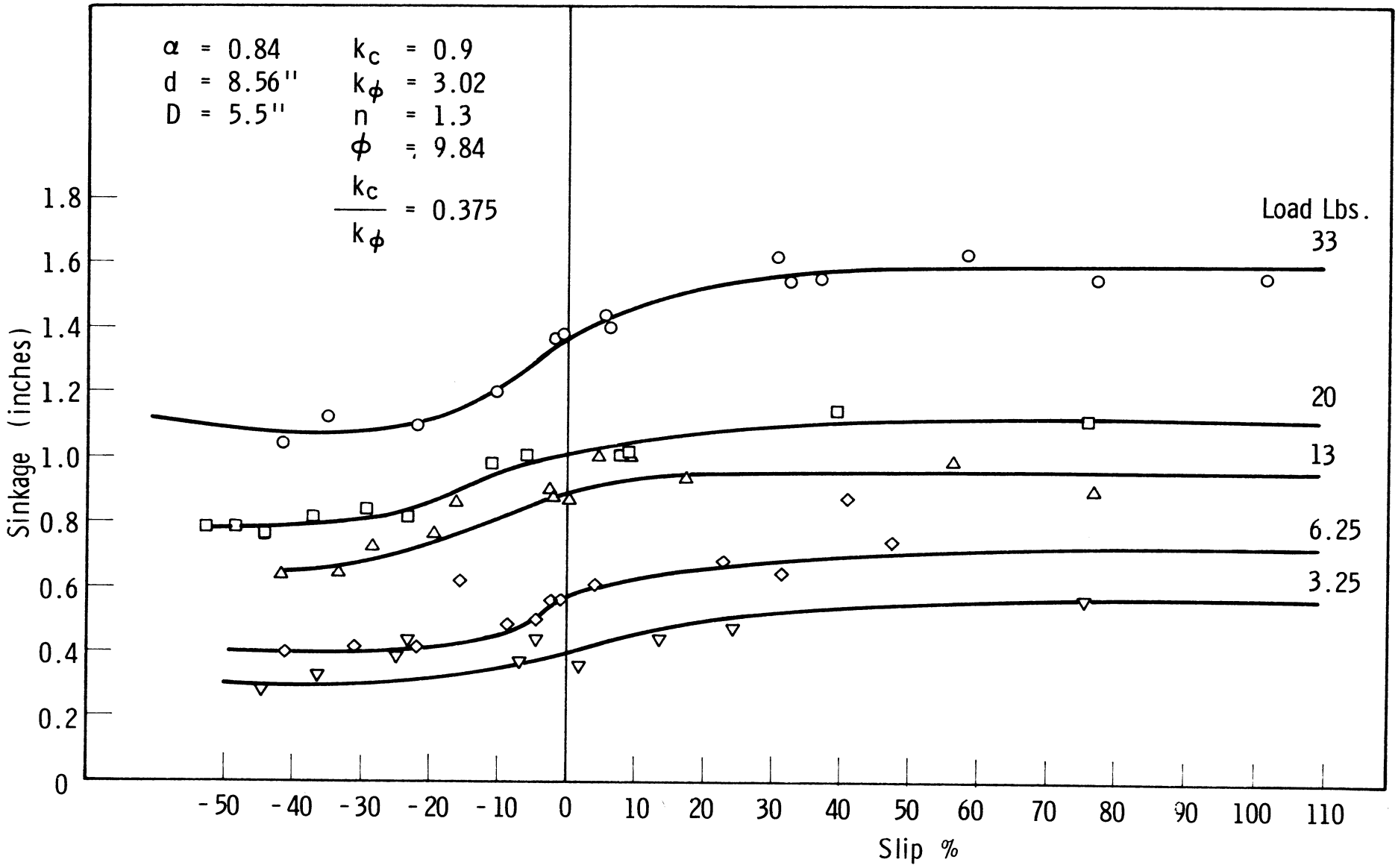

Fig. 41. Sinkage-slip curves for d = 8.56 in., α = 0.84, D = 5.5 in.

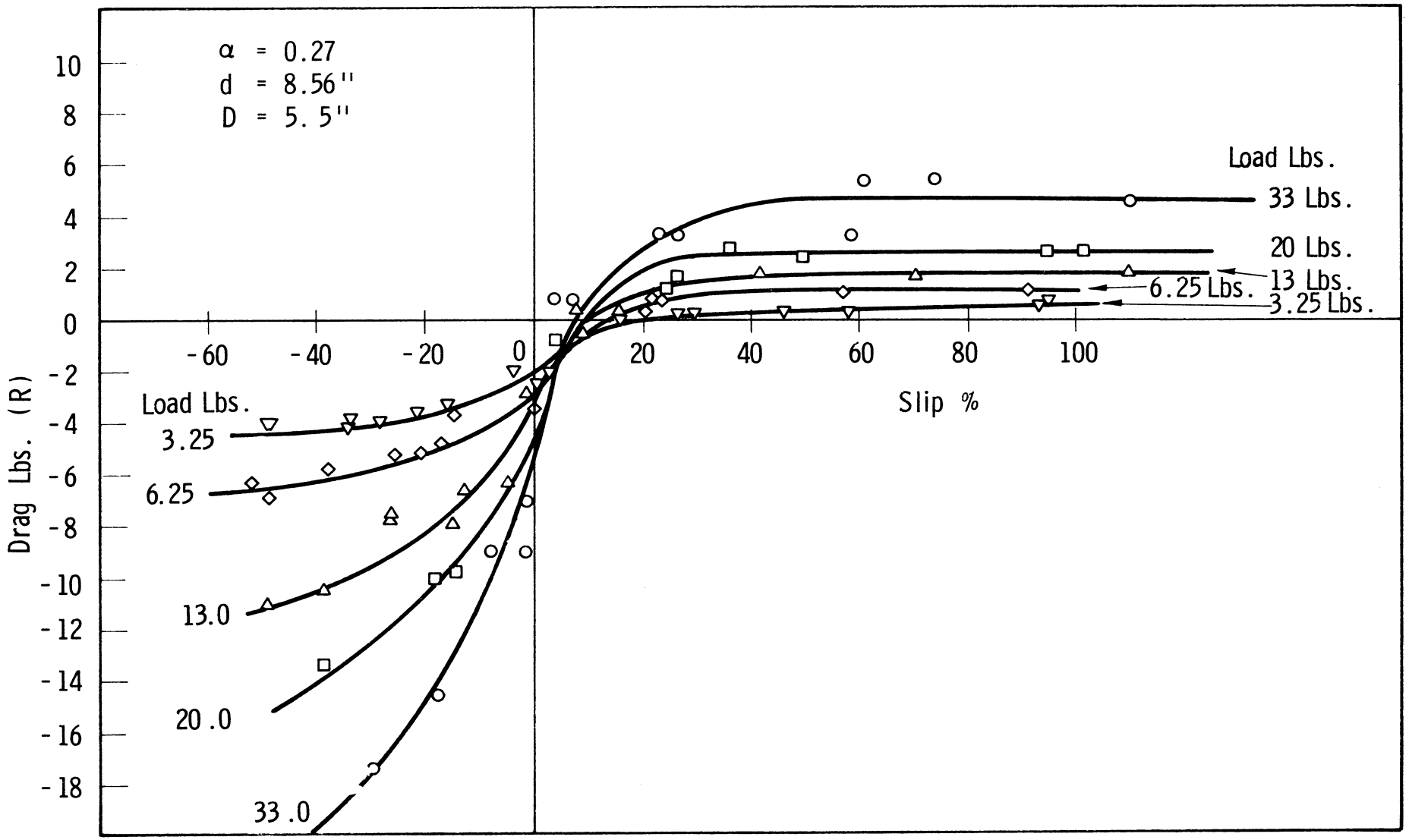

Fig. 42. Drag-slip curves for d = 8.56 in., α = 0.27, D = 5.5 in.

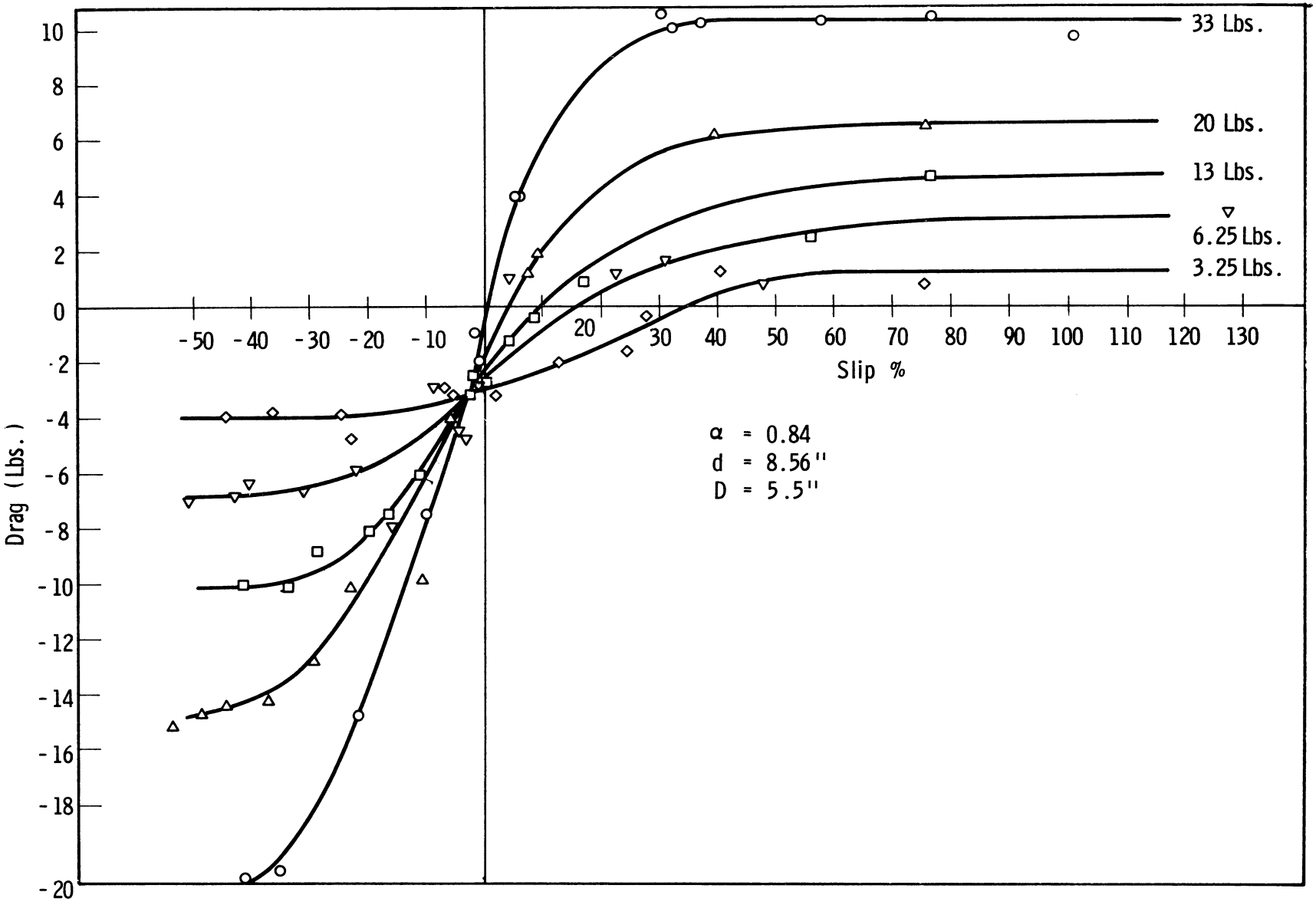

Fig. 43. Drag-slip curves for d = 8.56 in., α = 0.84, D = 5.5 in.

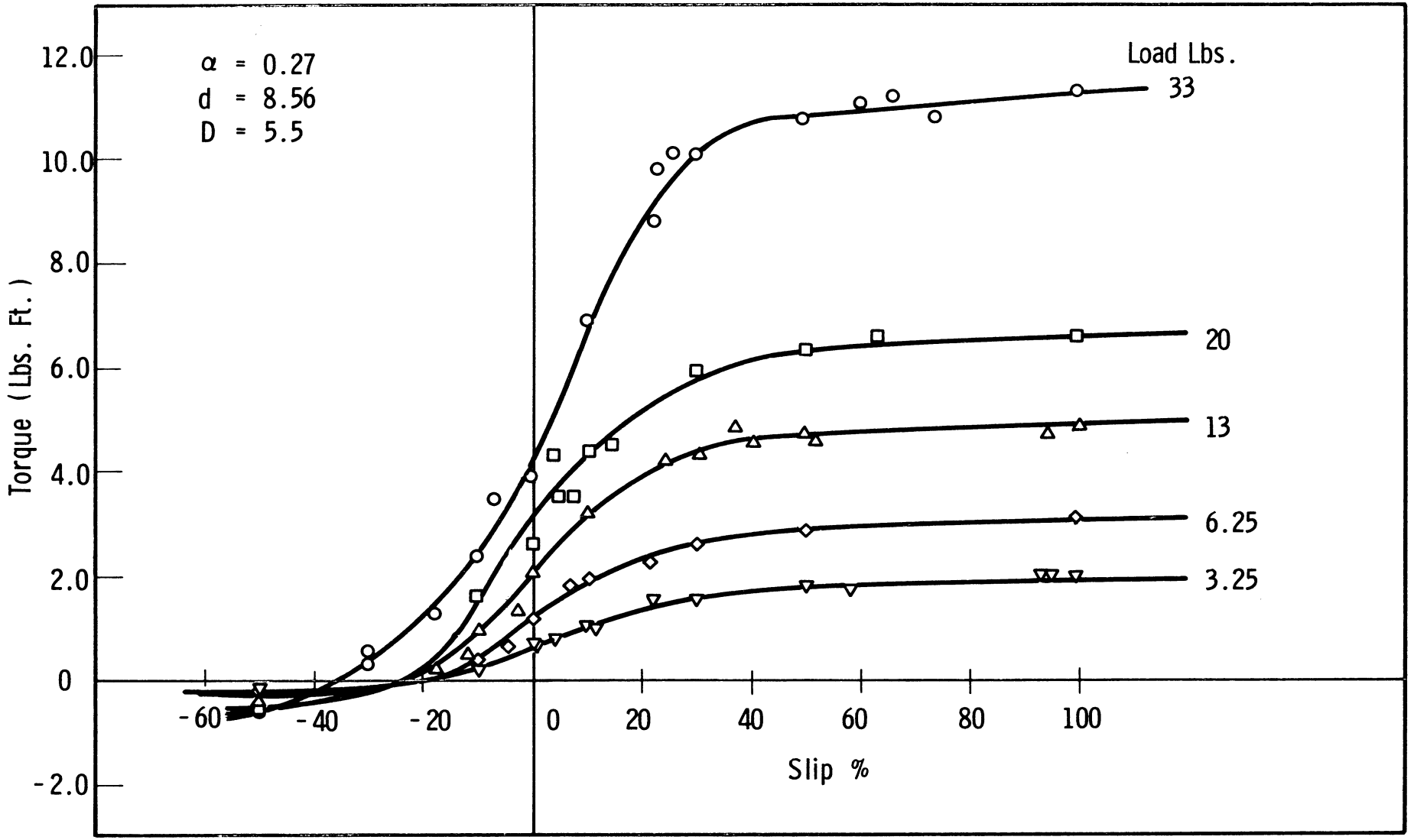

Fig. 44. Torque-slip curves for d = 8.56 in., α = 0.27, D = 5.5 in.

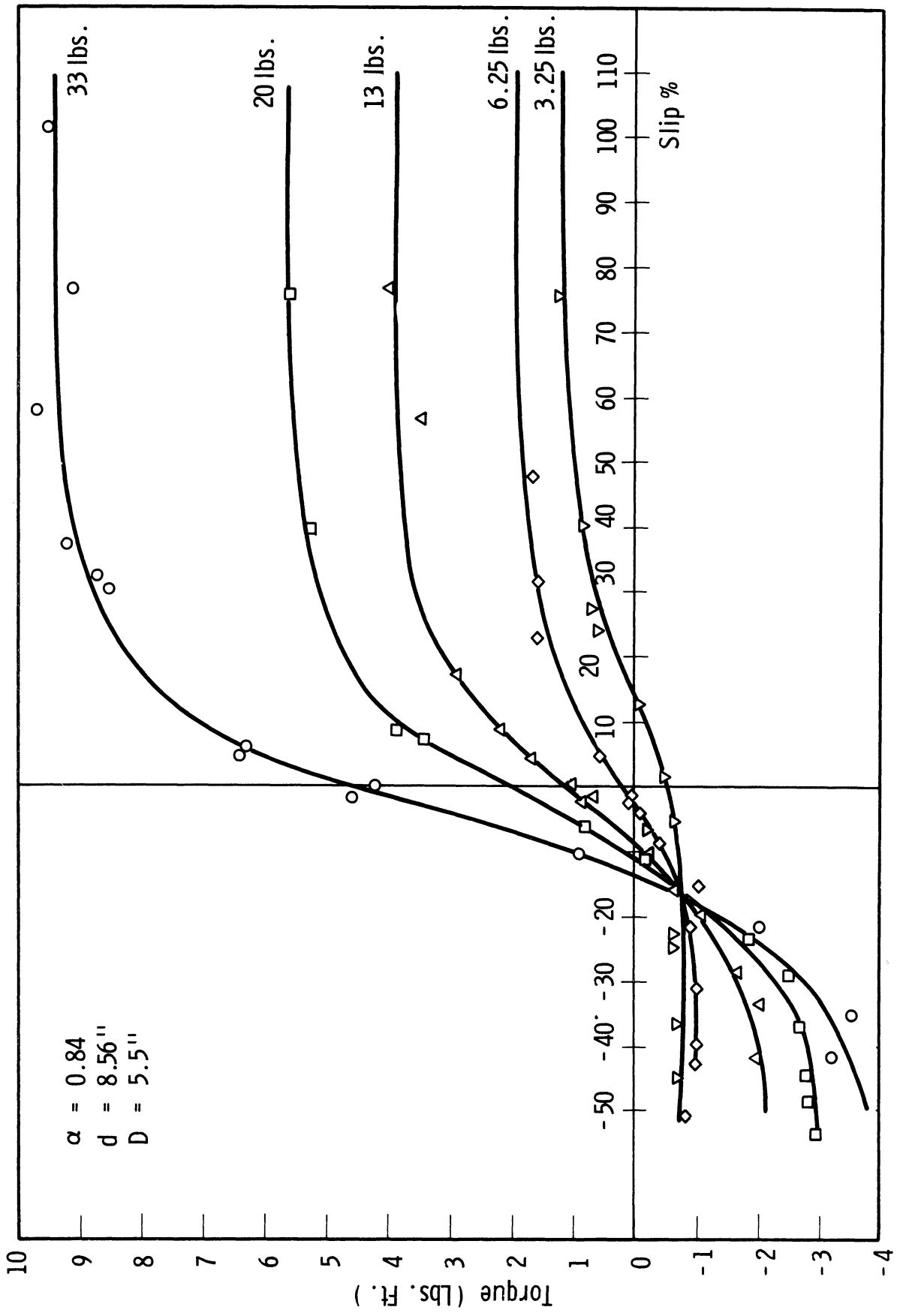

Fig. 45. Torque-slip curves for d = 8.56 in., α = 0.84, D = 5.5 in.

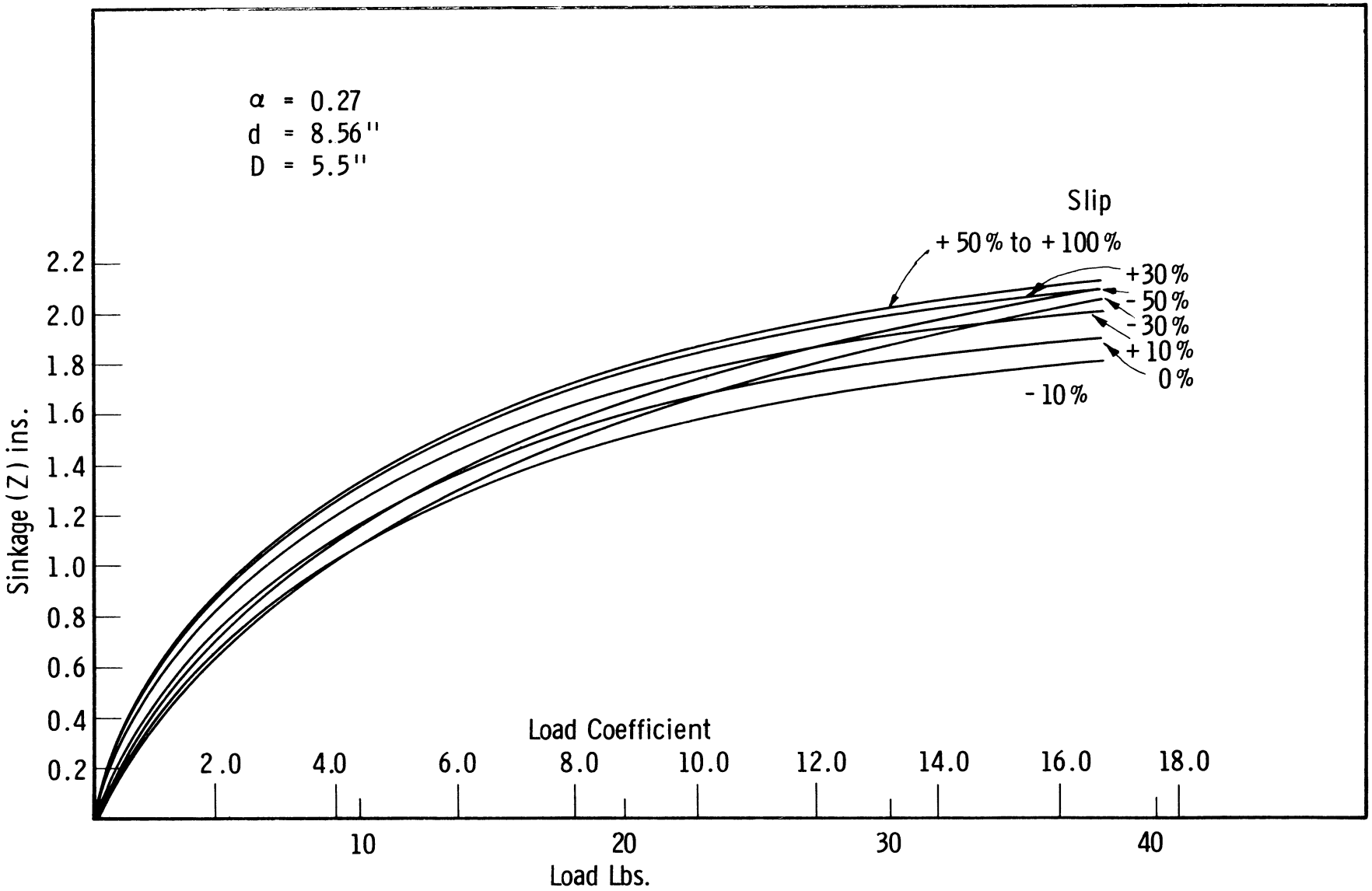

Fig. 46. Sinkage-load curves for d = 8.56 in., α = 0.27, D = 5.5 in.

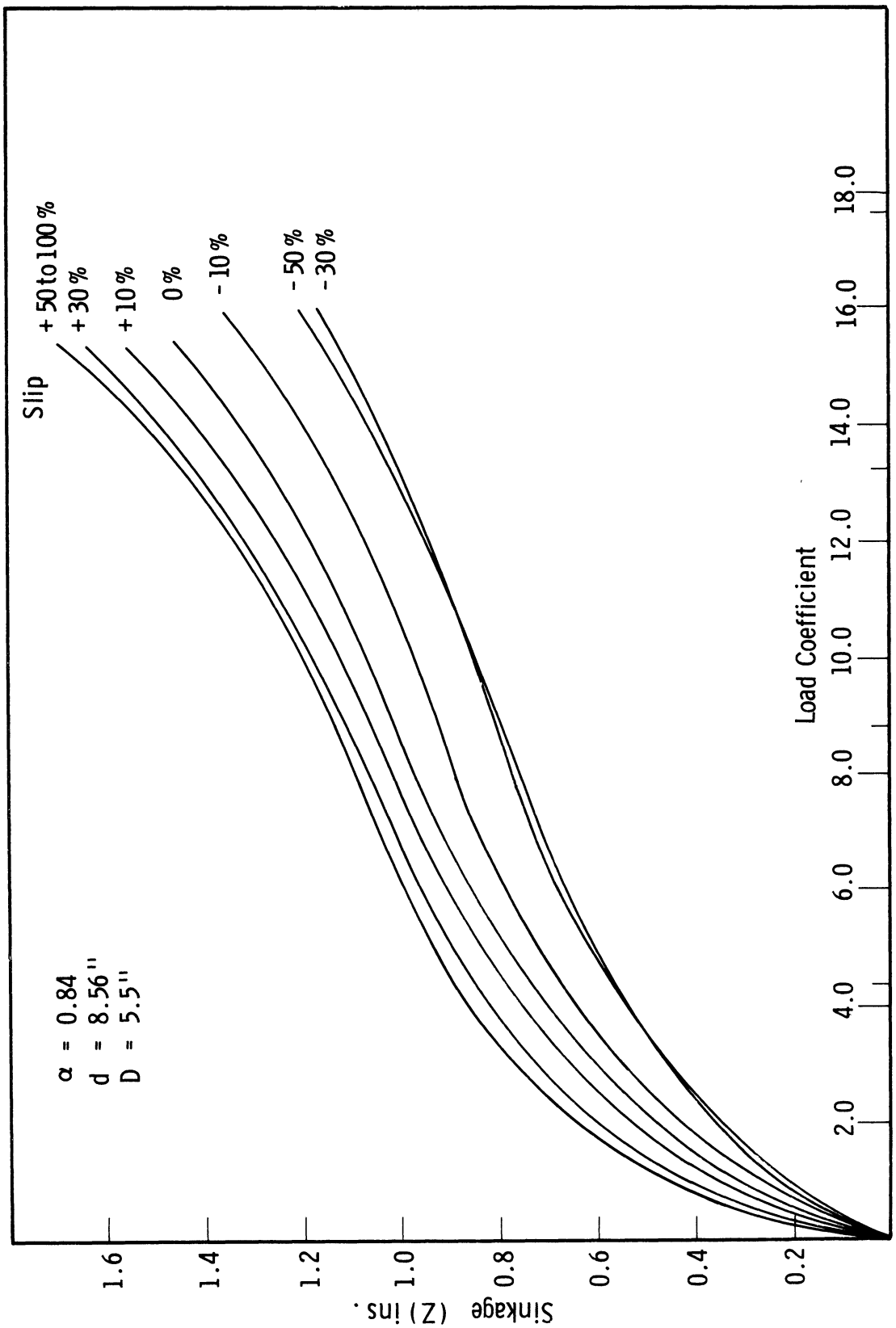

Fig. 47. Sinkage-load curves for d = 8.56 in., α = 0.84, D = 5.5 in.

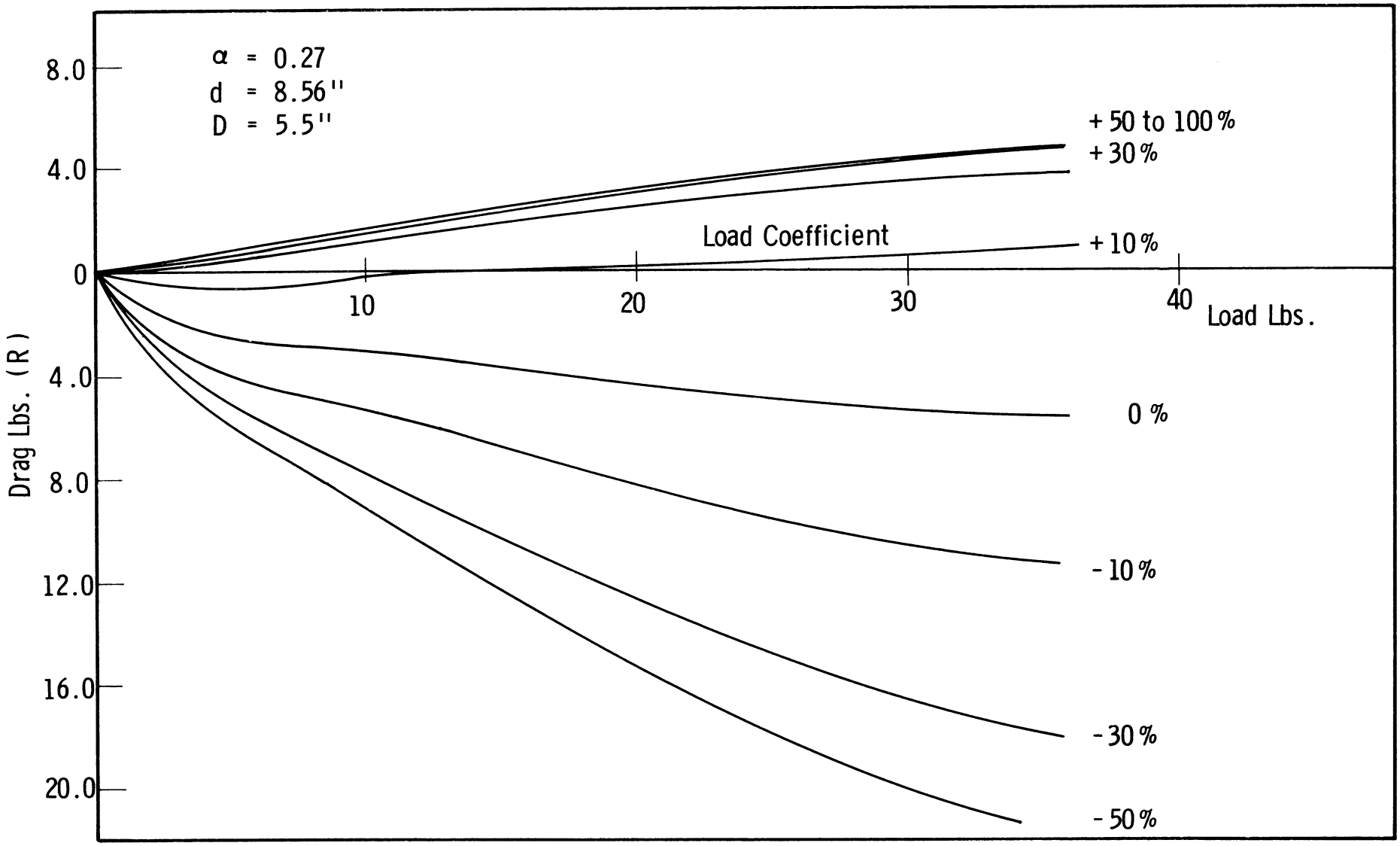

Fig. 48. Drag-load curves for d = 8.56 in., α = 0.27, D = 5.5 in.

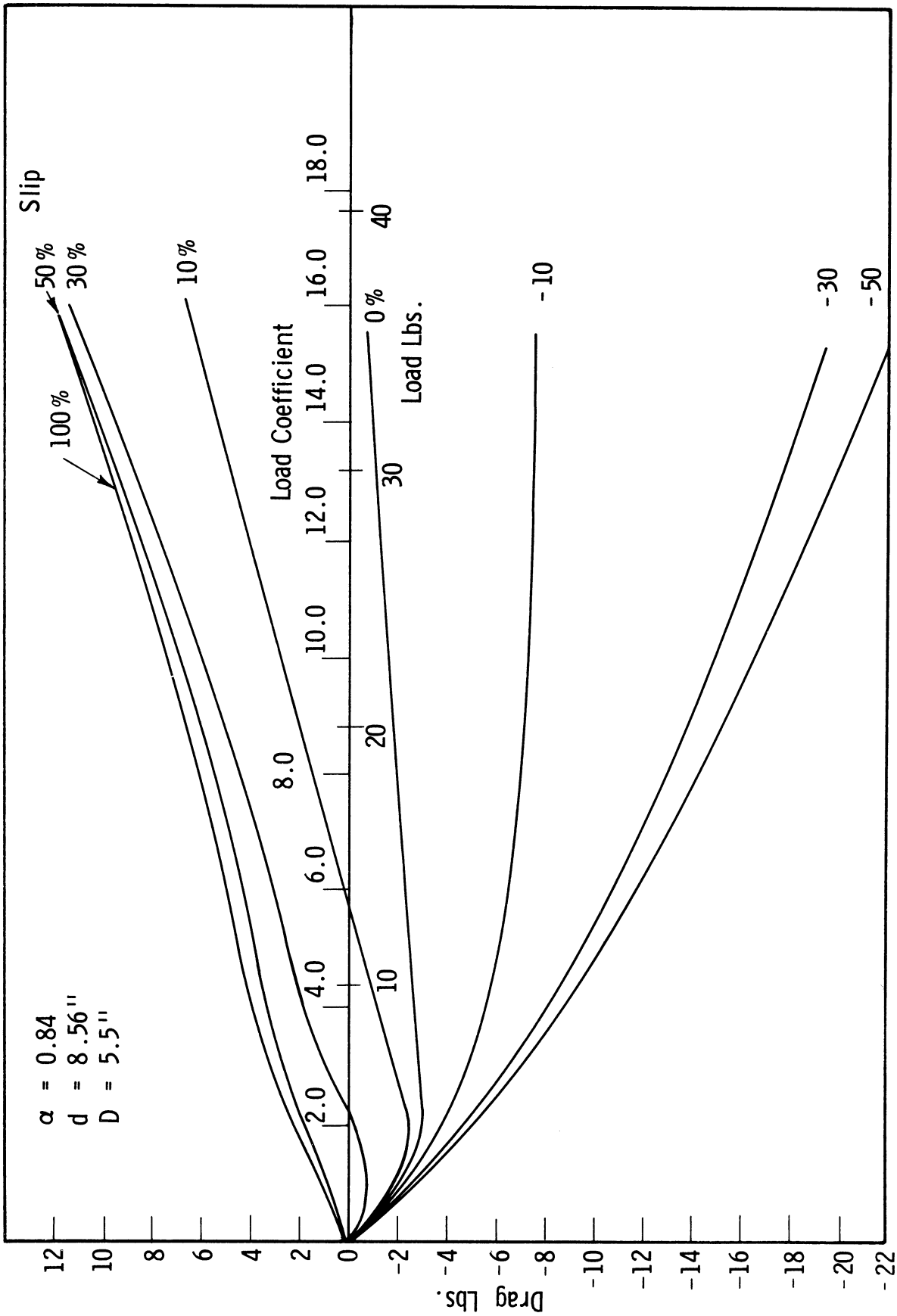

Fig. 49. Drag-load curves for d = 8.56 in., α = 0.84, D = 5.5 in.

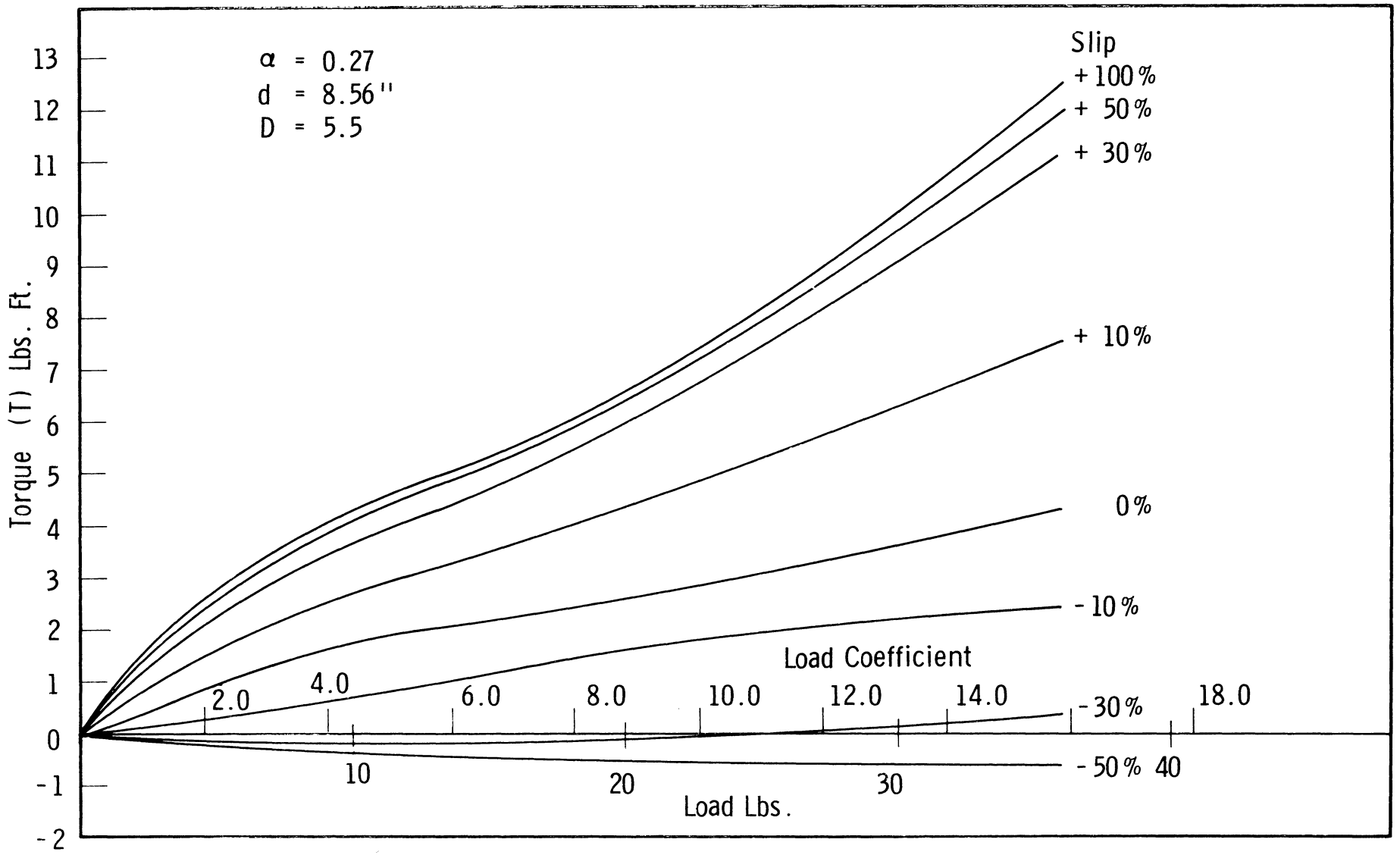

Fig. 50. Torque-load curves for d = 8.56 in., α = 0.27, D = 5.5 in.

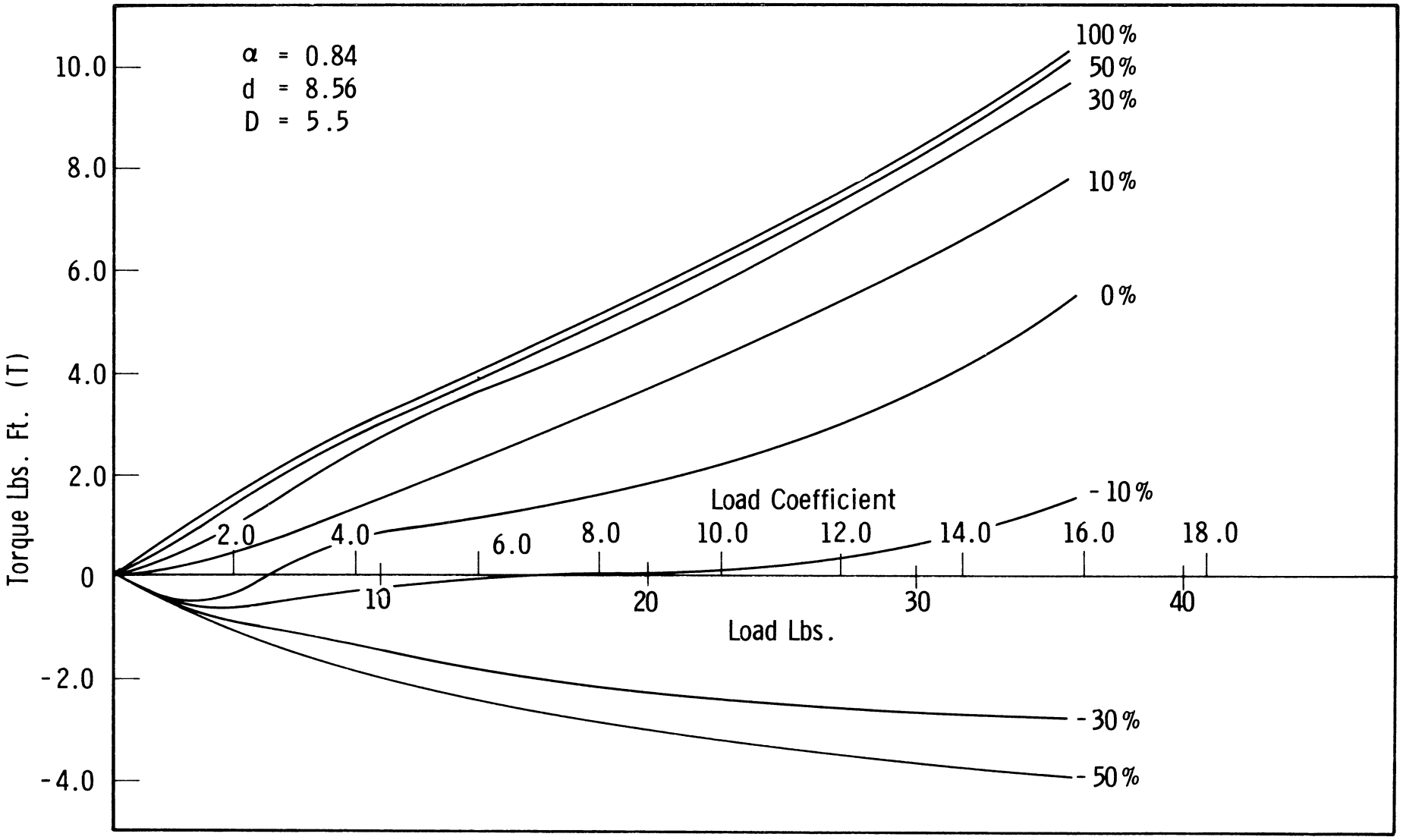

Fig. 51. Torque-load curves for d = 8.56 in., α = 0.84, D = 5.5 in.

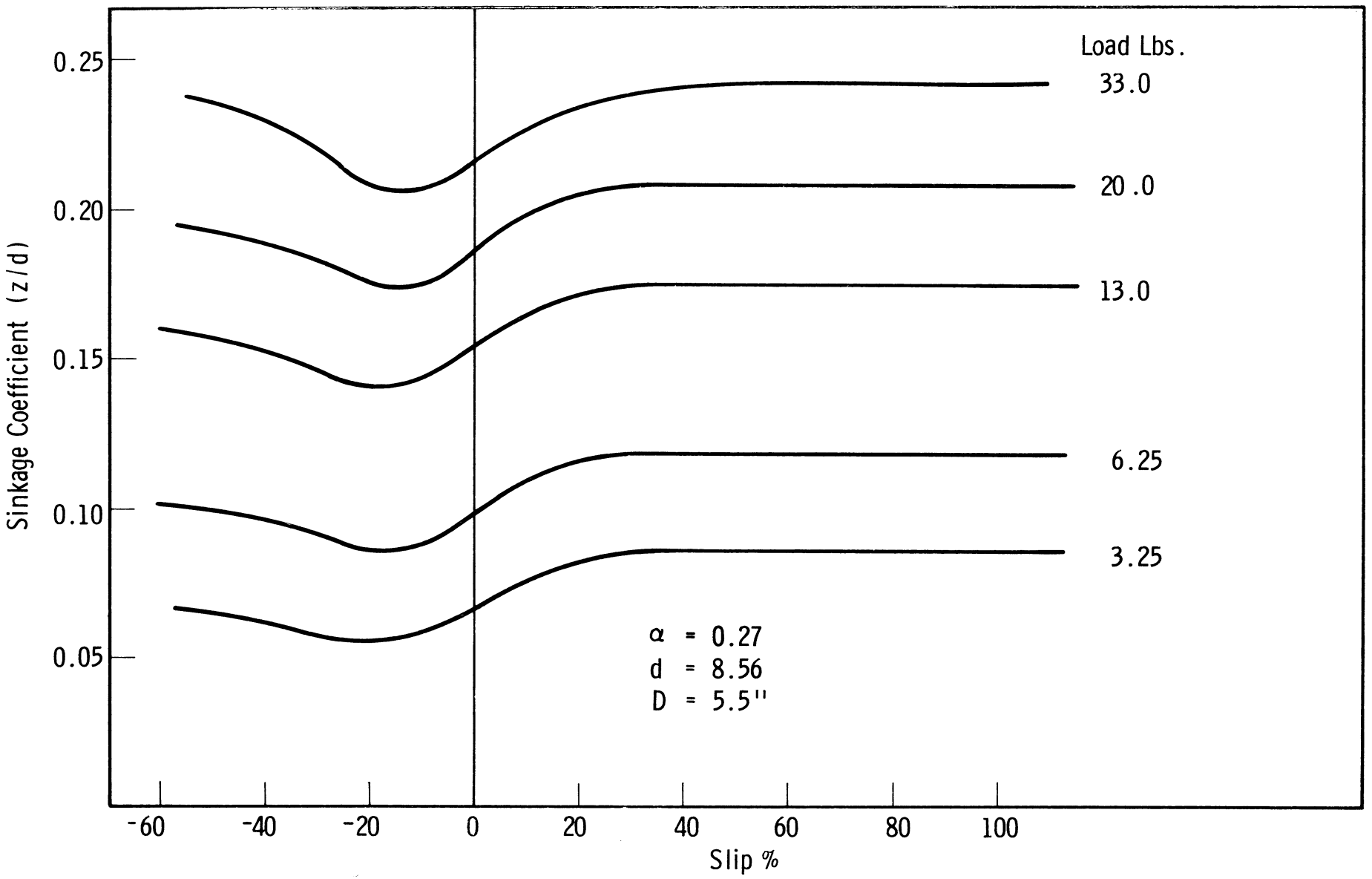

Fig. 52. Sinkage coefficient-slip curves for d = 8.56 in., α = 0.27, D = 5.5 in.

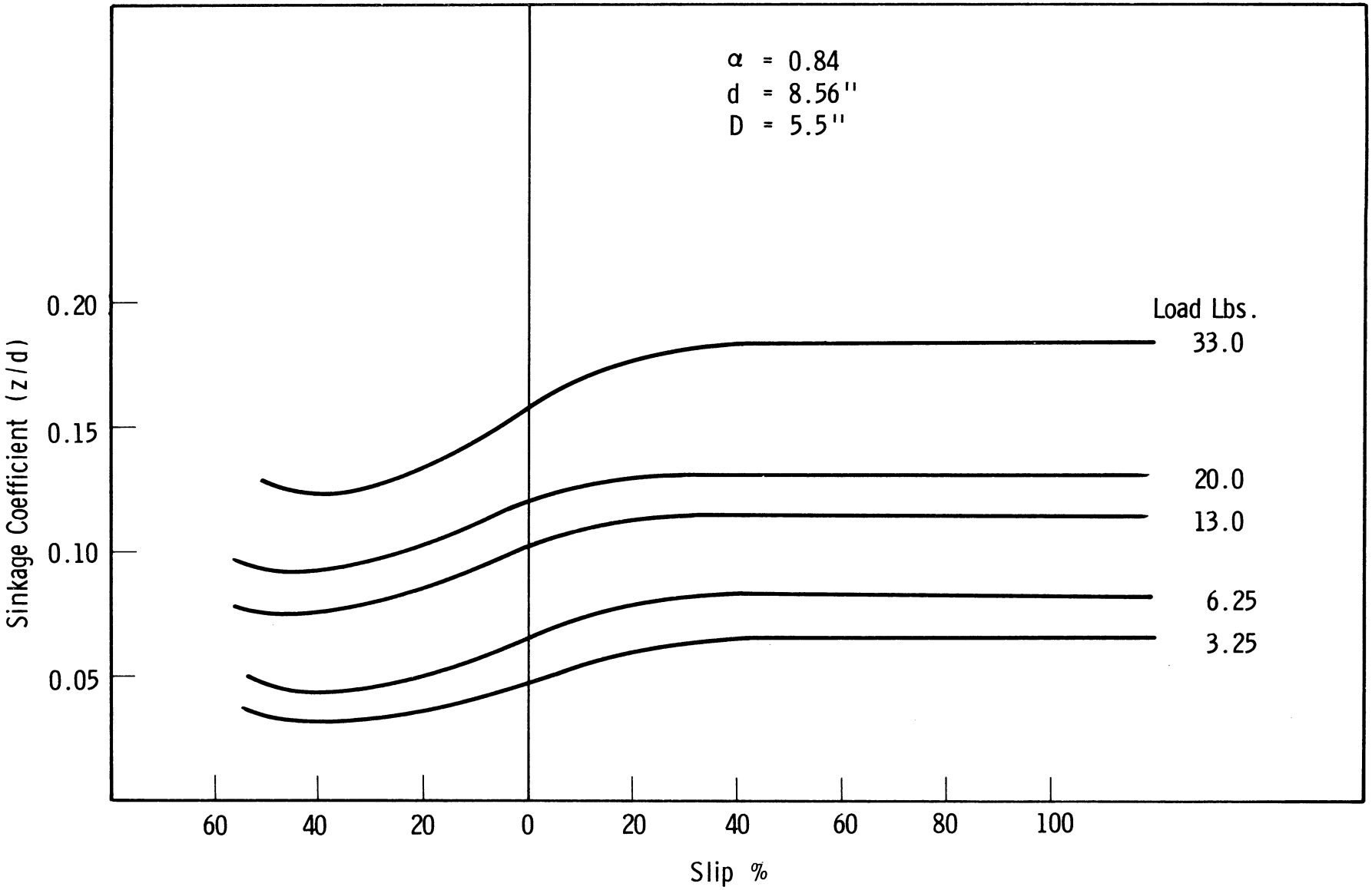

Fig. 53. Sinkage coefficient-slip curves for d = 8.56 in., α = 0.84, D = 5.5 in.

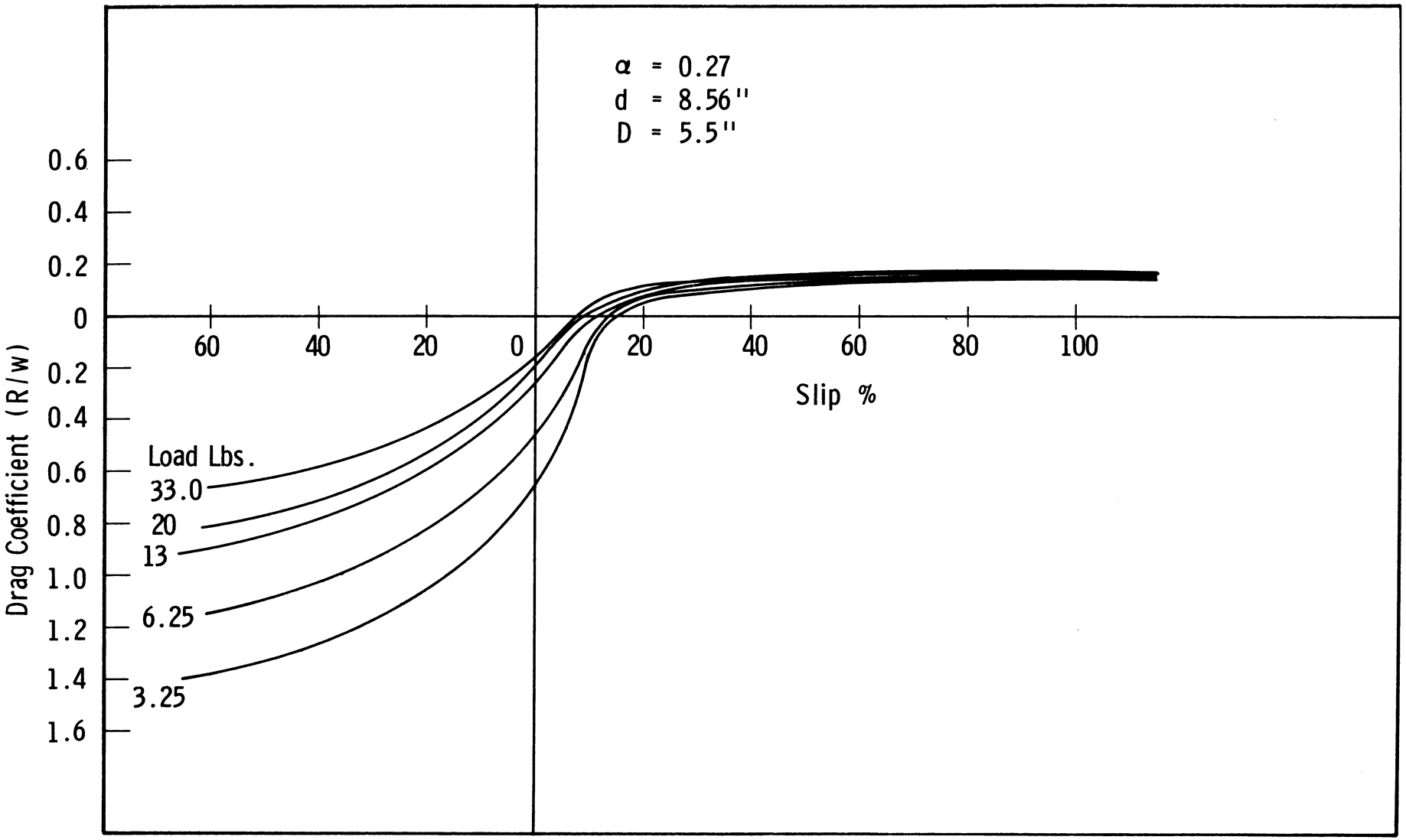

Fig. 54. Drag coefficient-slip curves for d = 8.56 in., α = 0.27, D = 5.5 in.

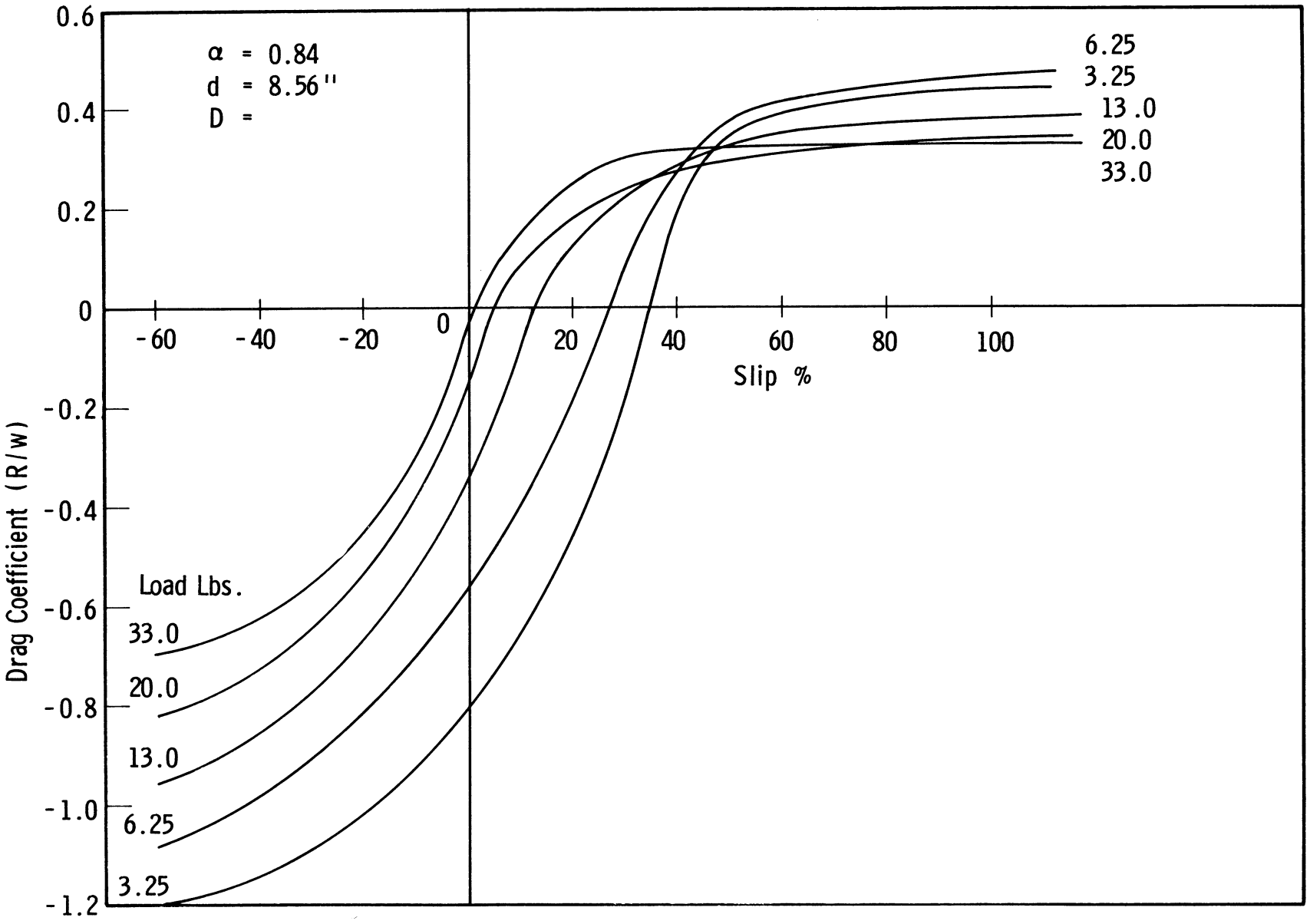

Fig. 55. Drag coefficient-slip curves for d = 8.56 in., α = 0.84, D = 5.5 in.

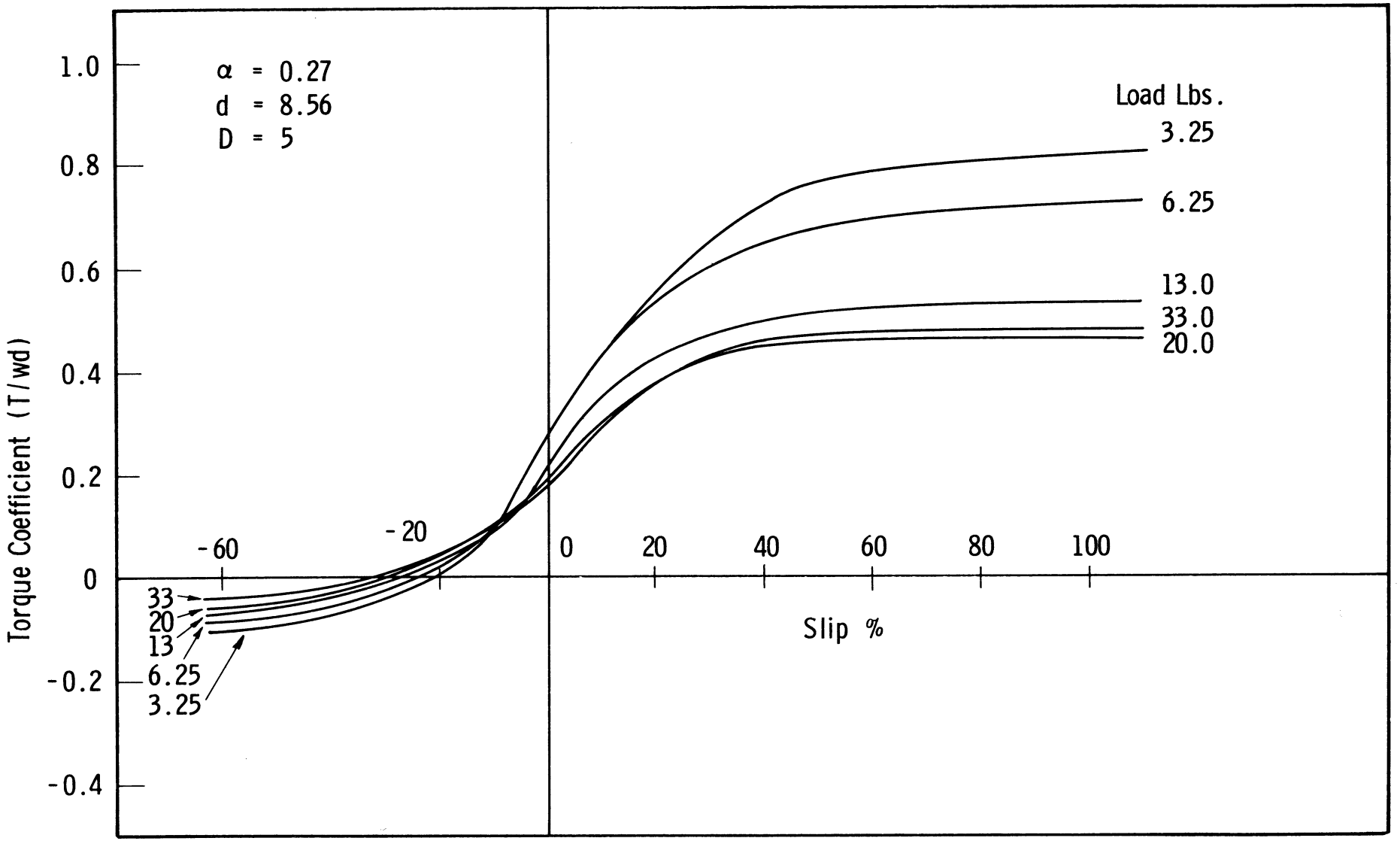

Fig. 56. Torque coefficient-slip curves for d = 8.56 in., α = 0.27, D = 5.5 in.

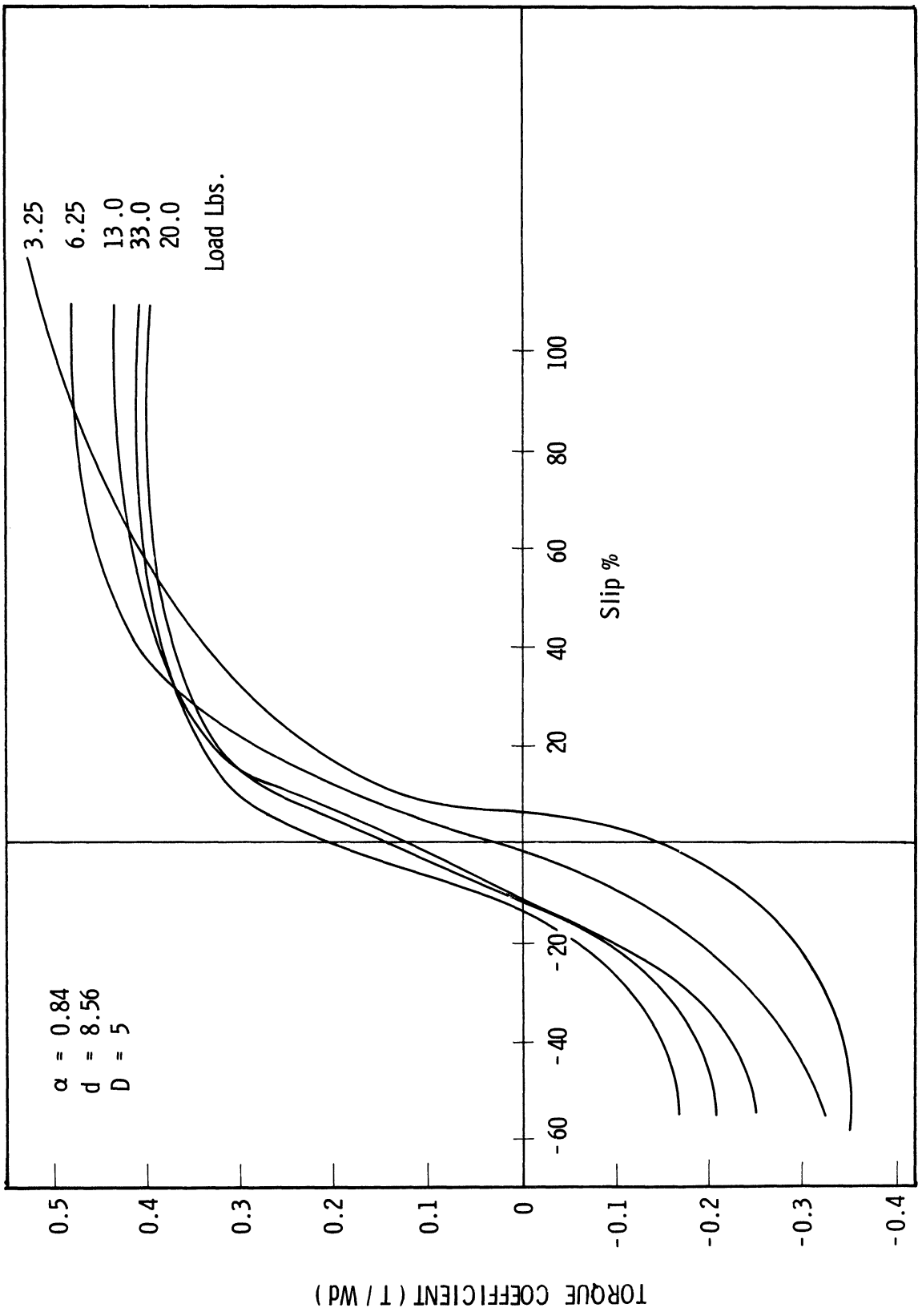

Fig. 57. Torque coefficient-slip curves for d = 8.56 in., α = 0.84, D = 5.5 in.

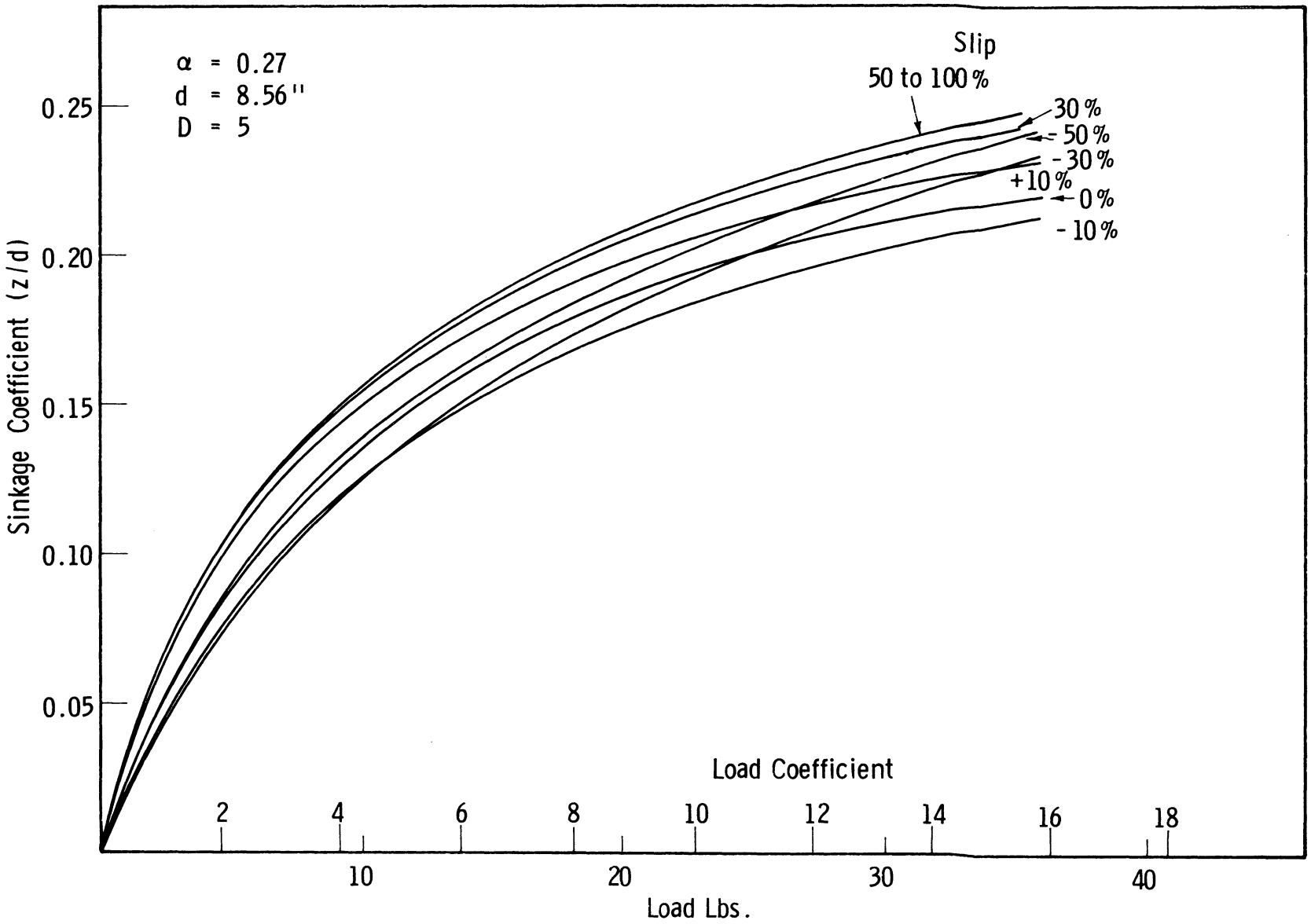

Fig. 58. Sinkage coefficient-load curves for d = 8.56 in., α = 0.27, D = 5.5 in.

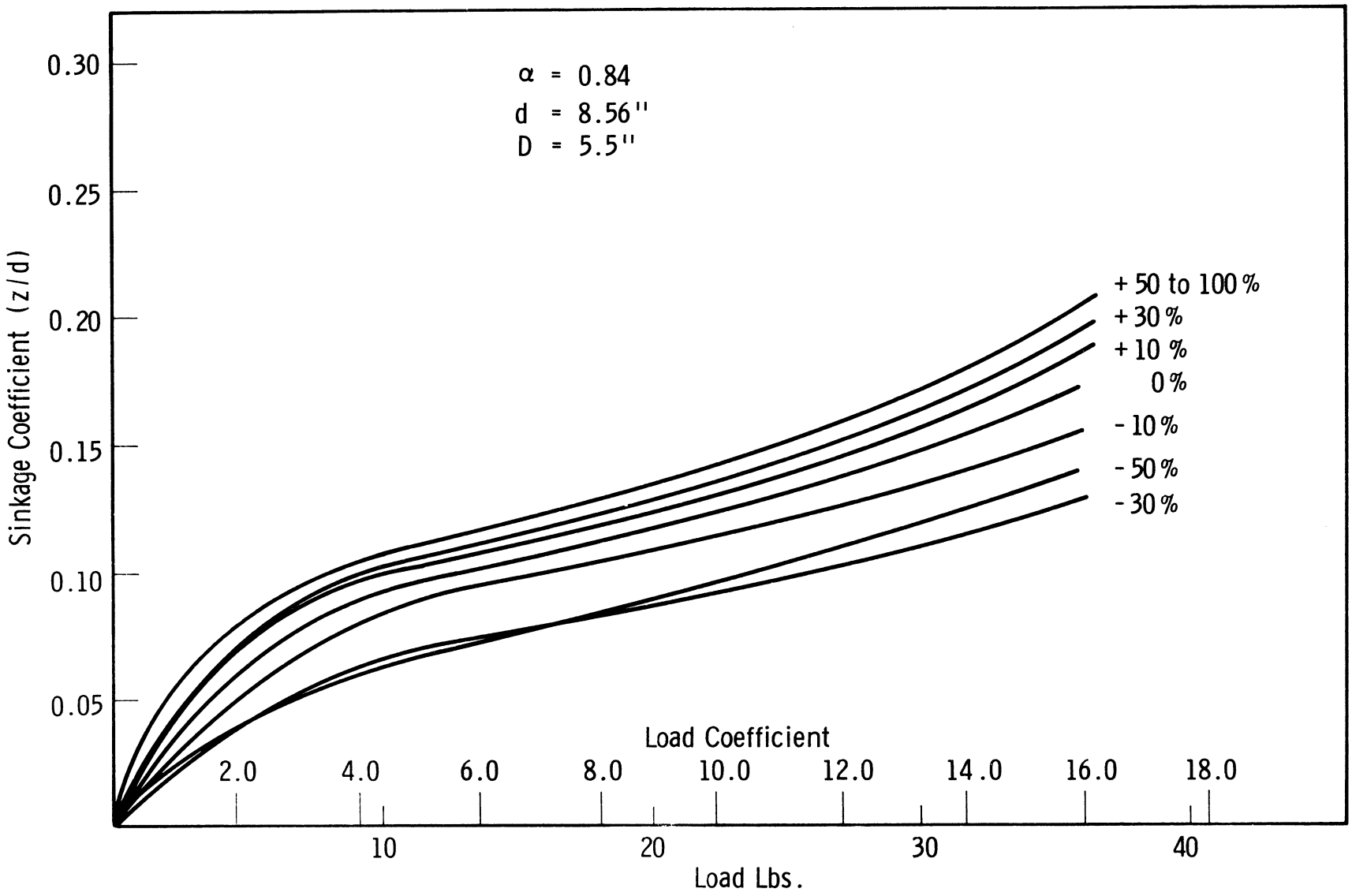

Fig. 59. Sinkage coefficient-load curves for d = 8.56 in., α = 0.84, D = 5.5 in.

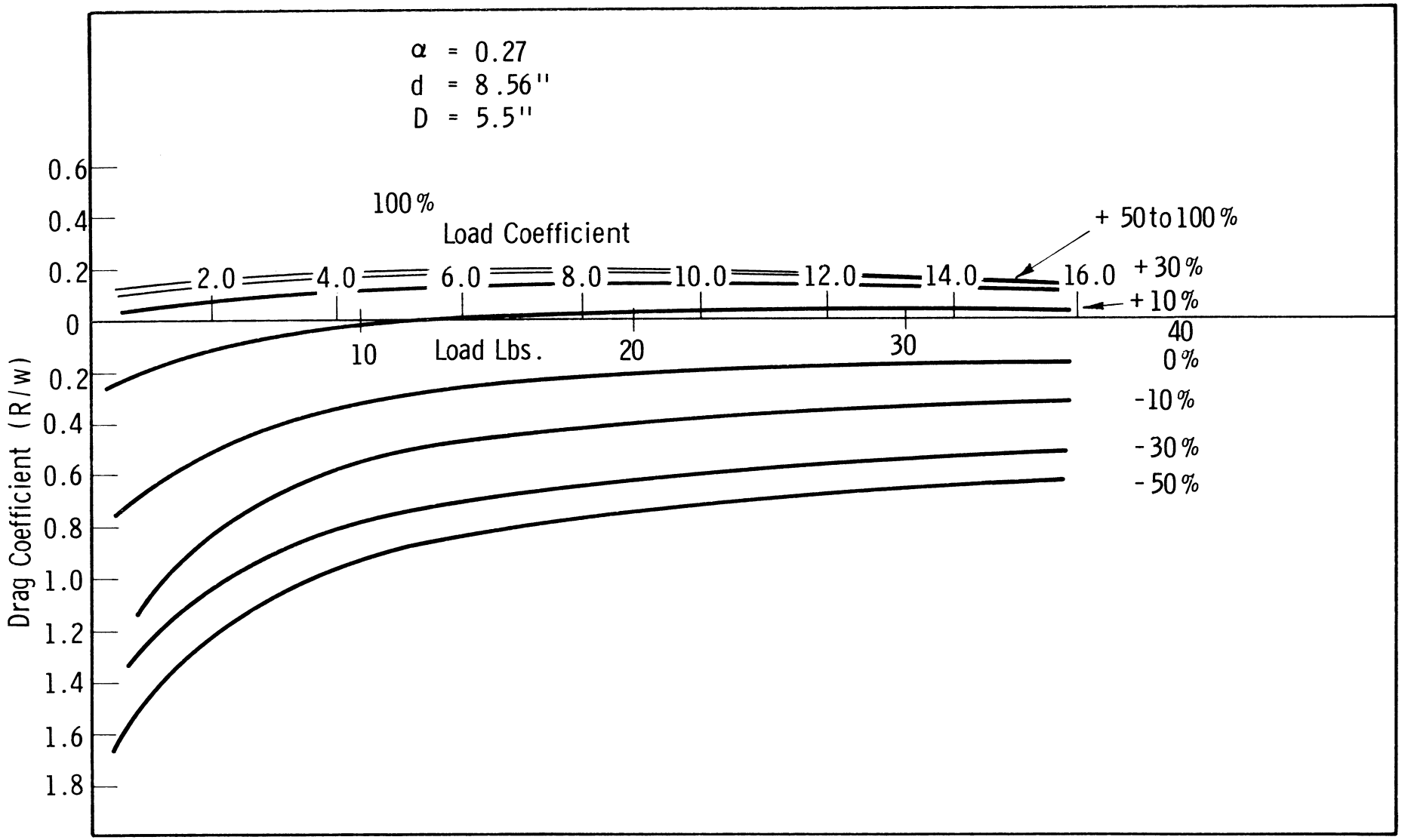

Fig. 60. Drag coefficient-load curves for d = 8.56 in., α = 0.27, D = 5.5 in.

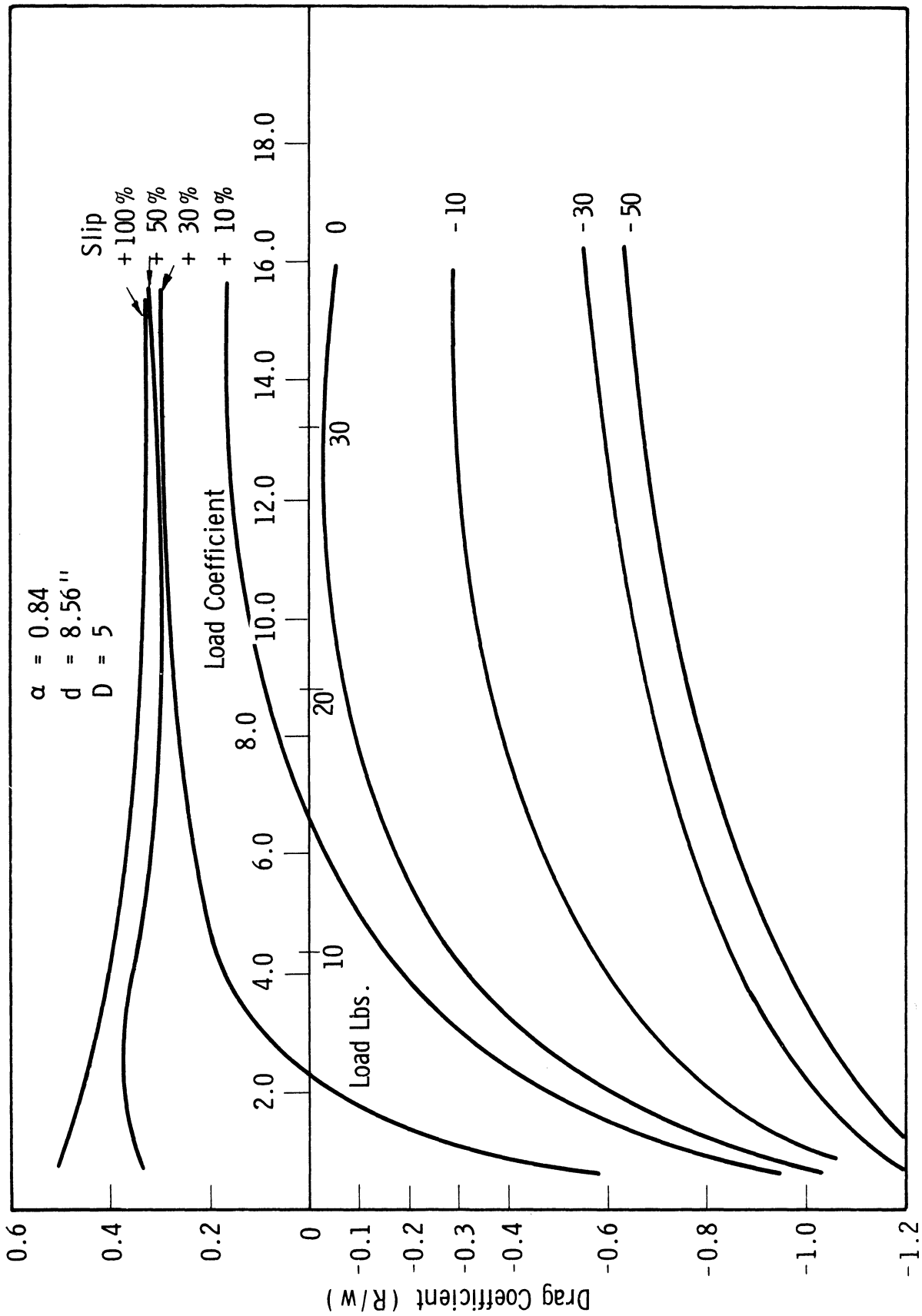

Fig. 61. Drag coefficient-load curves for d = 8.56 in., α = 0.84, D = 5.5 in.

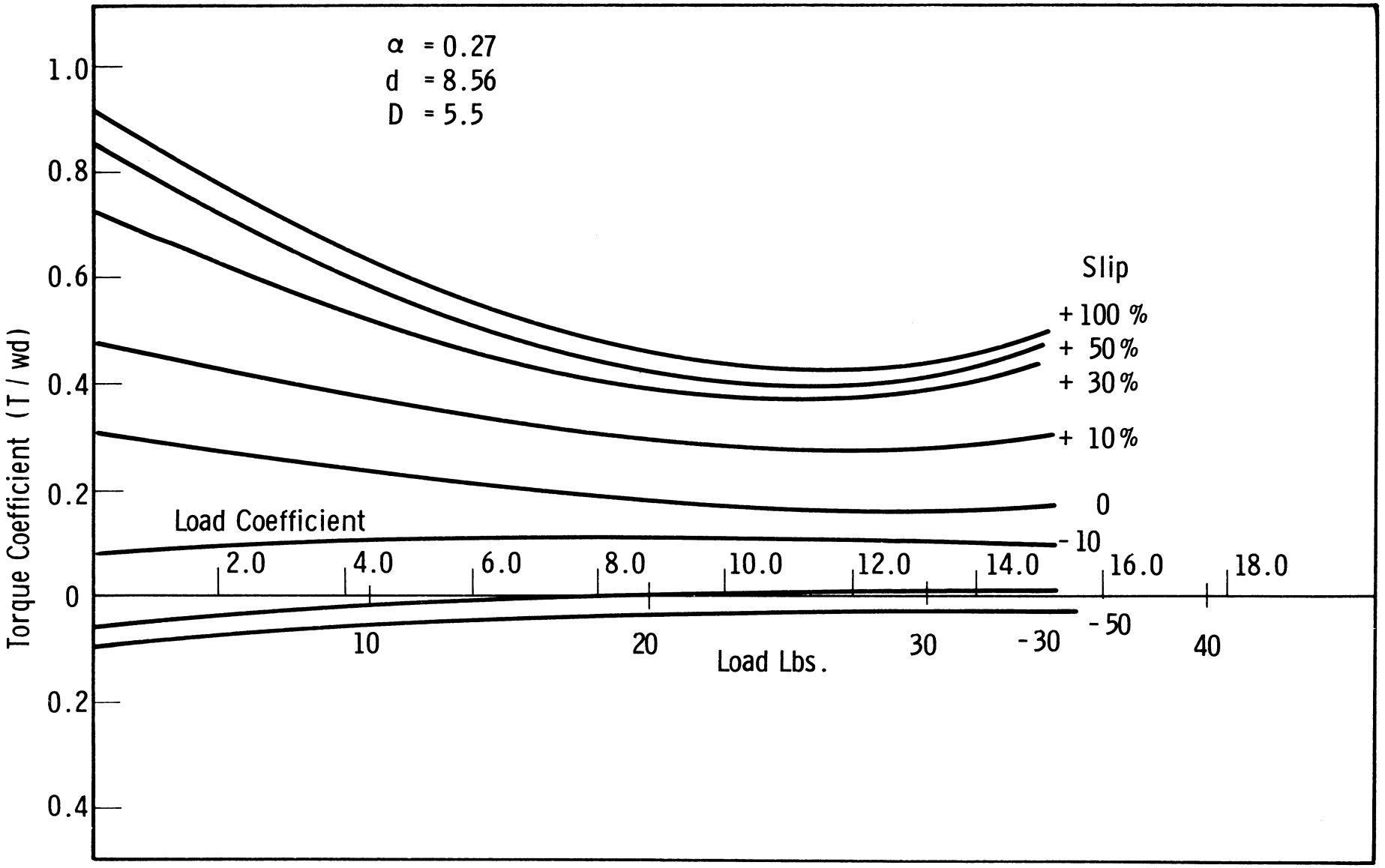

Fig. 62. Torque coefficient-load curves for d = 8.56 in., α = 0.27, D = 5.5 in.

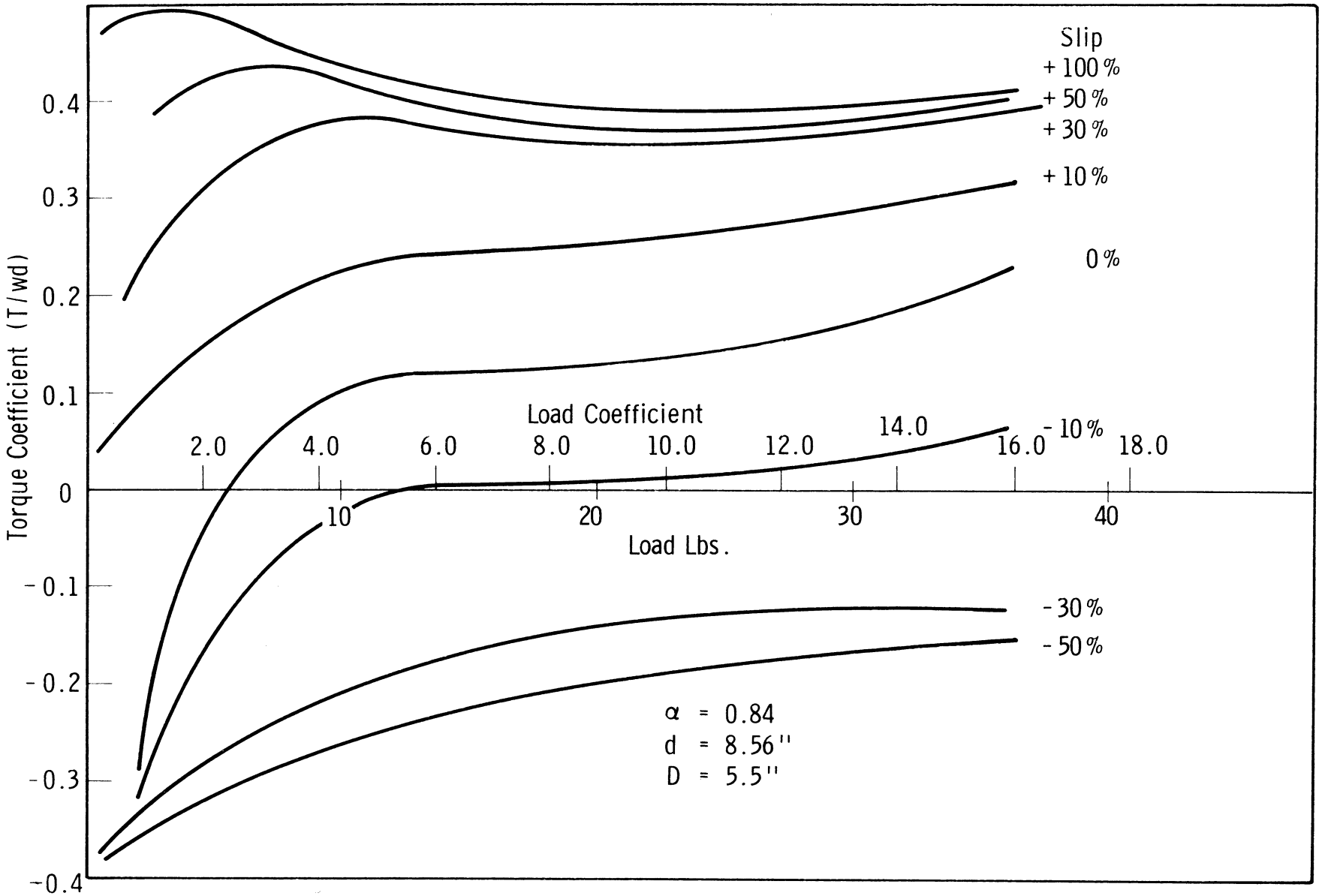

Fig. 63. Torque coefficient-load curves for d = 8.56 in., α = 0.84, D = 5.5 in.

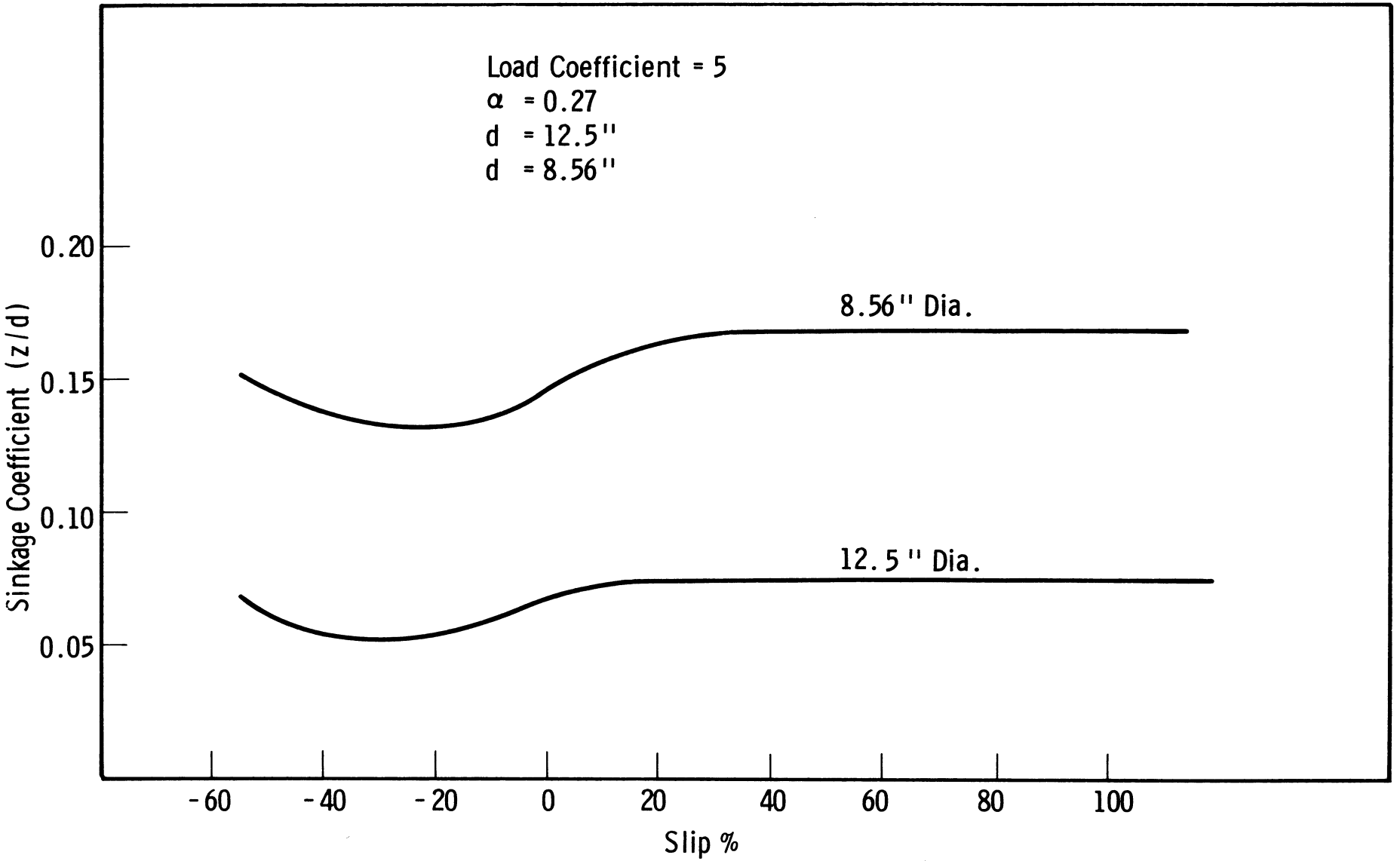

Fig. 64. Sinkage coefficient vs. slip for 12.5- and 8.56-in. dia wheels when load coefficient = 5.0, α = 0.27.

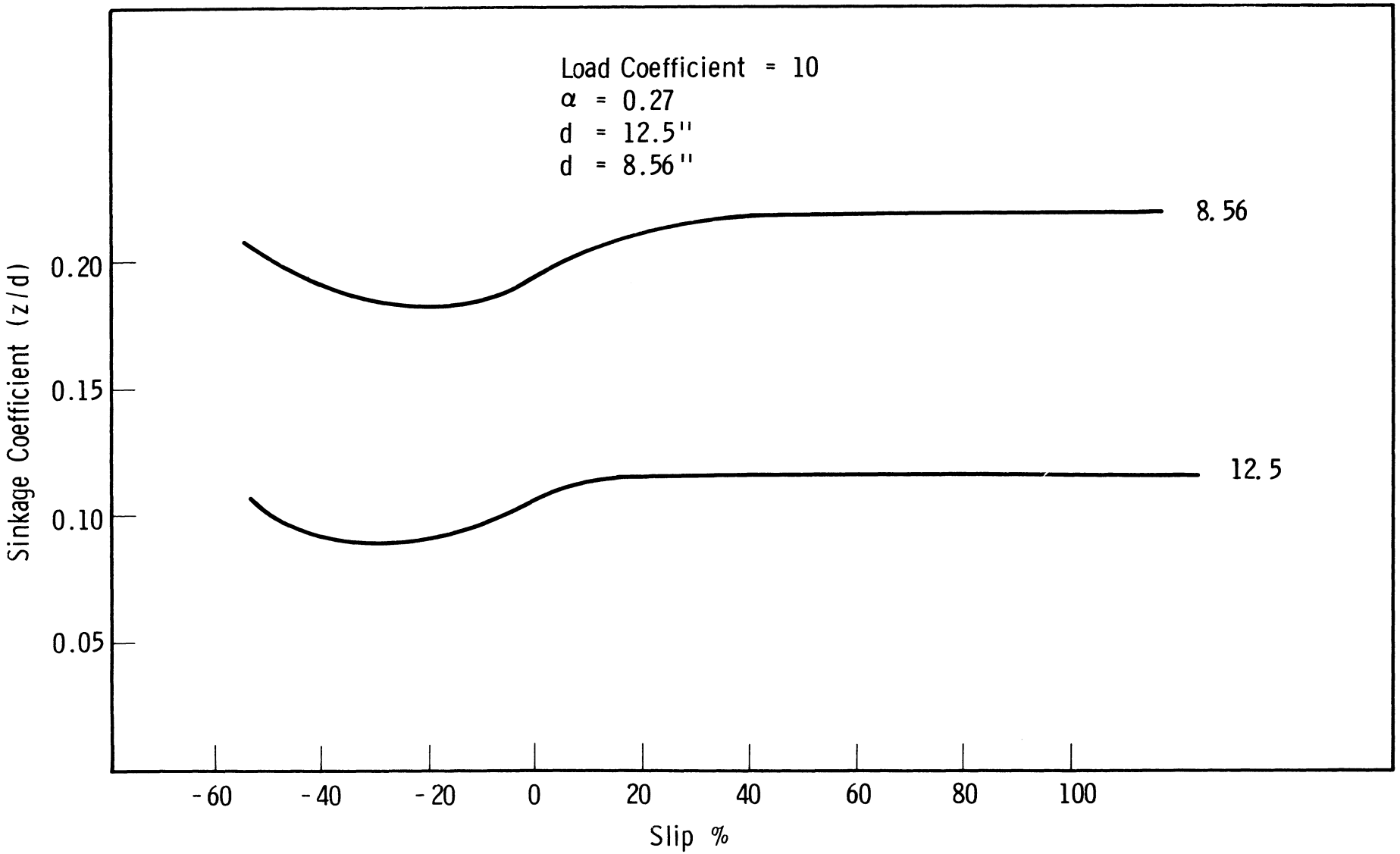

Fig. 65. Sinkage coefficient vs. slip for 12.5- and 8.56-in. dia wheels when load coefficient = 10.0, α = 0.27.

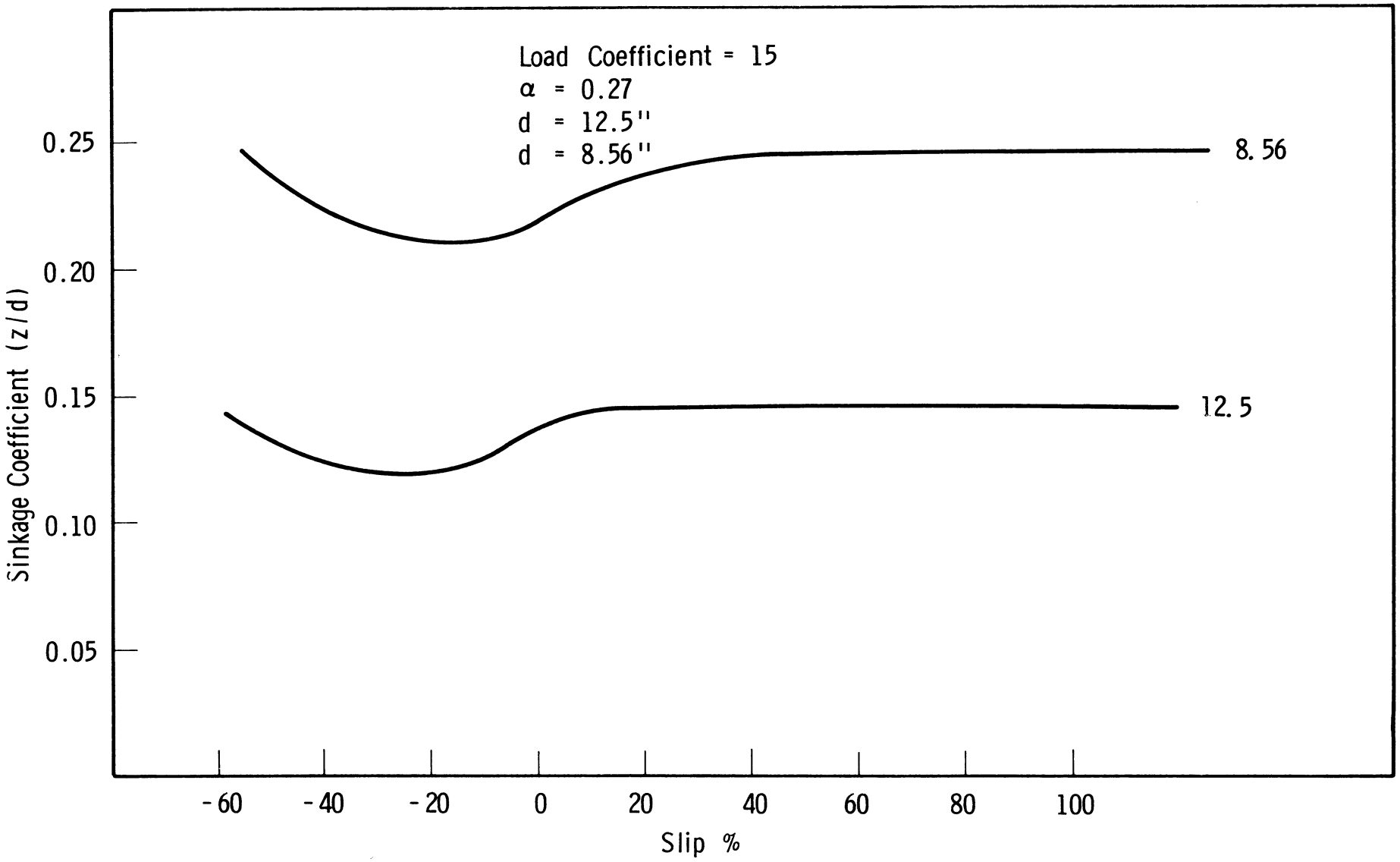

Fig. 66. Sinkage coefficient vs. slip for 12.5- and 8.56-in. dia wheels when load coefficient = 15.0, α = 0.27

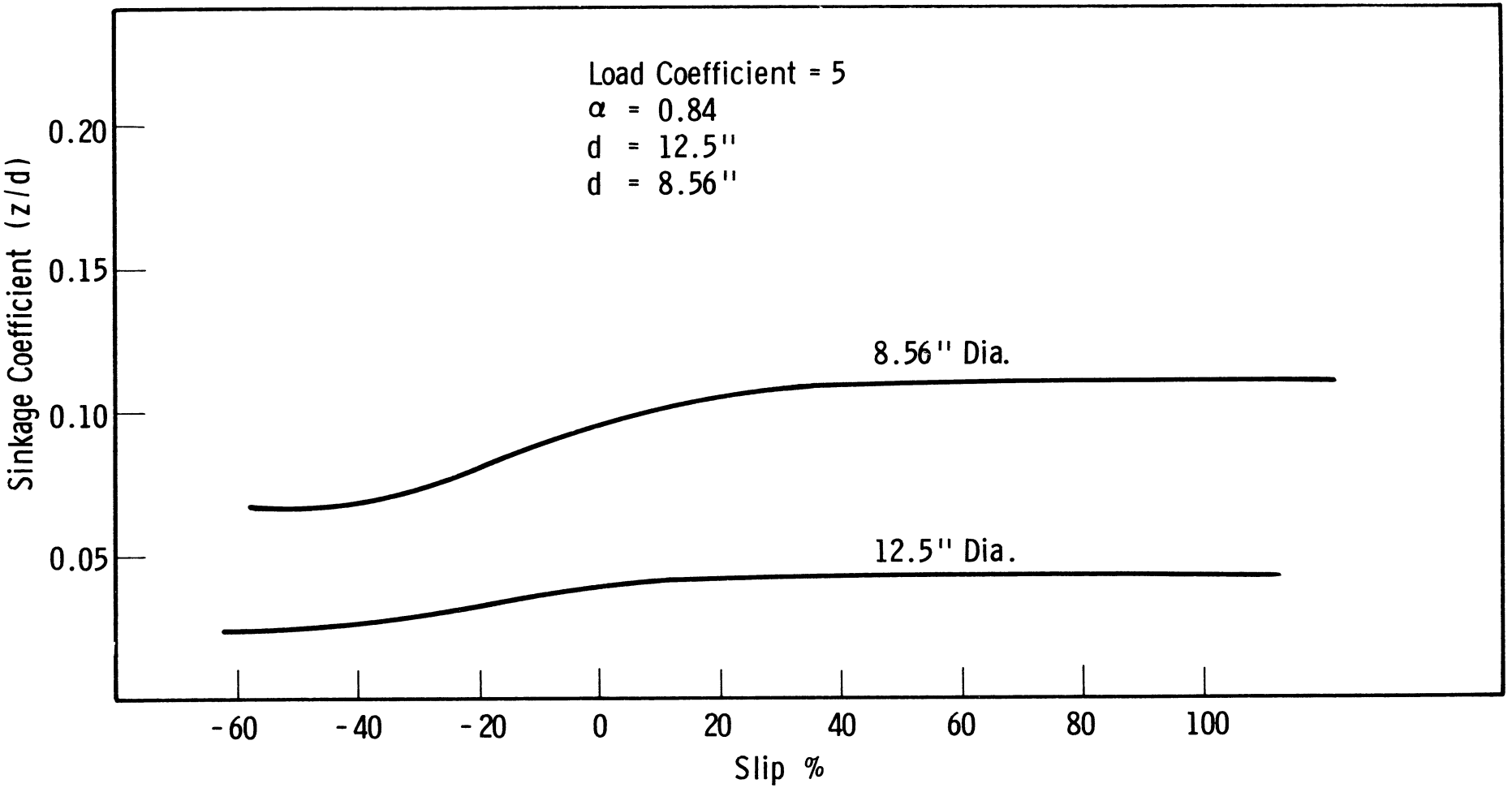

Fig. 67. Sinkage coefficient vs. slip for 12.5- and 8.56-in. dia wheels when load coefficient = 5.0, α = 0.84.

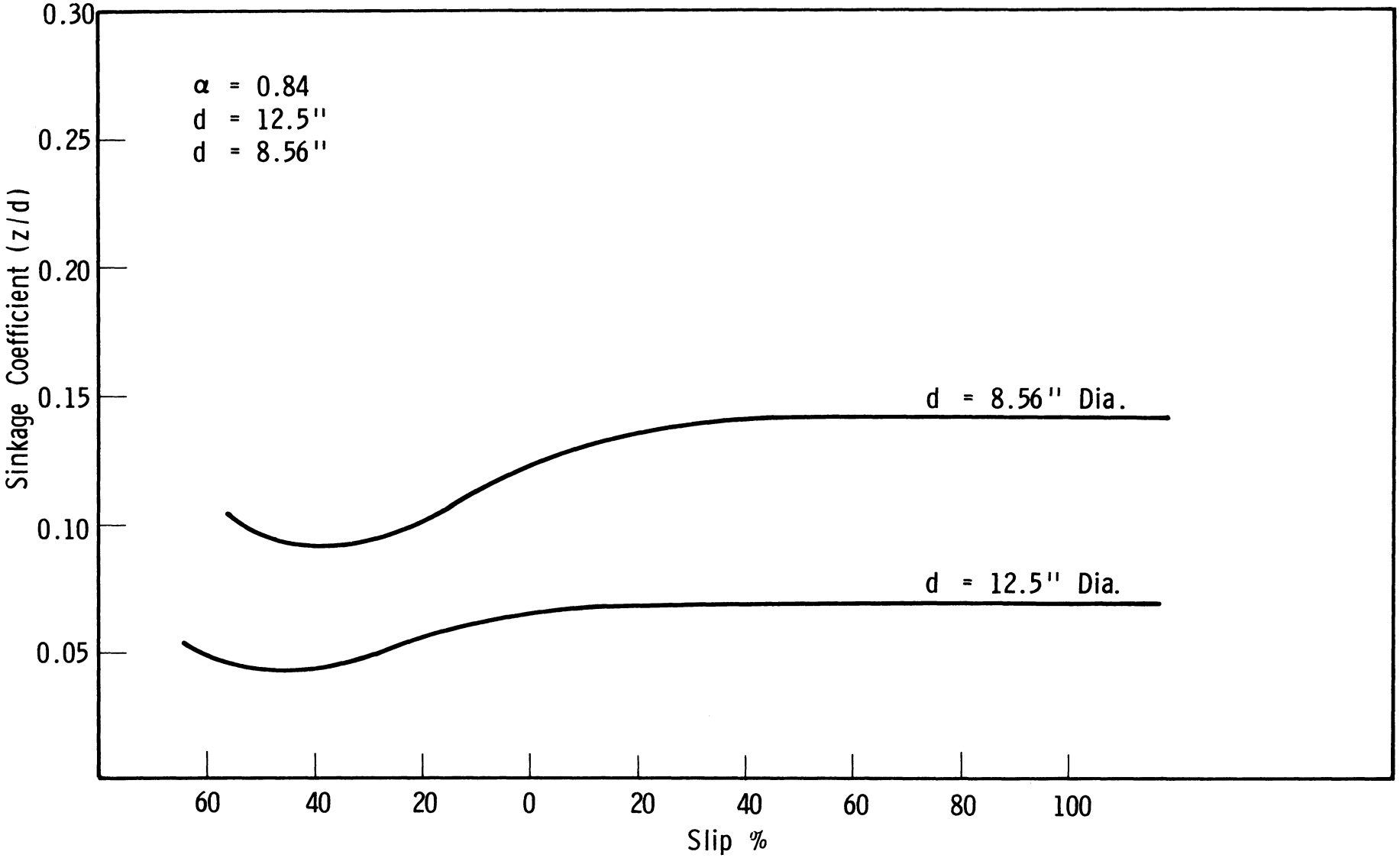

Fig. 68. Sinkage coefficient vs. slip for 12.5- and 8.56-in. dia wheels when load coefficient = 10.0, α = 0.84.

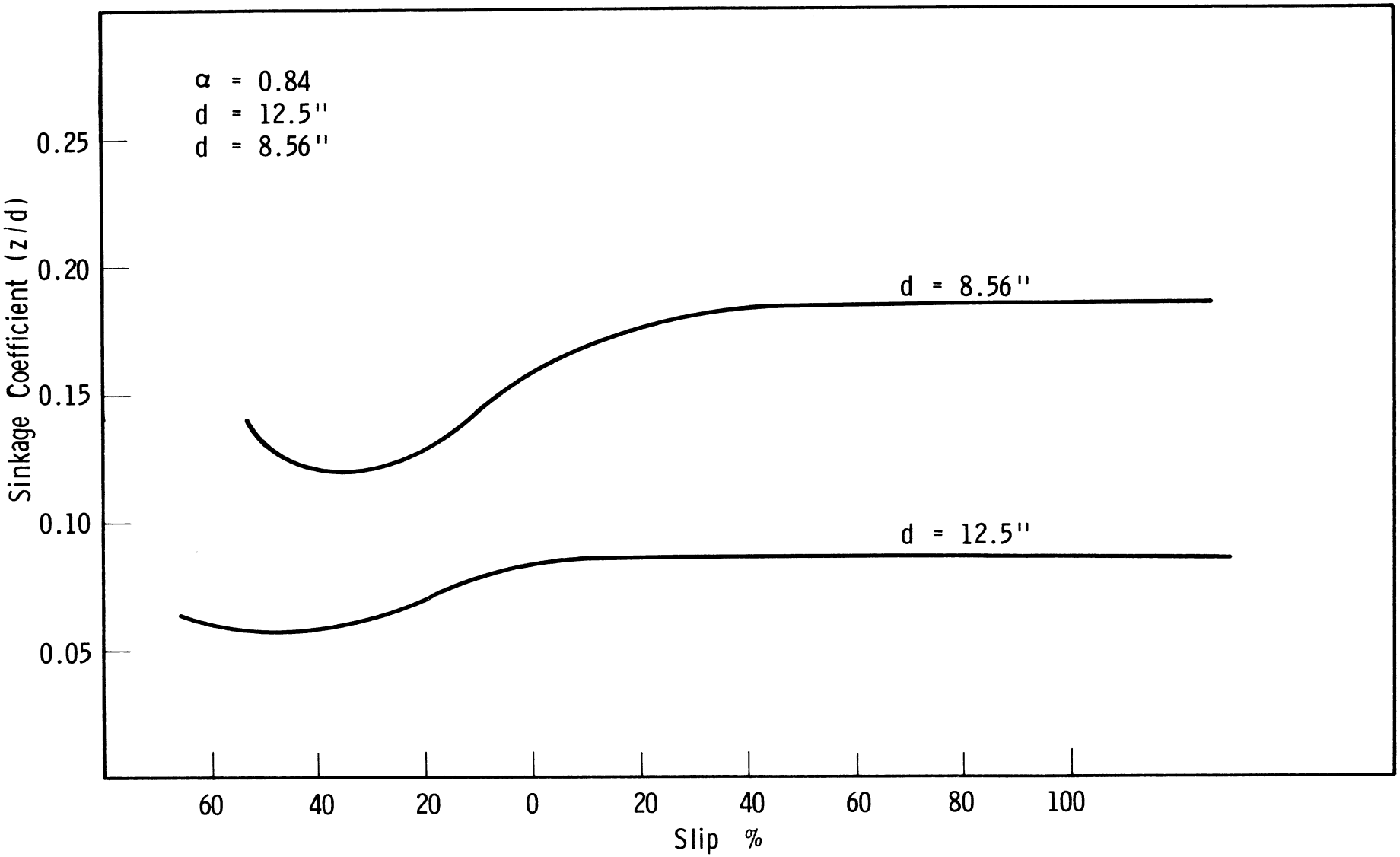

Fig. 69. Sinkage coefficient vs. slip for 12.5- and 8.56-in. dia wheels when load coefficient = 15.0, α = 0.84.

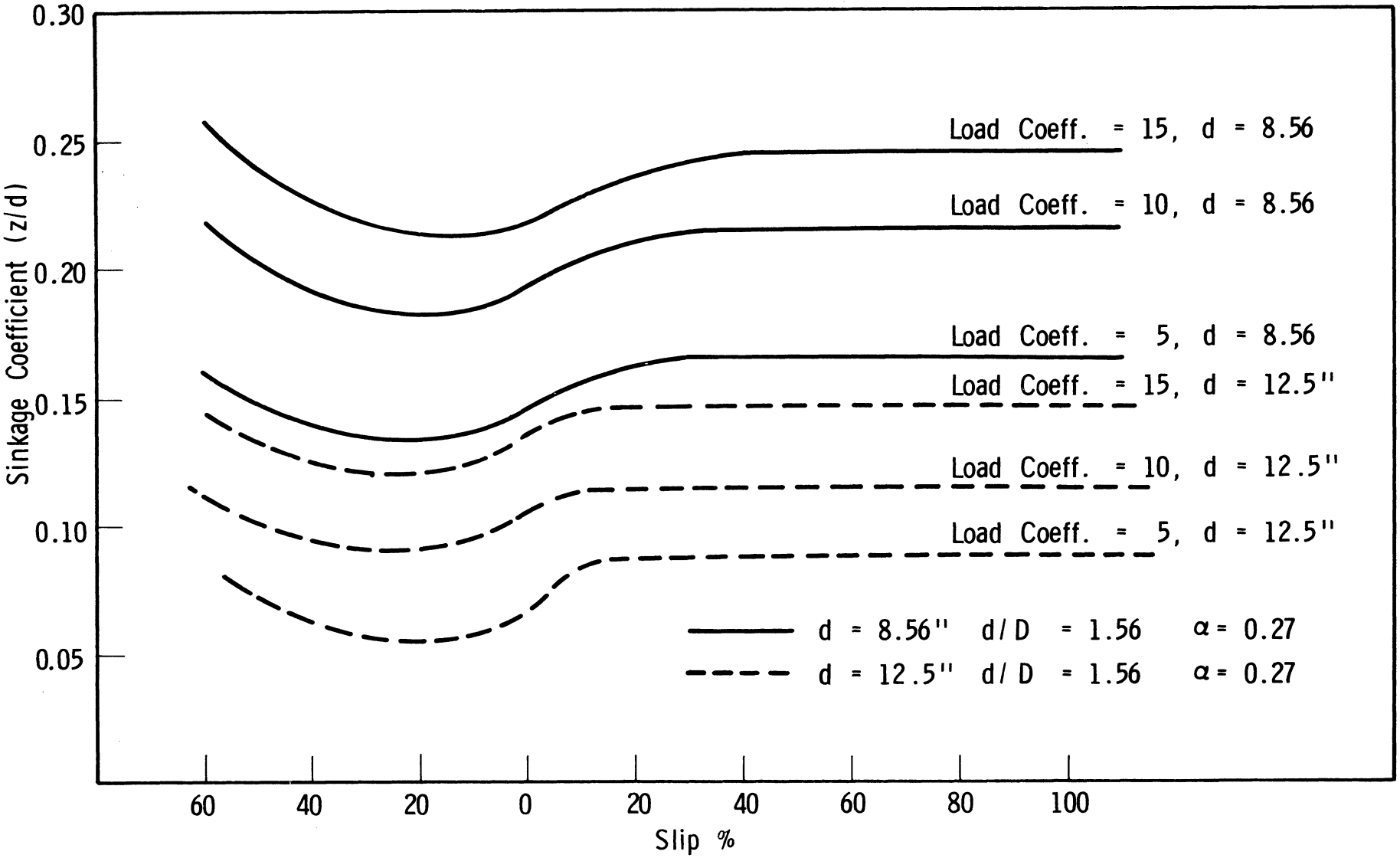

Fig. 70. Comparison of sinkage-coefficient for load coefficients of 5.0, 10.0, and 15.0 for α = 0.27, d = 12.5- and 8.56-in. dia wheels with d/D = 1.56.

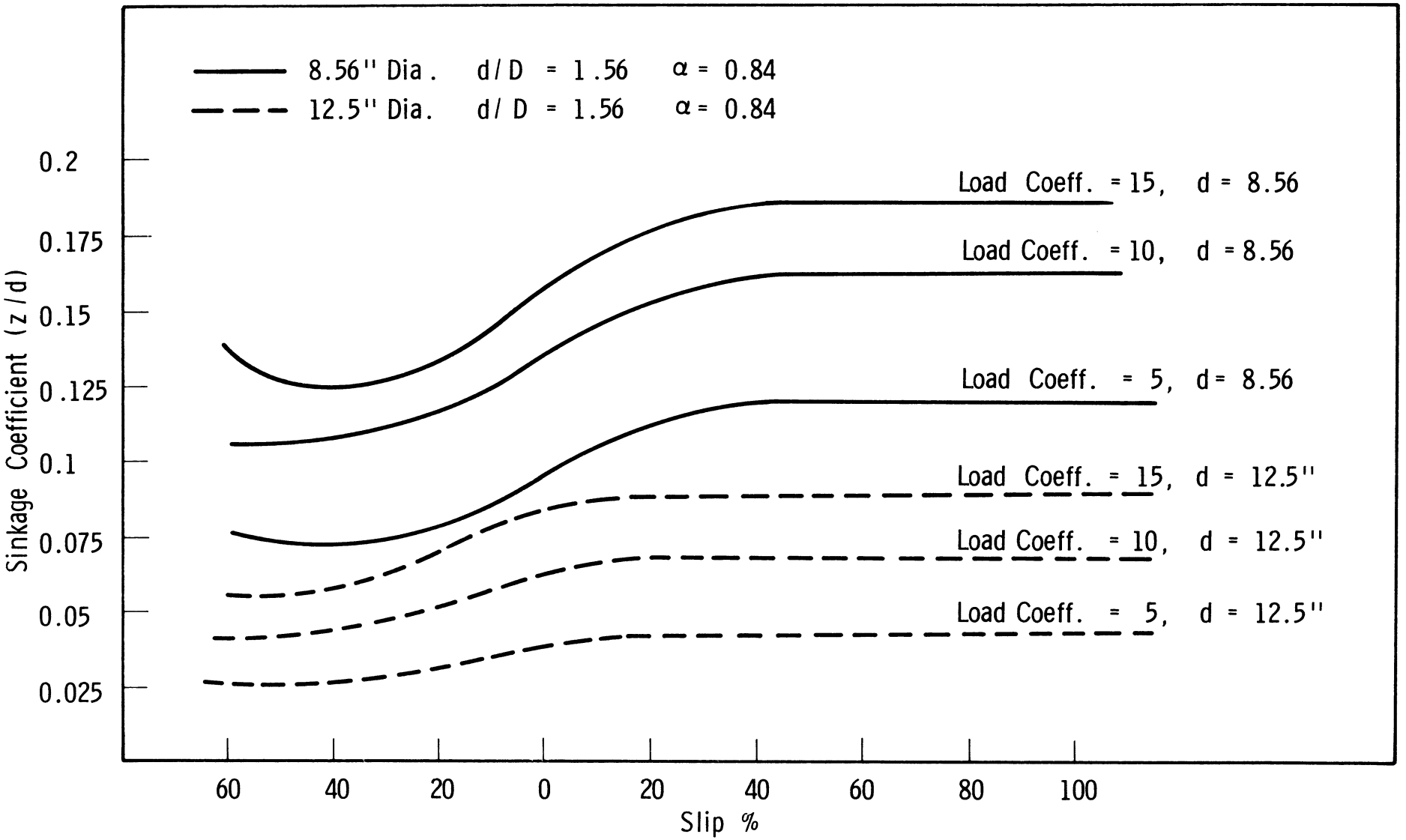

Fig. 71. Comparison of sinkage-coefficient for load coefficients of 5.0, 10.0, and 15.0 for α = 0.84, d = 12.5- and 8.56-in. dia wheels with d/D = 1.56.

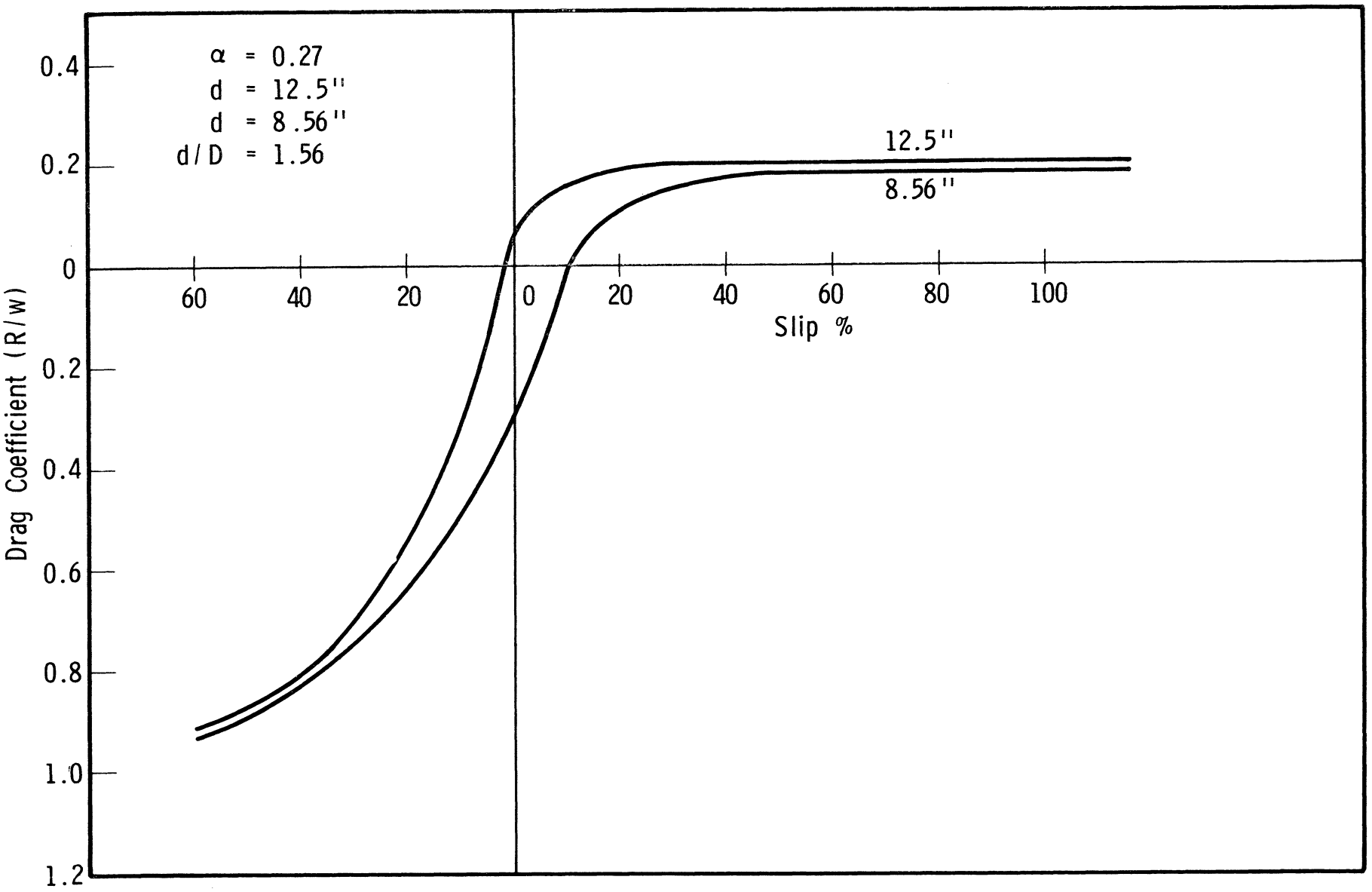

Fig. 72. Drag coefficient-slip for 12.5- and 8.56-in. dia wheels when $\alpha = 0.27$, d/D = 1.56, and load coefficient = 5.0.

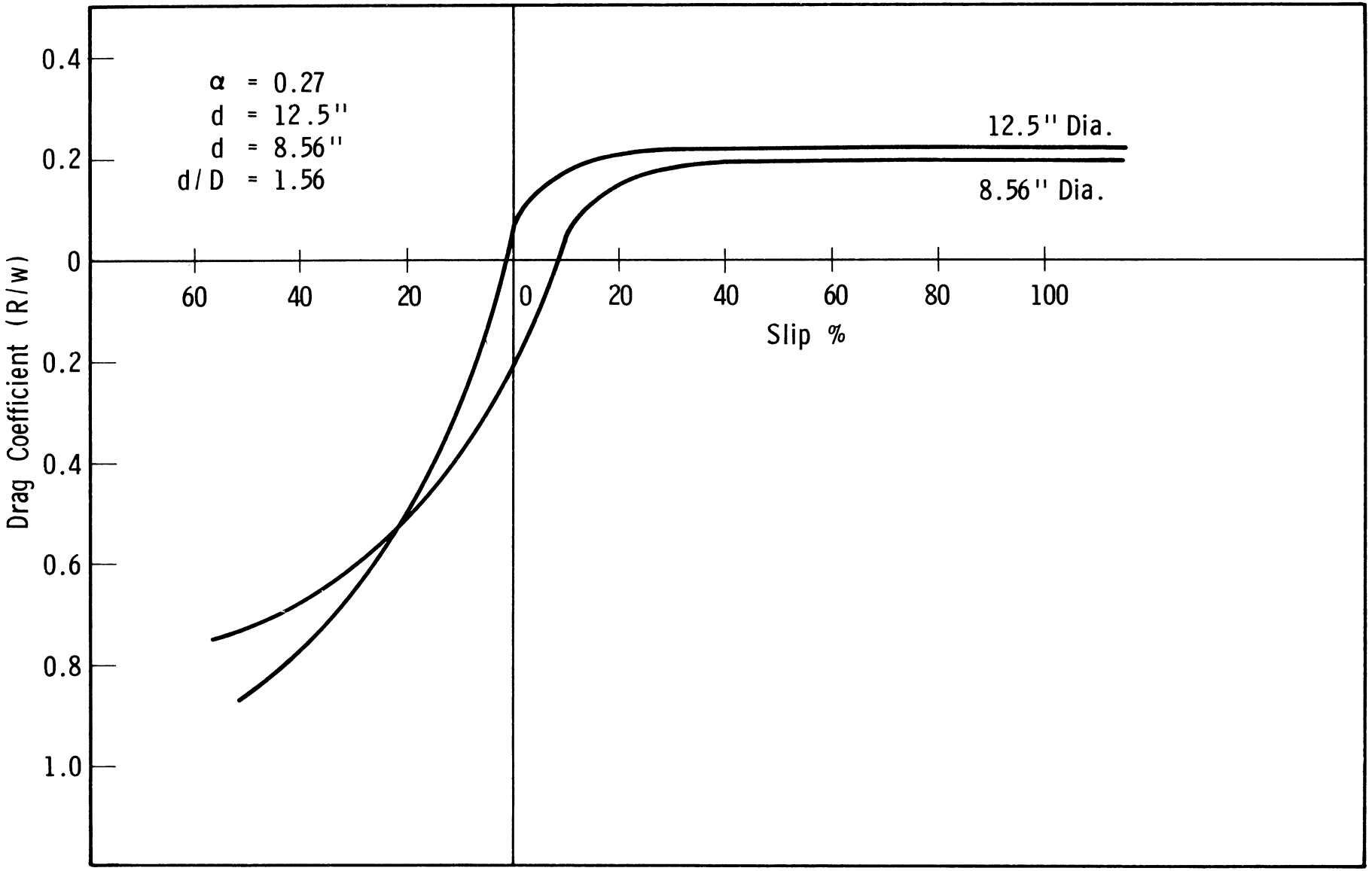

Fig. 73. Drag coefficient-slip for 12.5- and 8.56-in. dia wheels when $\alpha = 0.27$, $d/D = 1.56$, and load coefficient = 10.0

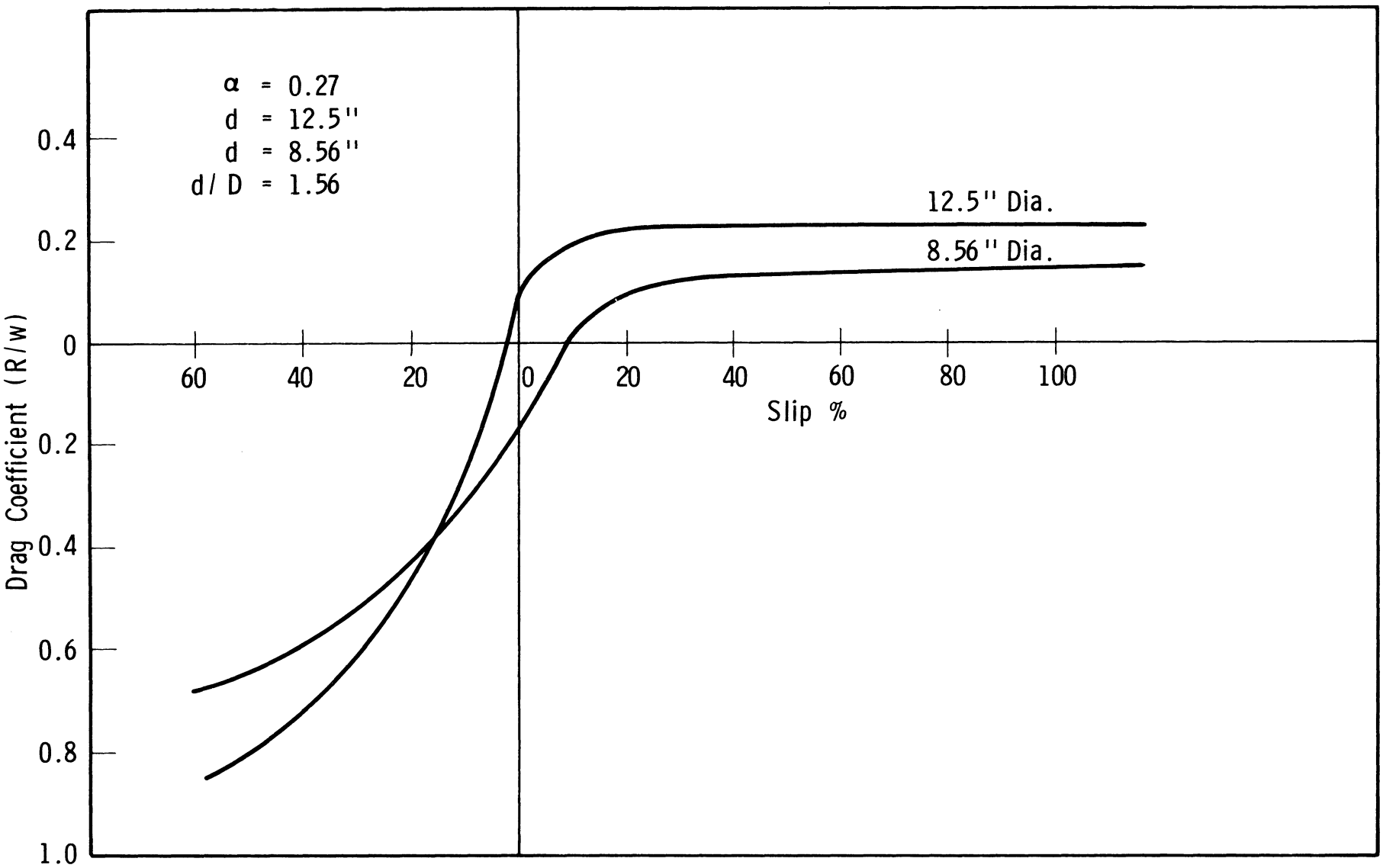

Fig. 74. Drag coefficient-slip for 12.5- nad 8.56-in. dia wheels when $\alpha = 0.27$, $d/D = 1.56$, and load coefficient = 15.0.

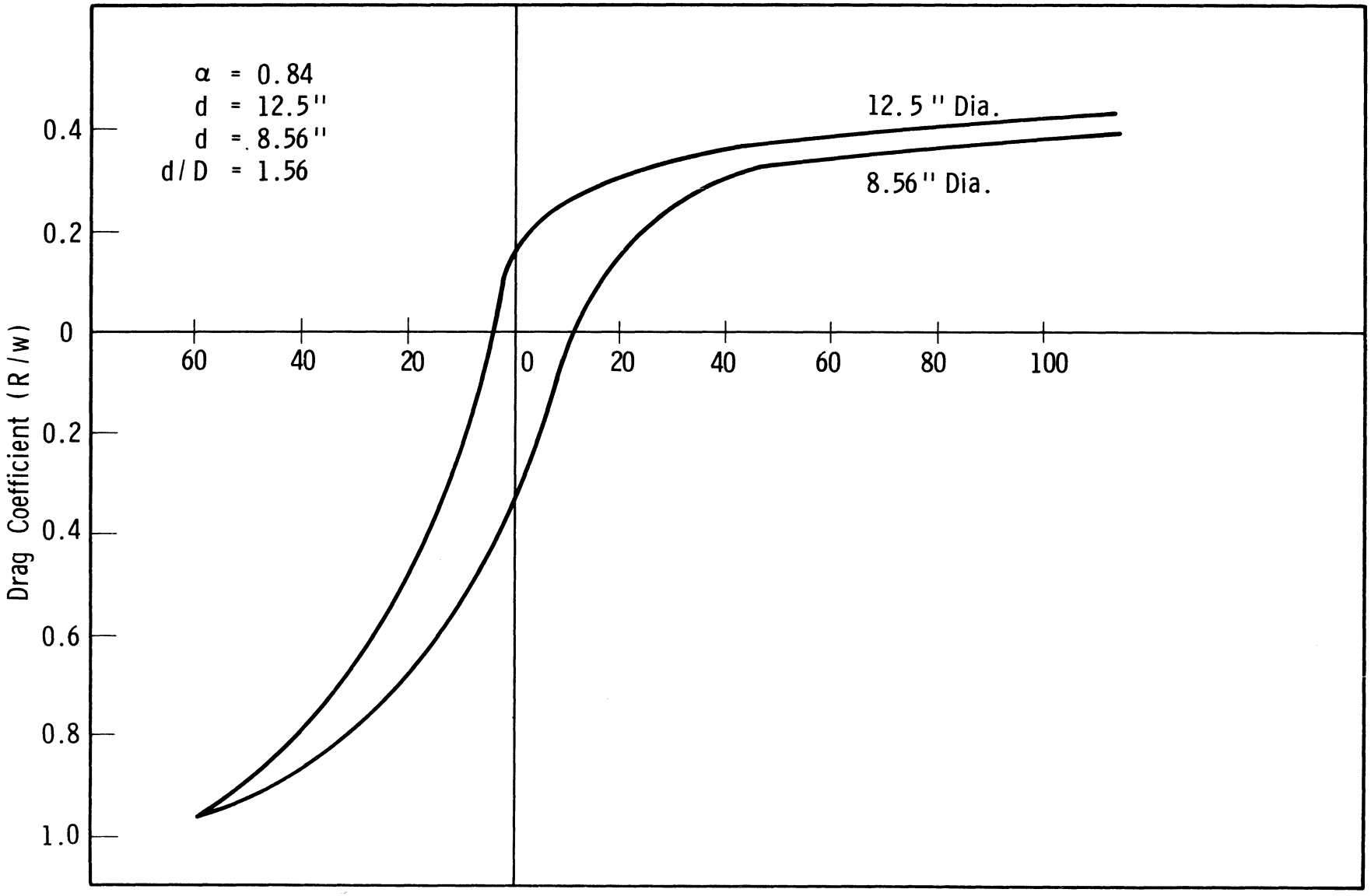

Fig. 75. Drag coefficient-slip for 12.5- and 8.56-in. dia wheels when $\alpha = 0.84$, $d/D = 1.56$, and load coefficient = 5.0.

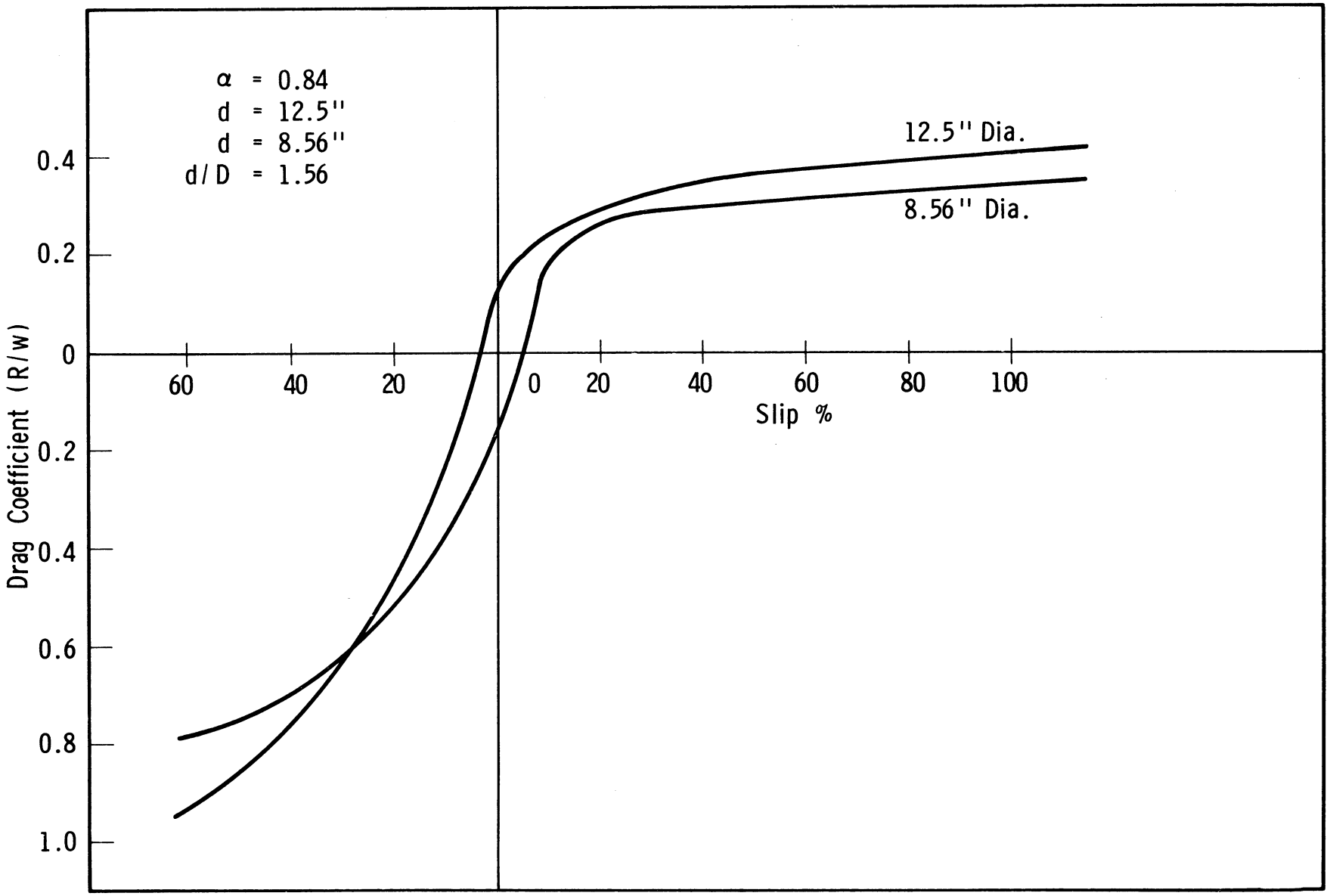

Fig. 76. Drag coefficient-slip for 12.5- and 8.56-in. dia wheels when $\alpha = 0.84$, $d/D = 1.56$, and load coefficient = 10.0.

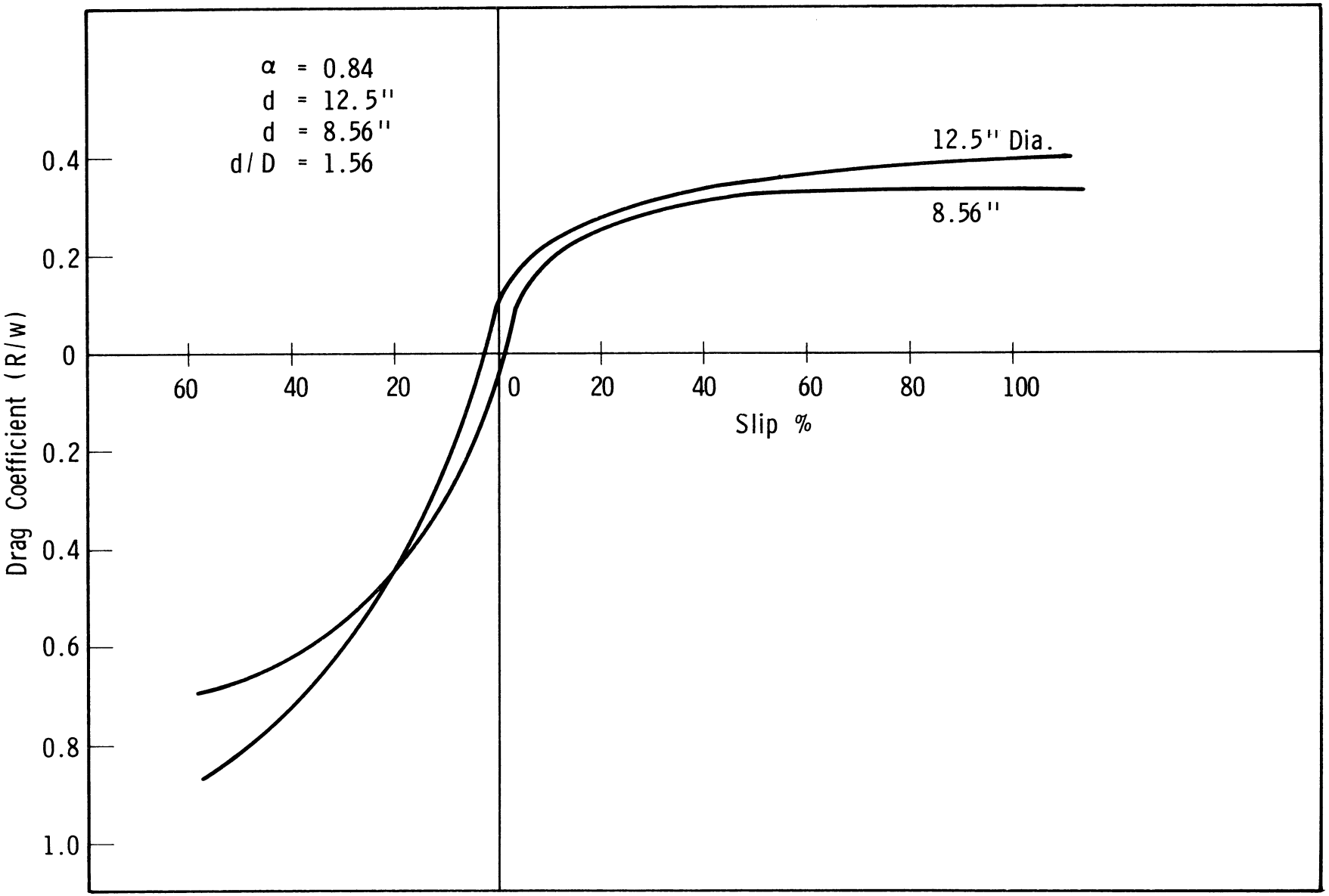

Fig. 77. Drag coefficient-slip for 12.5- and 8.56-in. dia wheels when $\alpha = 0.84$, $d/D = 1.56$, and load coefficient = 15.0.

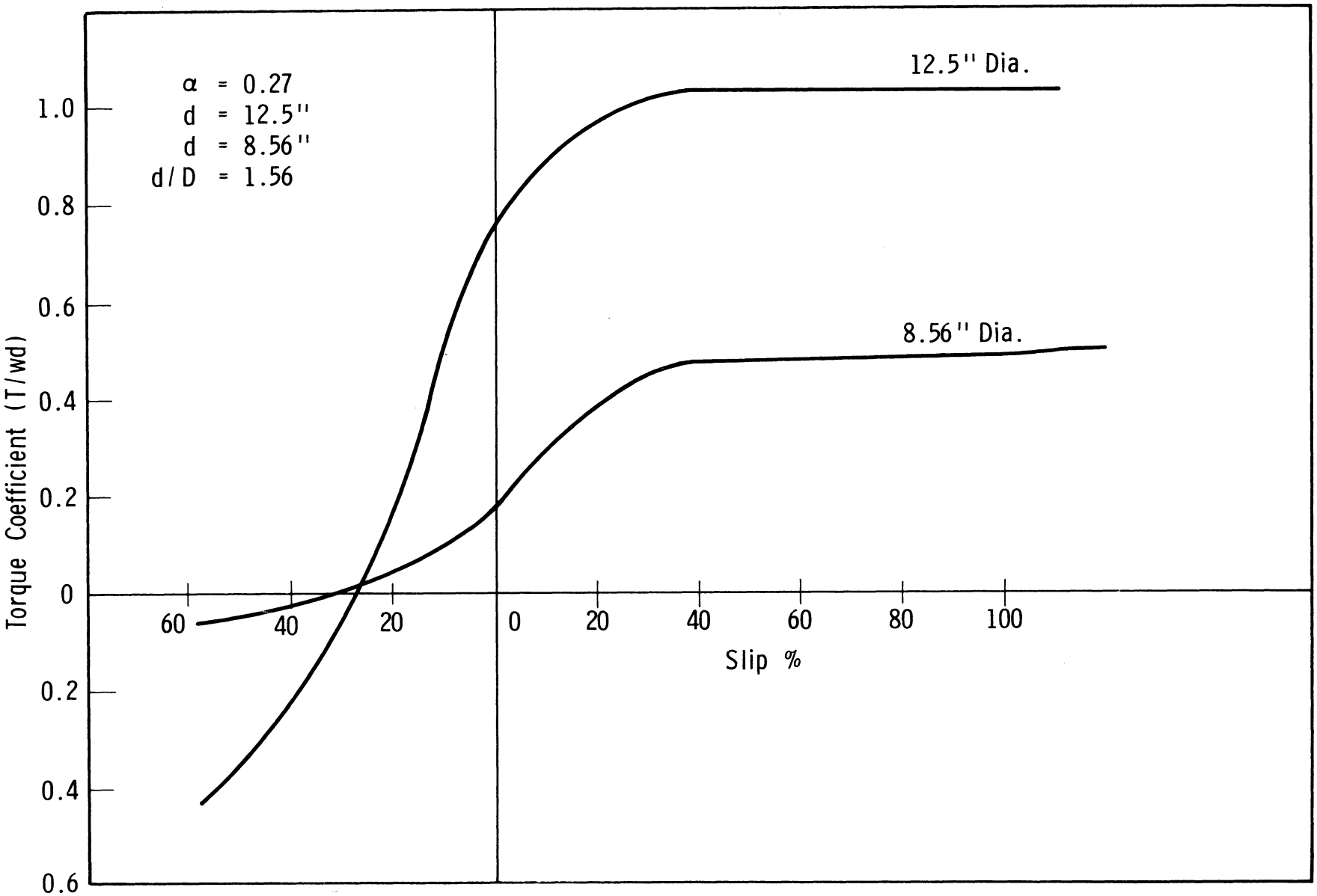

Fig. 78. Torque coefficient-slip for 12.5- and 8.56-in. dia wheels when $\alpha = 0.27$, $d/D = 1.56$, and load coefficient = 5.0.

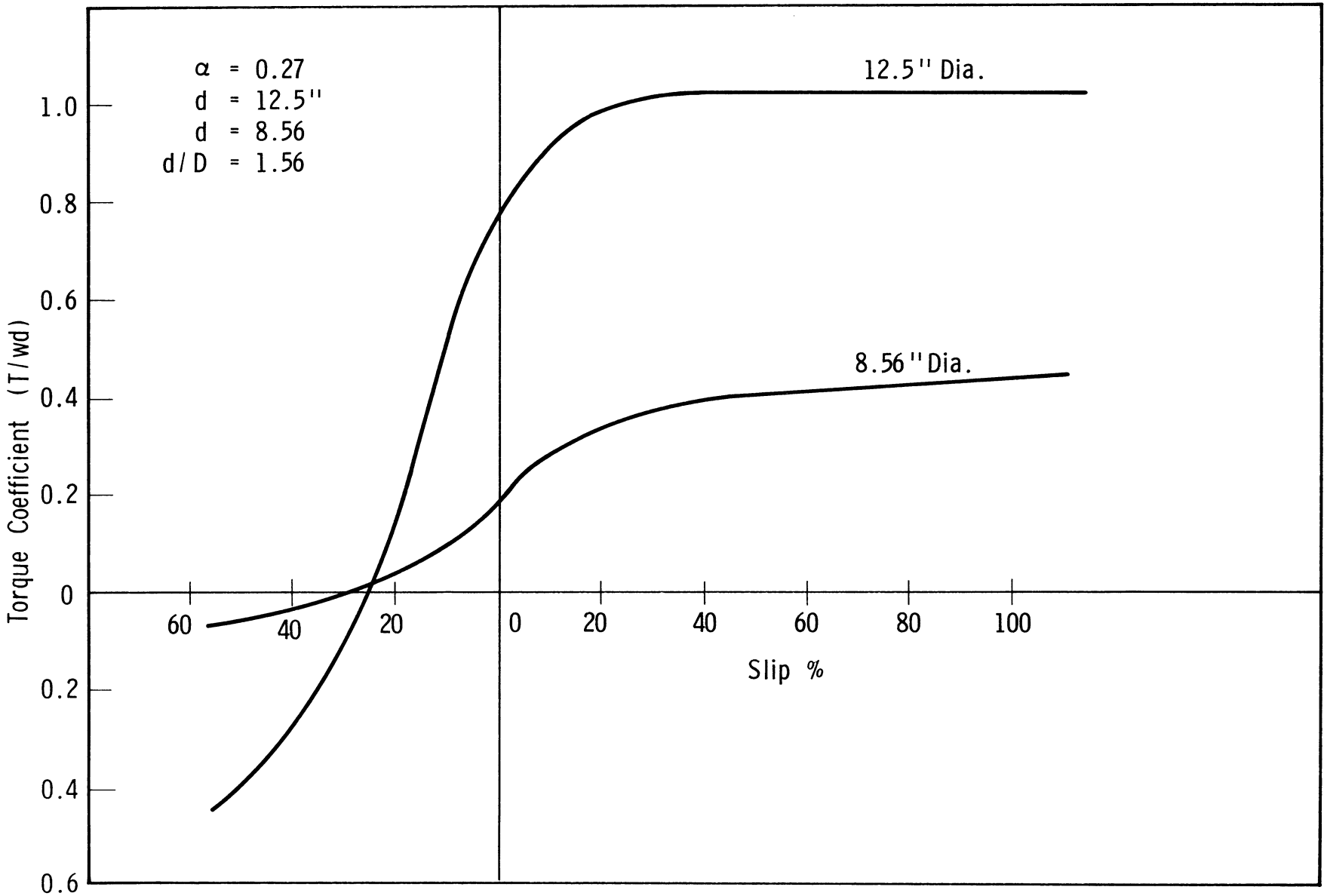

Fig. 79. Torque coefficient-slip for 12.5- and 8.56-in. dia wheels when $\alpha = 0.27$, $d/D = 1.56$, and load coefficient = 10.0.

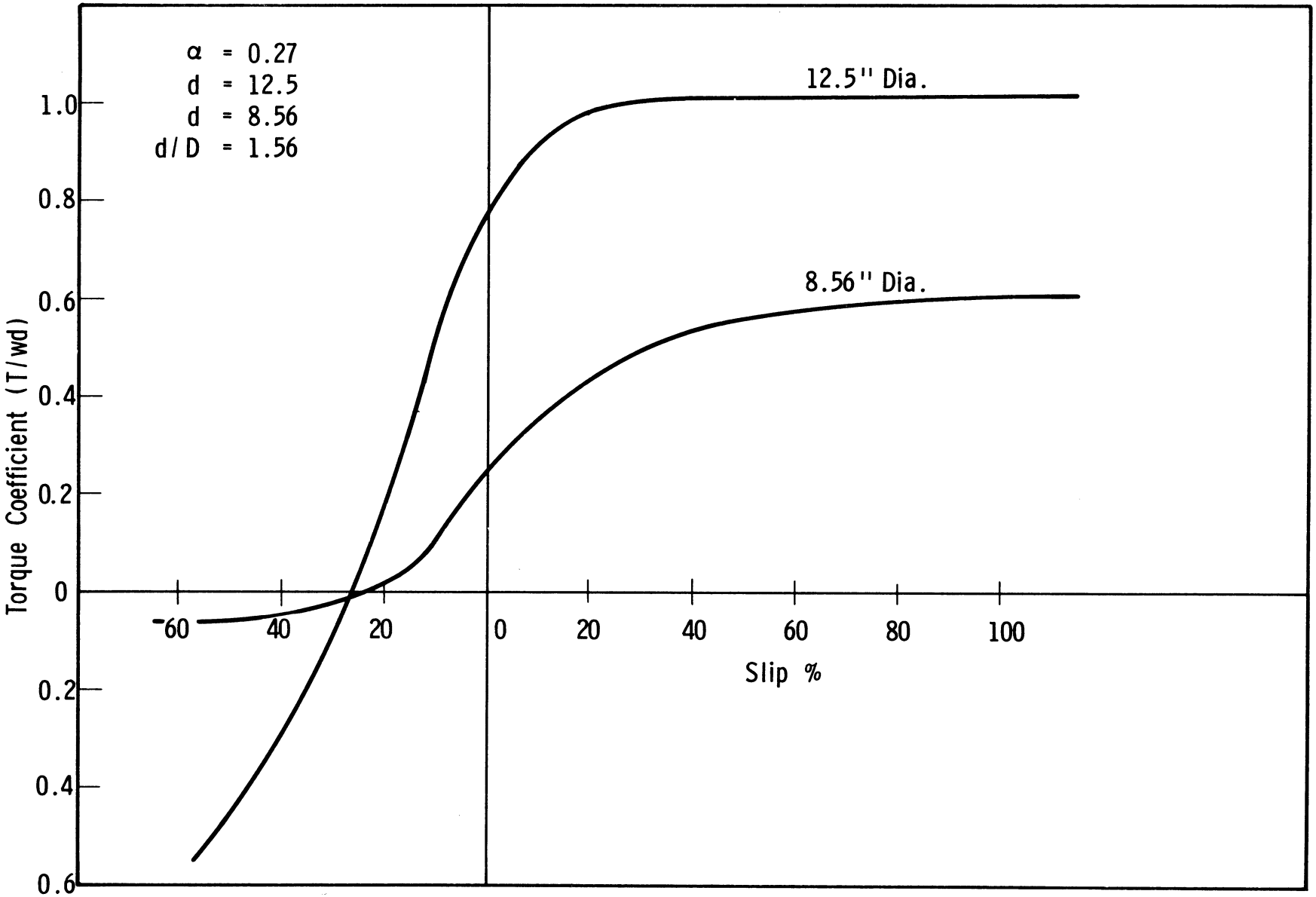

Fig. 80. Torque coefficient-slip for 12.5- and 8.56-in. dia wheels when $\alpha = 0.27$, $d/D = 1.56$, and load coefficient = 15.0.

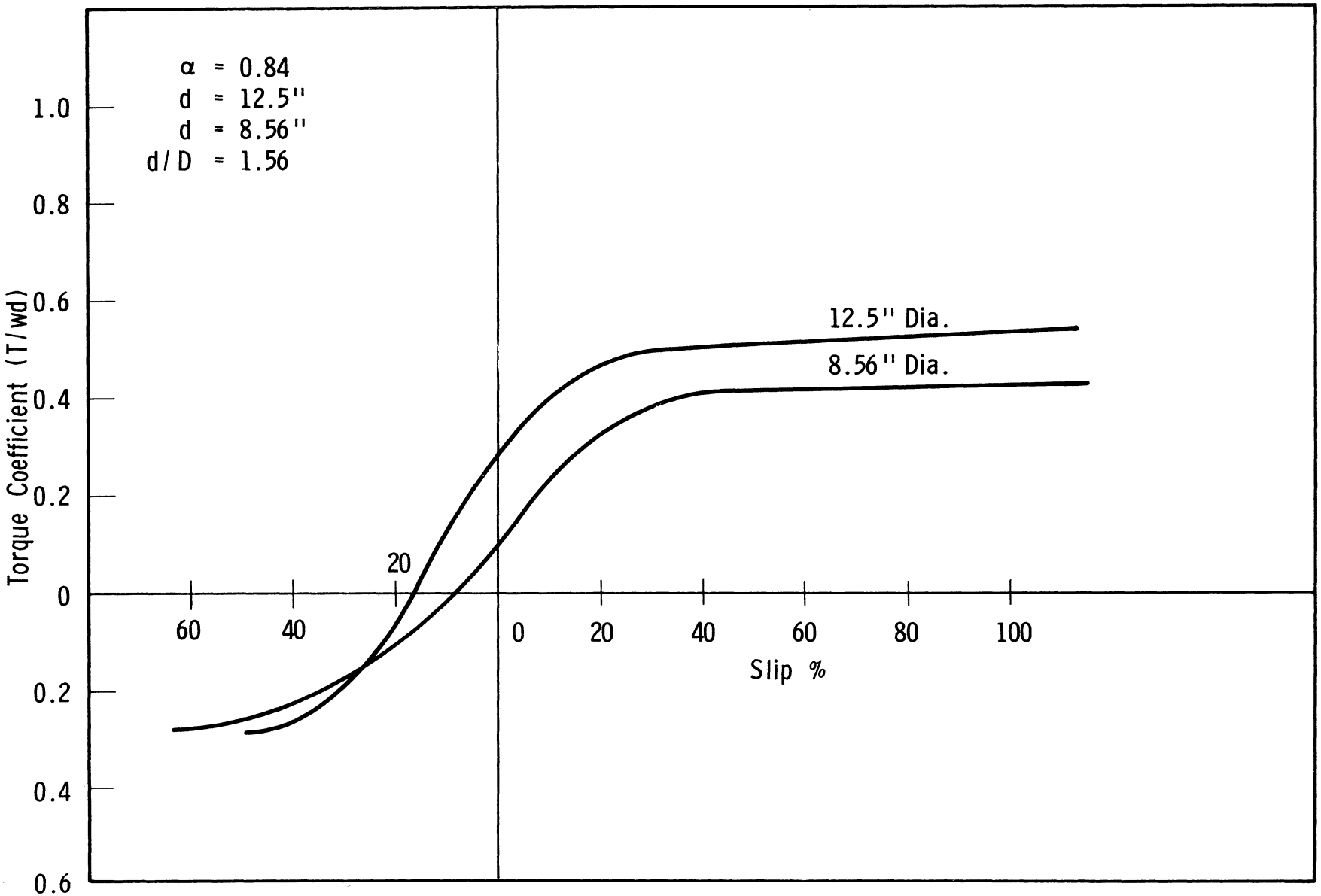

Fig. 81. Torque coefficient-slip for 12.5- and 8.56-in. dia wheels when $\alpha = 0.84$, $d/D = 1.56$, and load coefficient = 5.0.

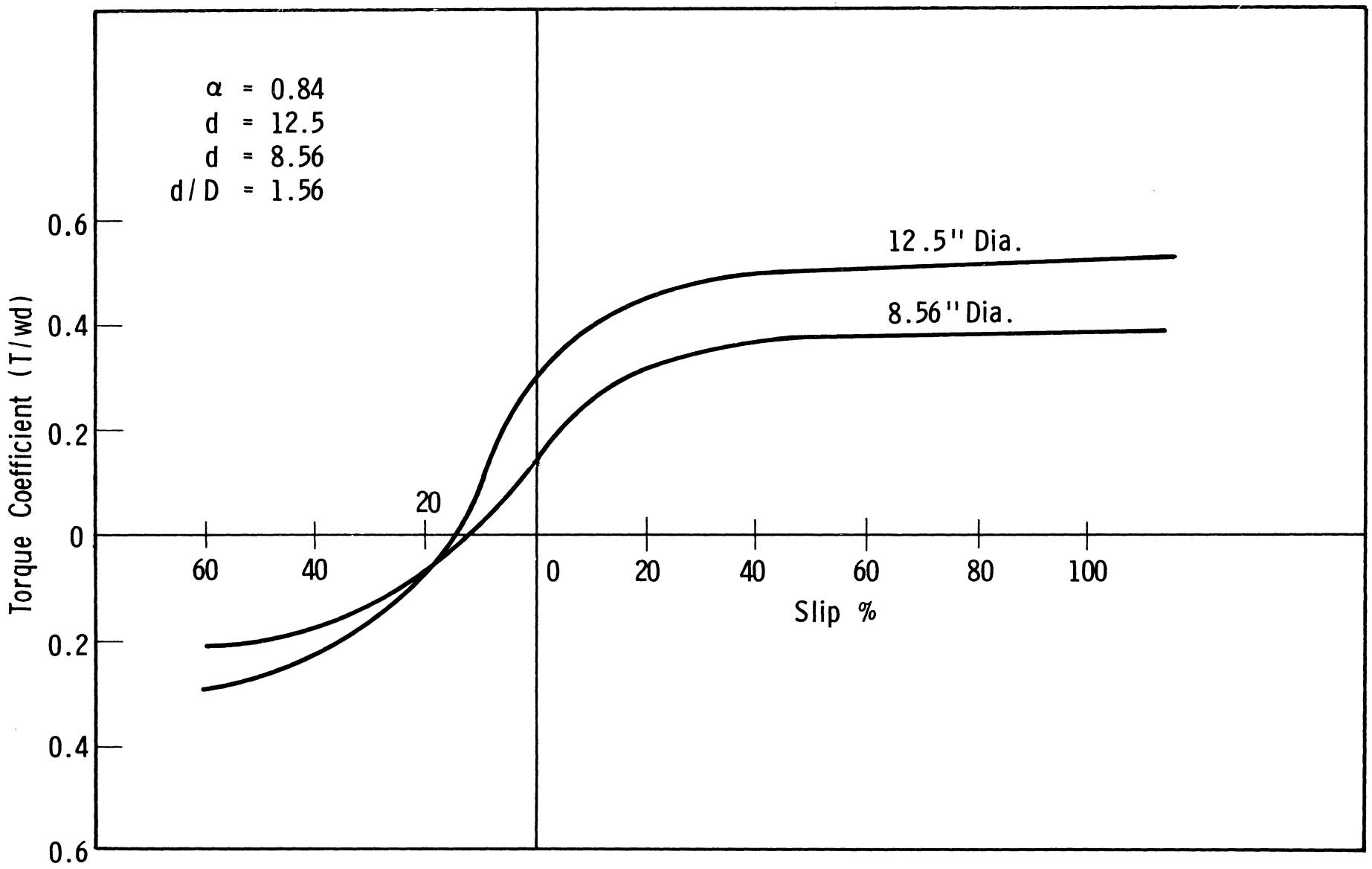

Fig. 82. Torque coefficient-slip for 12.5- and 8.56-in. dia wheels when $\alpha = 0.84$, $d/D = 1.56$, and load coefficient = 10.0.

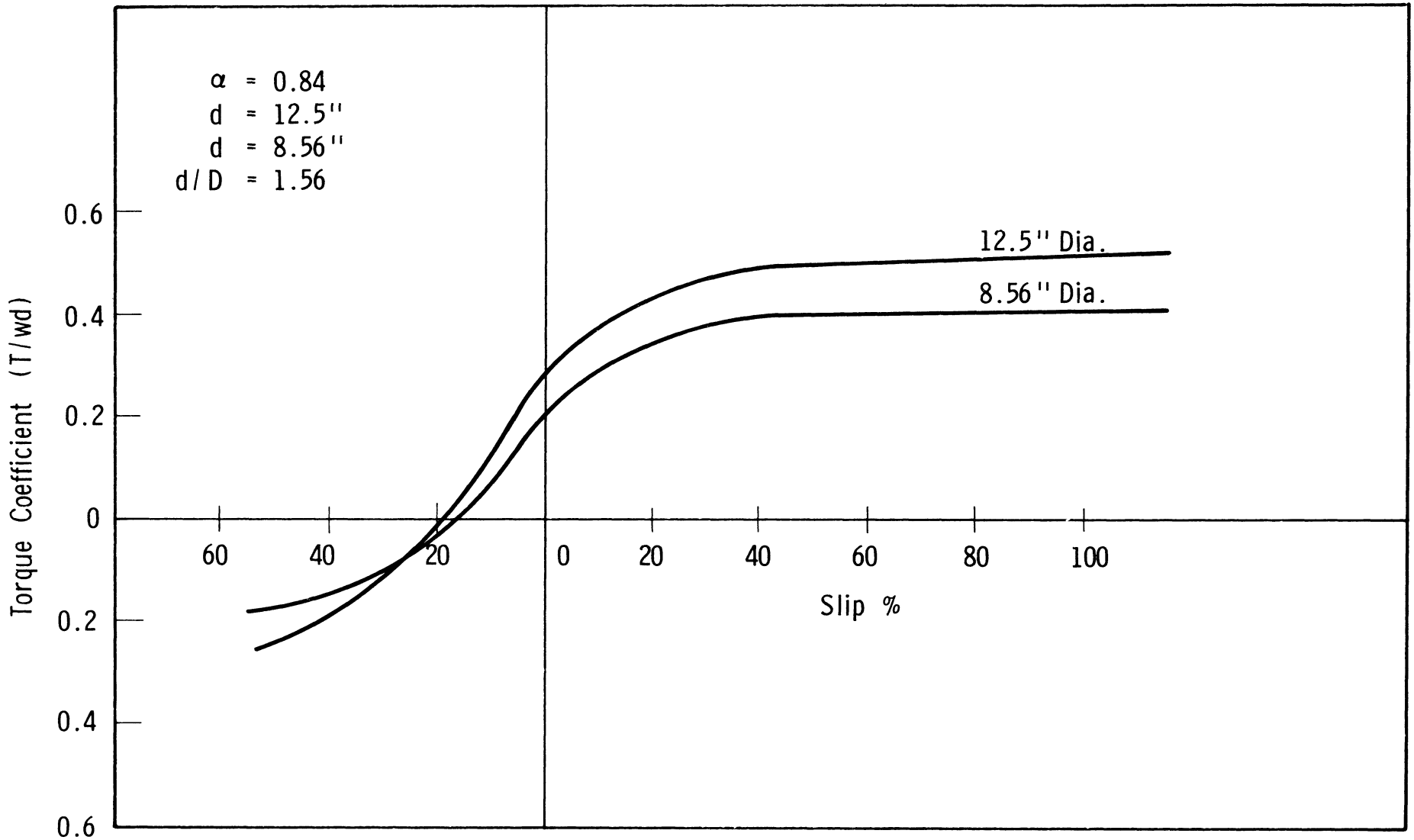

Fig. 83. Torque coefficient-slip for 12.5- and 8.56-in. dia wheels when $\alpha = 0.84$, $d/D = 1.56$, and load coefficient = 15.0.

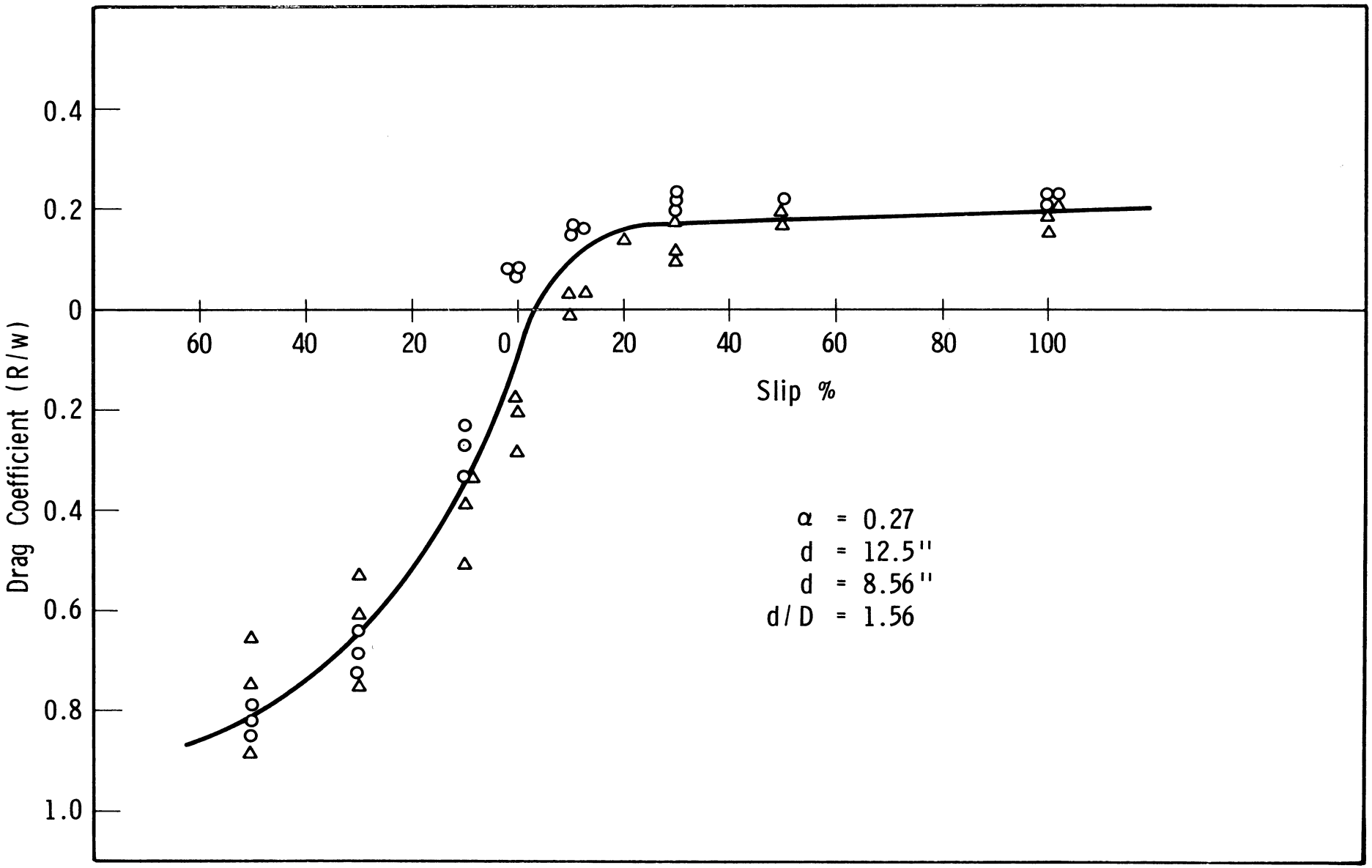

Fig. 84. Dimensionless plot of drag coefficient for load coefficients of 5.0, 10.0, and 15.0 when d = 12.5 and 8.56 in., d/D = 1.56, α = 0.27.

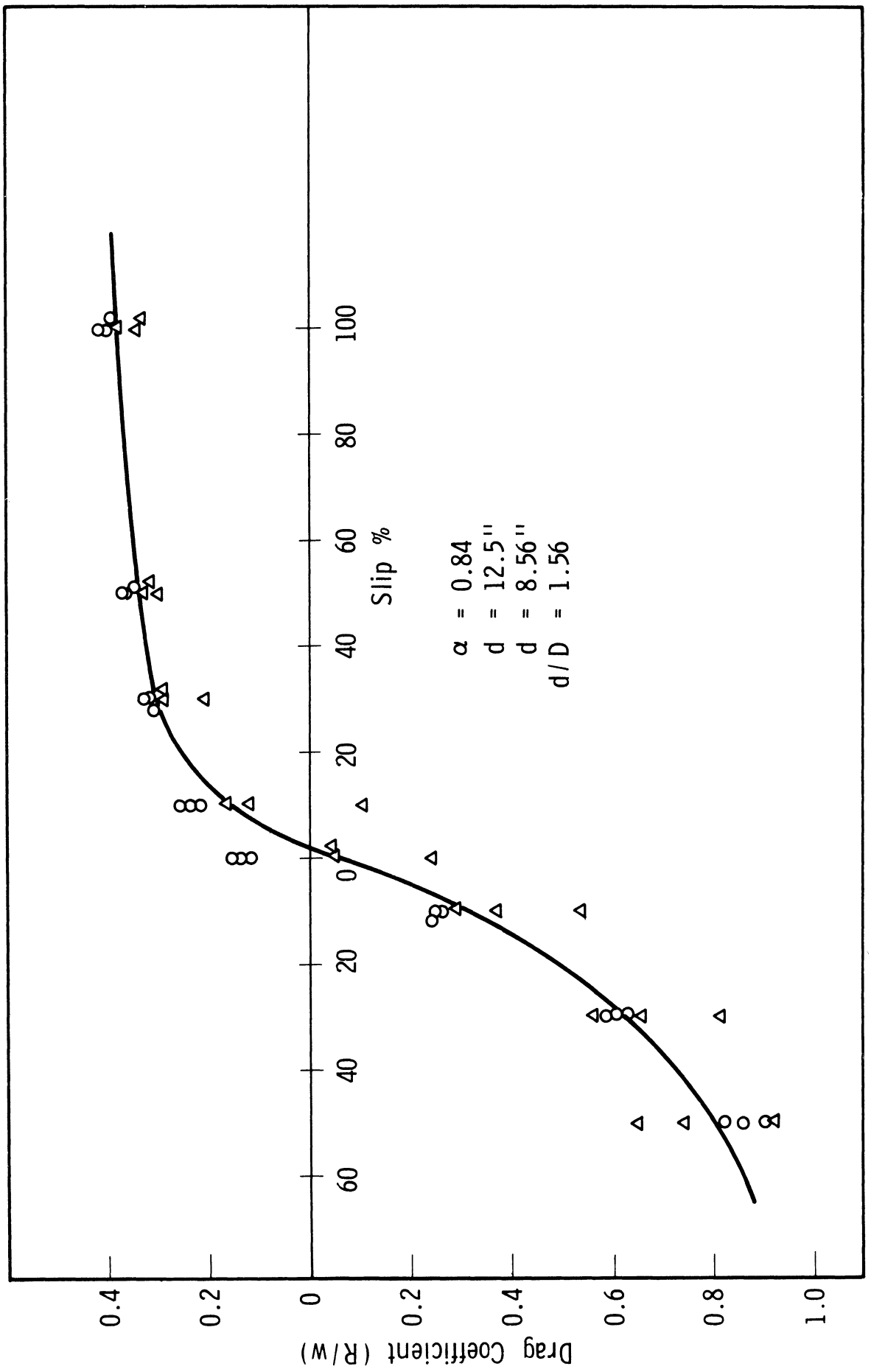

Fig. 85. Dimensionless plot of drag coefficient for load coefficients of 5.0, 10.0, and 15.0 when d = 12.5 and 8.56 in., d/D = 1.56, α = 0.84.

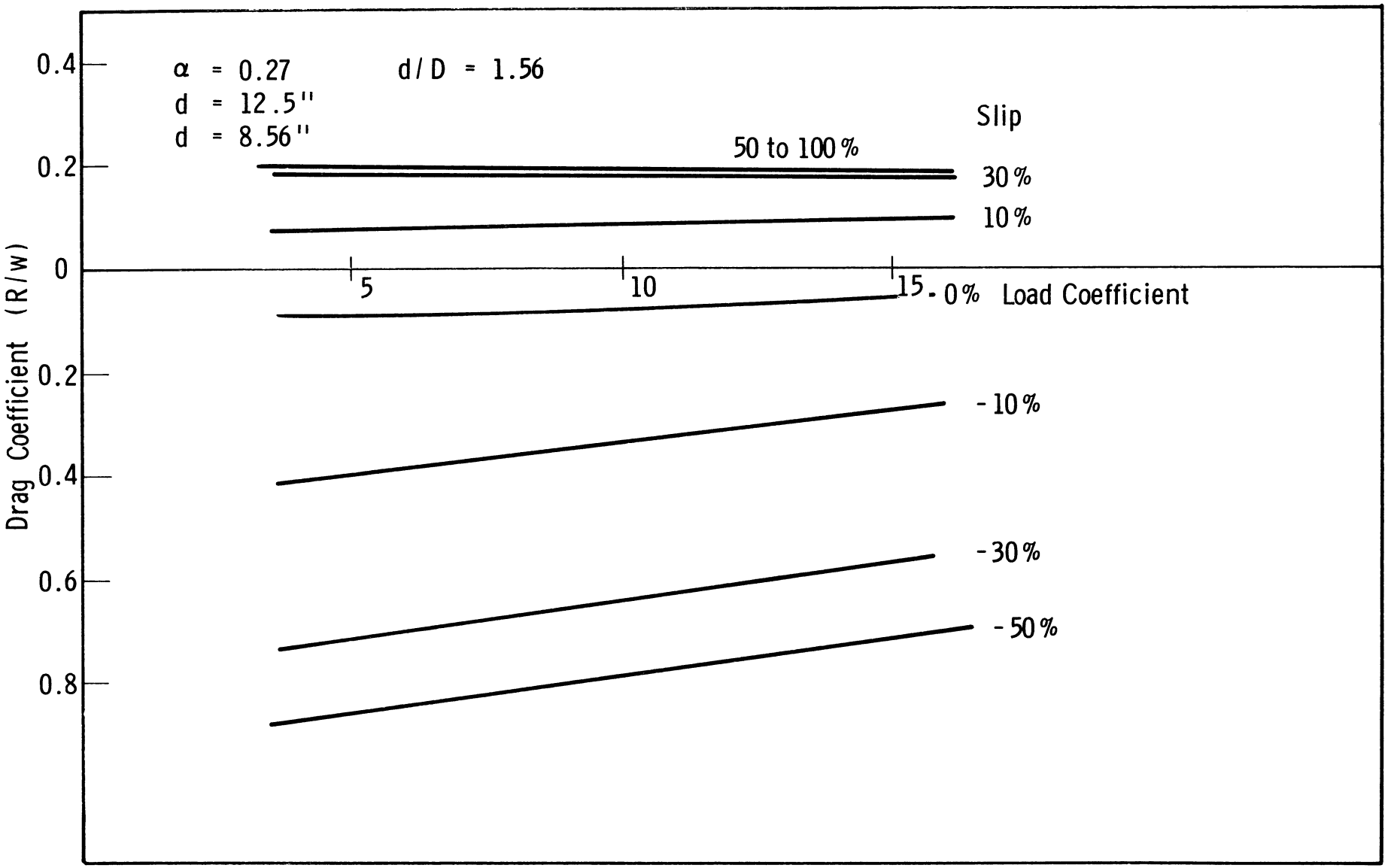

Fig. 86. Average drag coefficient-load coefficient curves for various slips when d = 12.5 and 8.56 in., d/D = 1.56, α = 0.27.

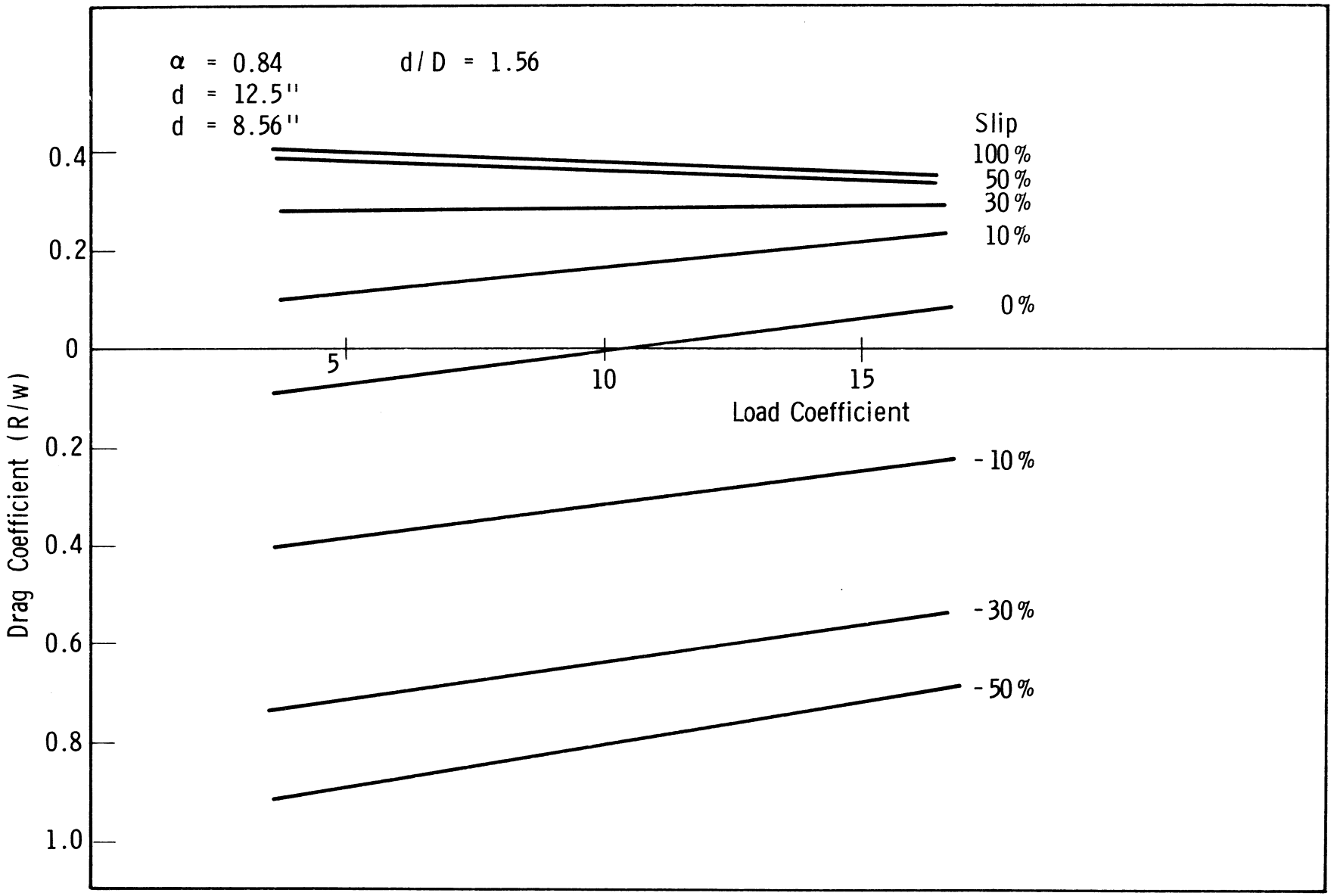

Fig. 87. Average drag coefficient-load coefficient curves for various slips when d = 12.5 and 8.56 in., d/D = 1.56, α = 0.84.

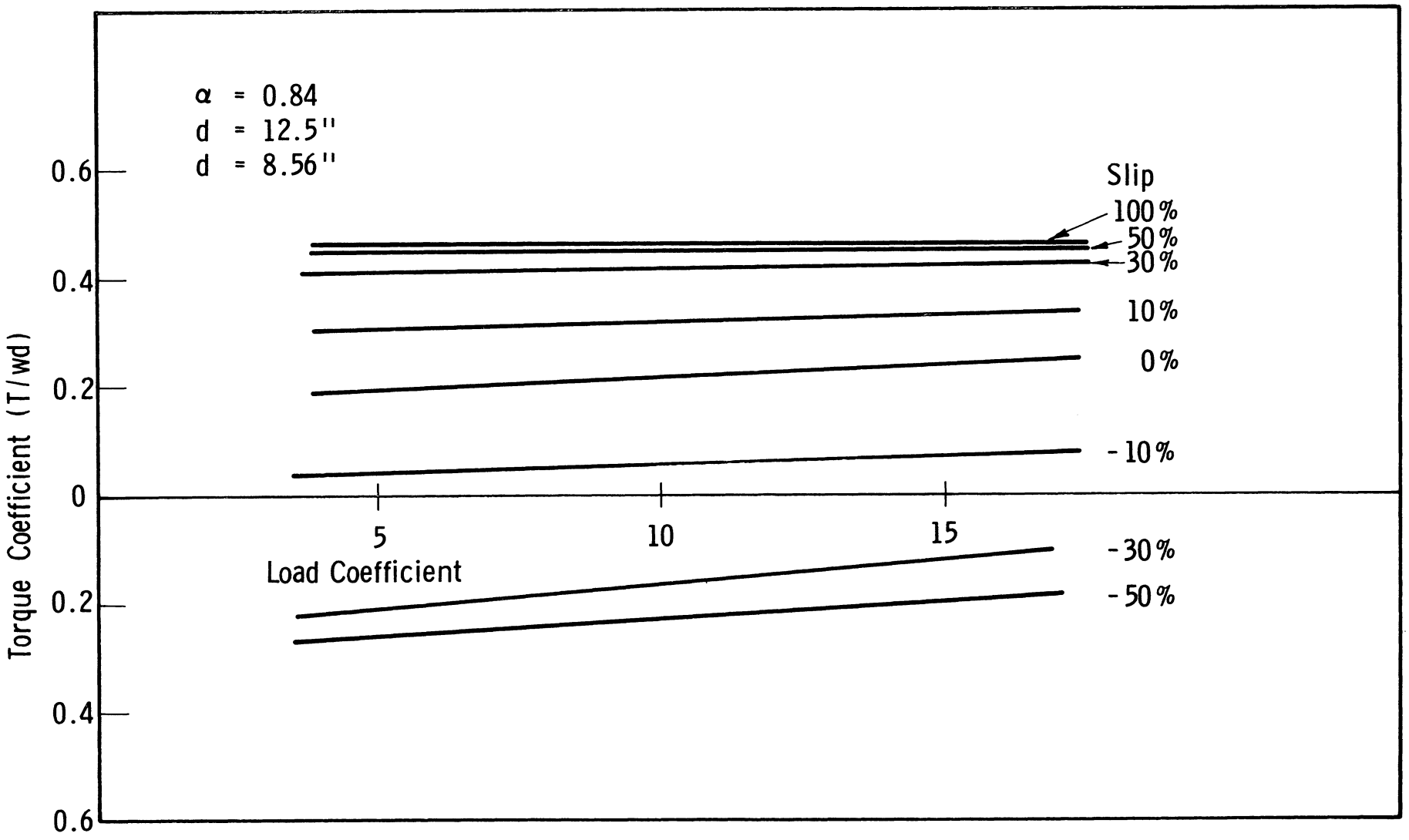

Fig. 88. Average torque coefficient-load coefficient curves for various slips when α = 0.27, d = 12.5 and 8.56 in., d/D = 1.56.

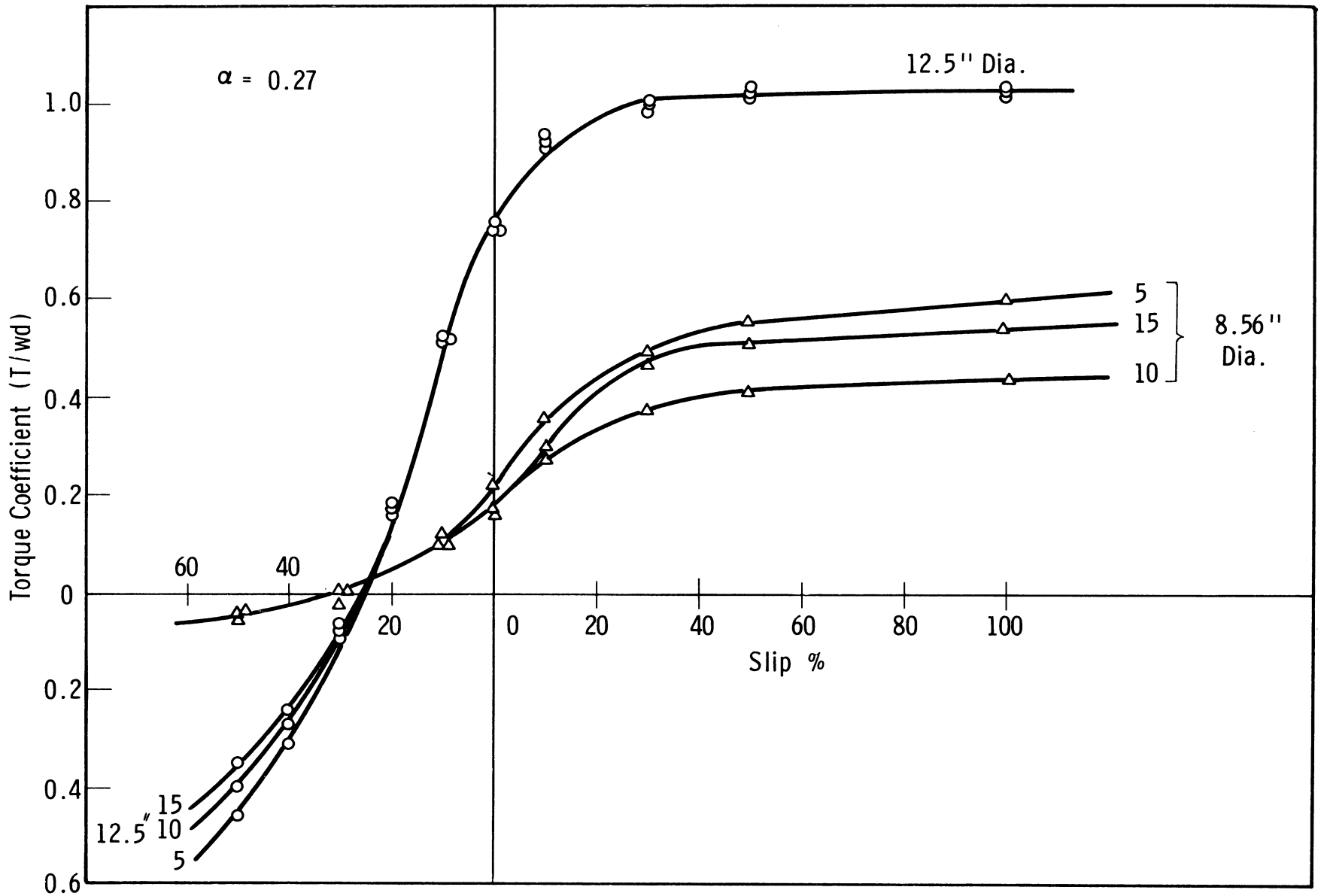

Fig. 89. Torque coefficient-slip curves for load coefficients of 5.0, 10.0, and 15.0 when α = 0.27, d = 12.5 and 8.56 in.

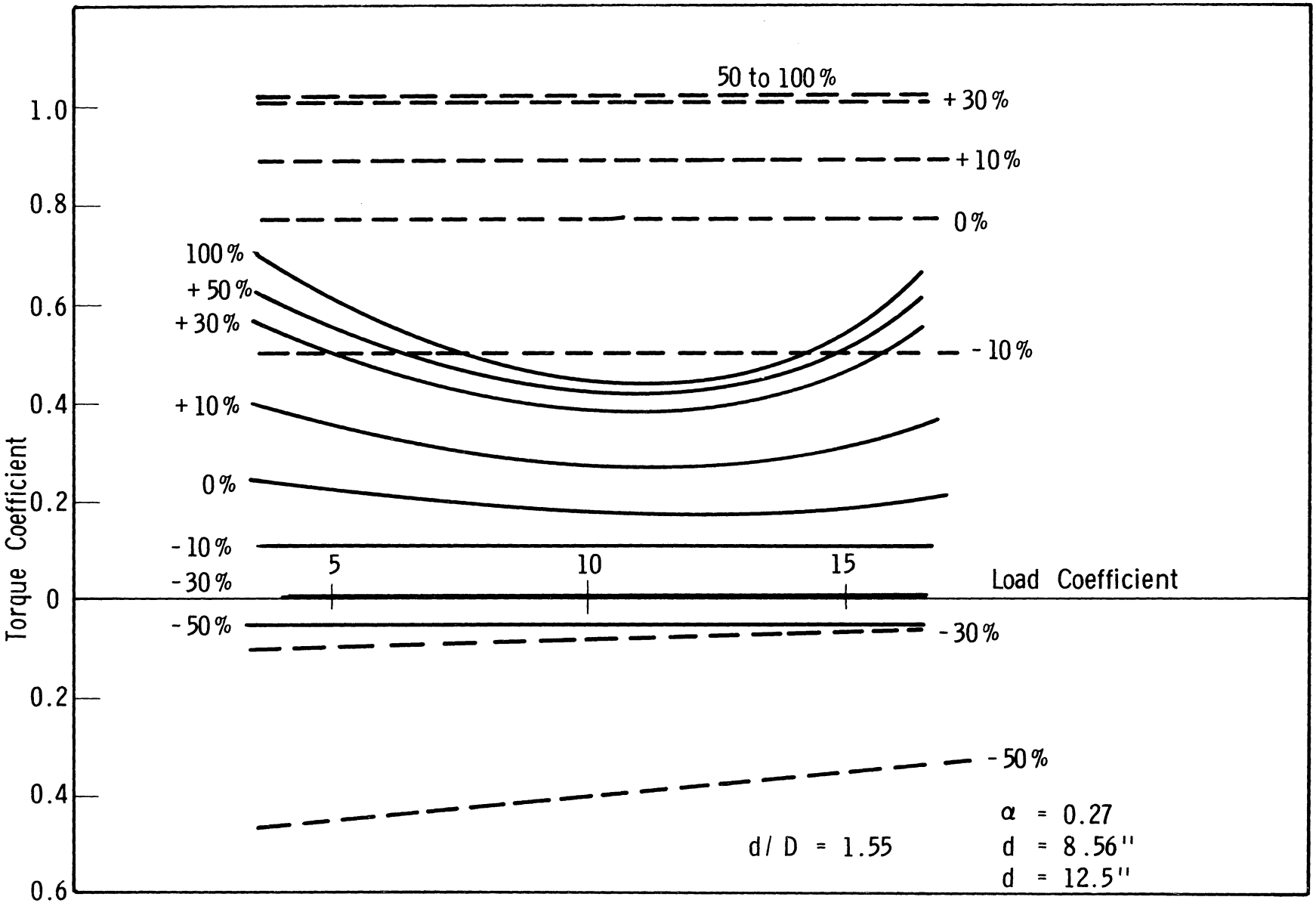

Fig. 90. Torque coefficient-load curves for $\alpha = 0.27$, d = 12.5 and 8.56 in., d/D = 1.56 at various slips.

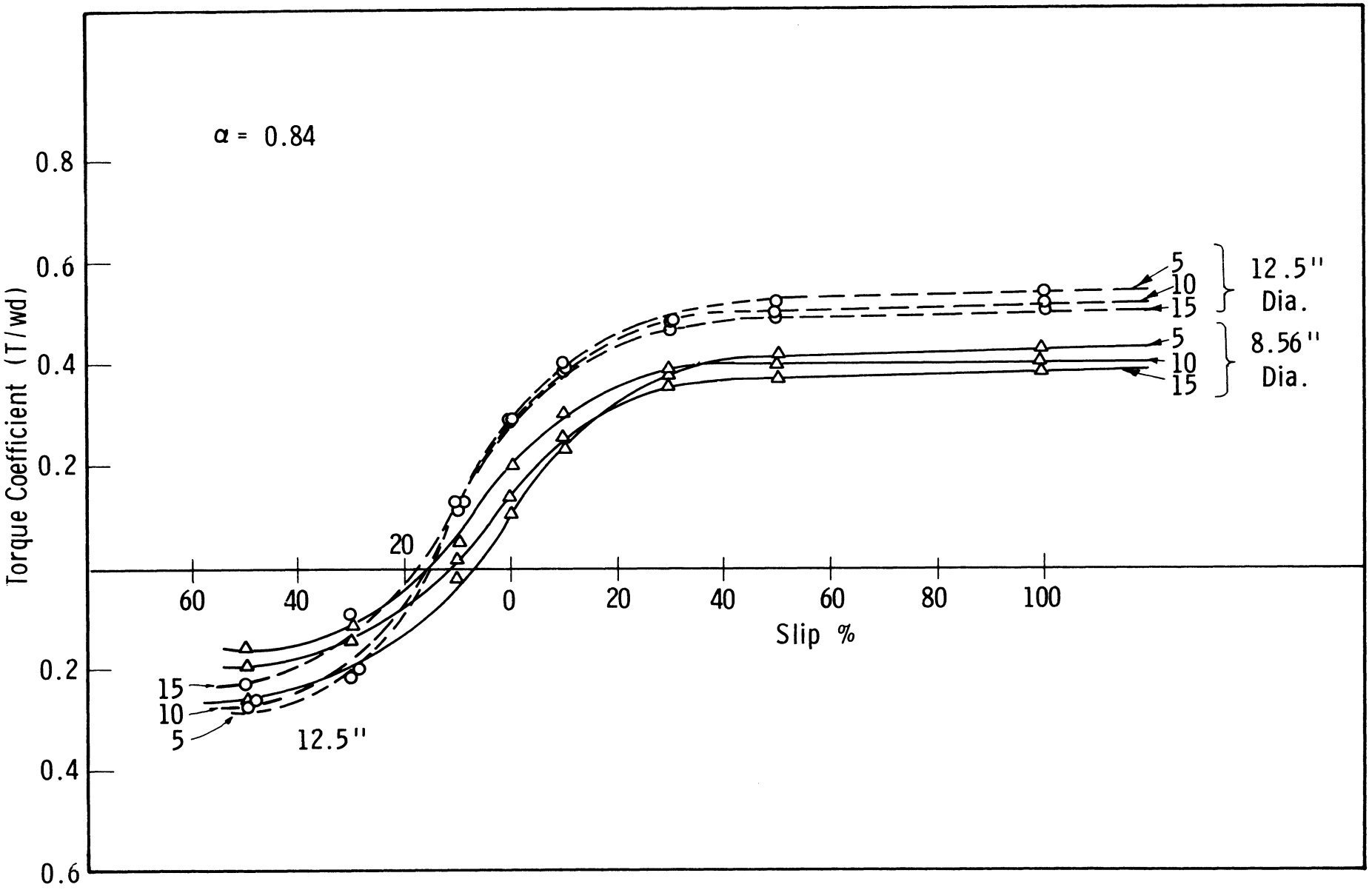

Fig. 91. Torque coefficient-slip curves for load coefficients of 5.0, 10.0, and 15.0 when α = 0.84.

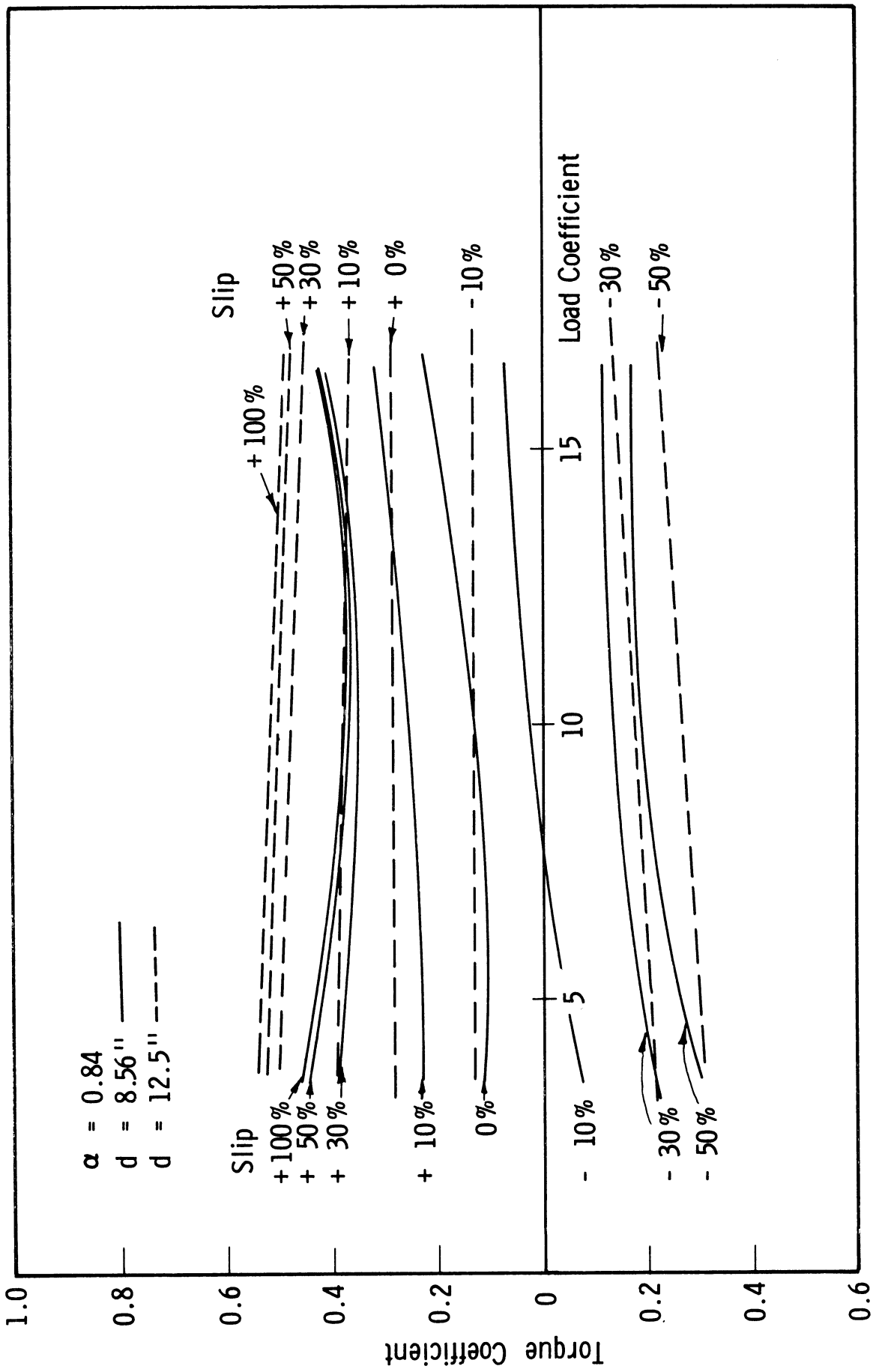

Fig. 92. Torque coefficient-load coefficient curves for $\alpha = 0.84$.

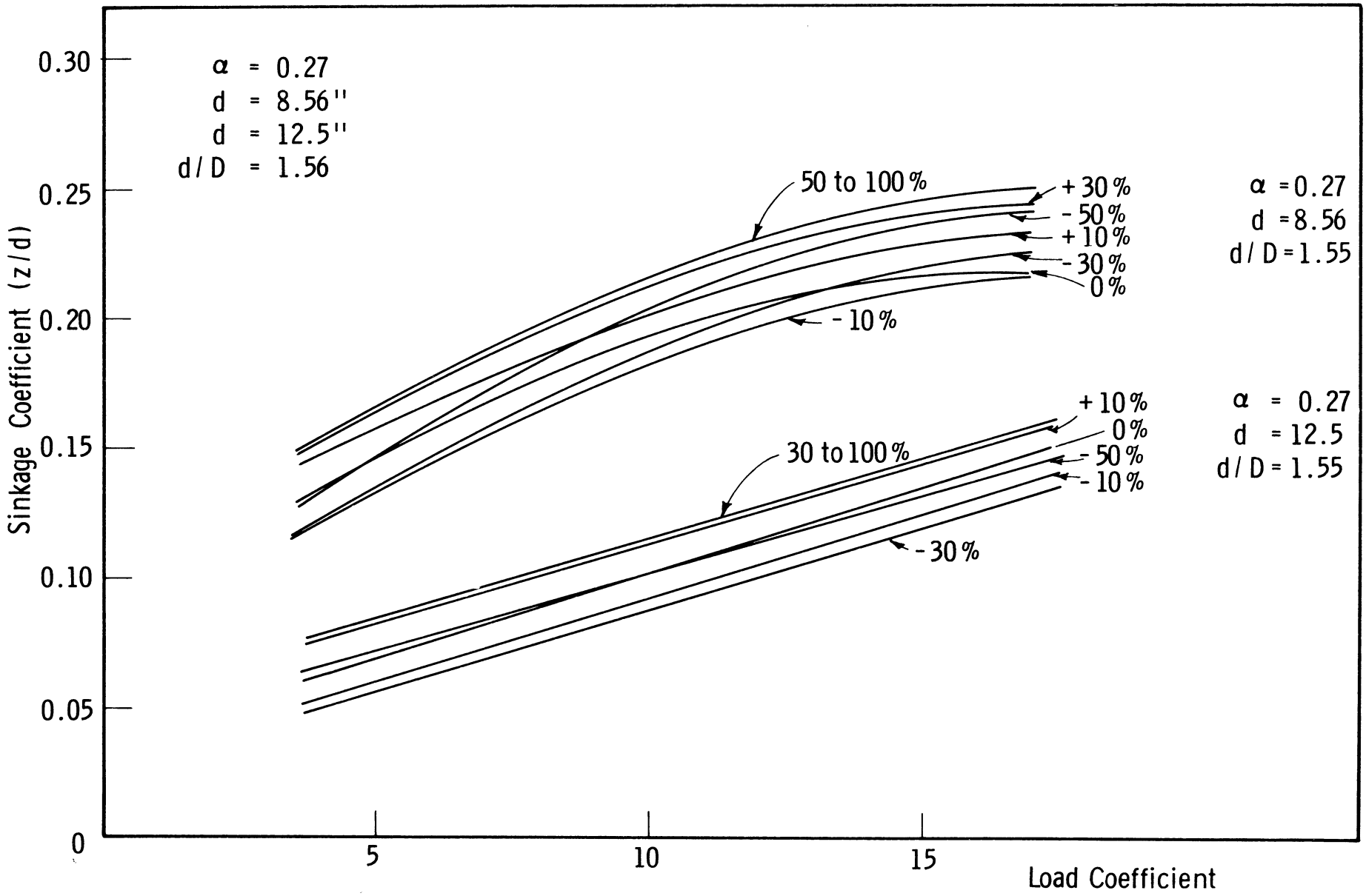

Fig. 93. Sinkage coefficient-load coefficient curves for $\alpha = 0.27$.

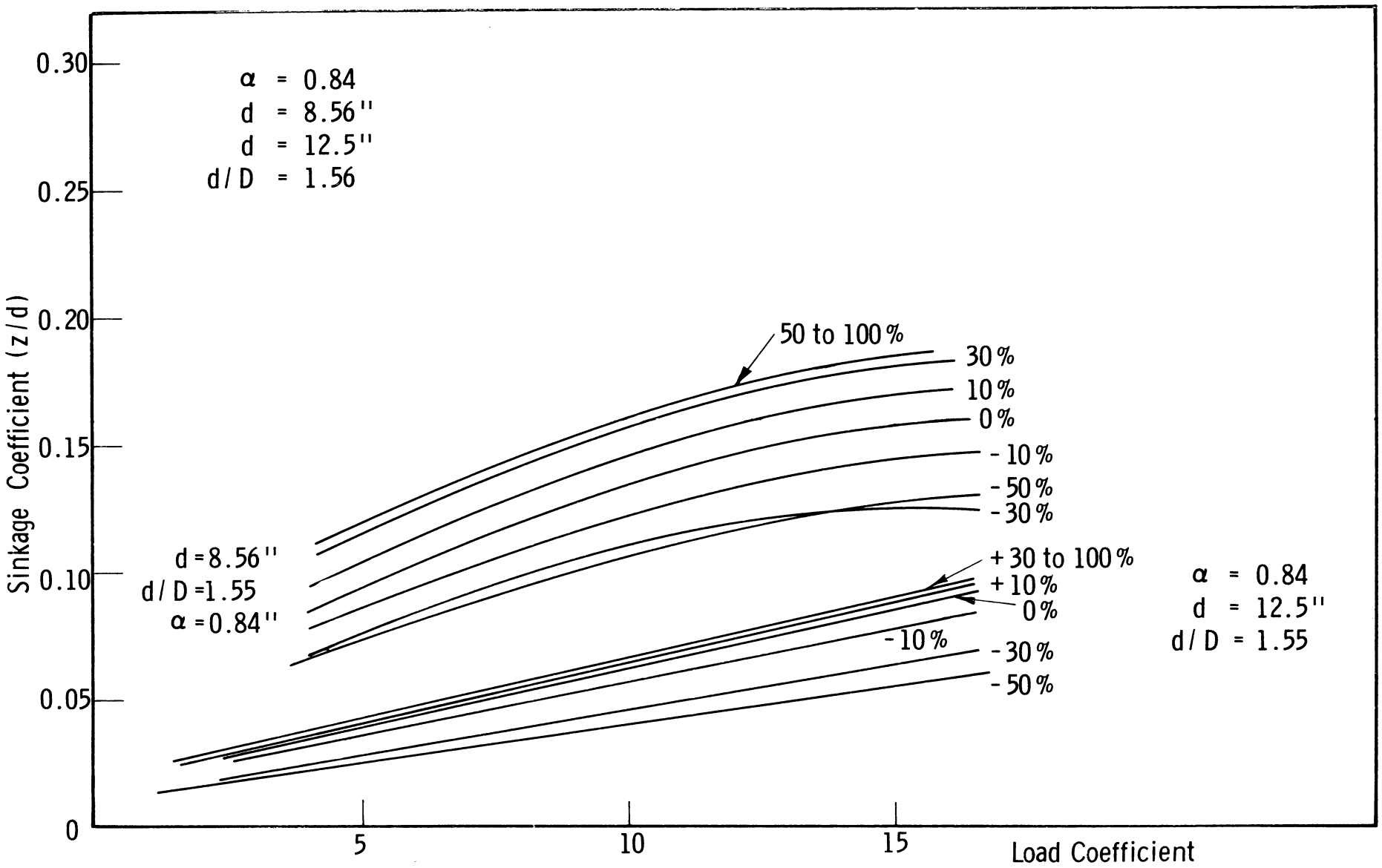

Fig. 94. Sinkage coefficient-load coefficient curves for $\alpha = 0.84$.

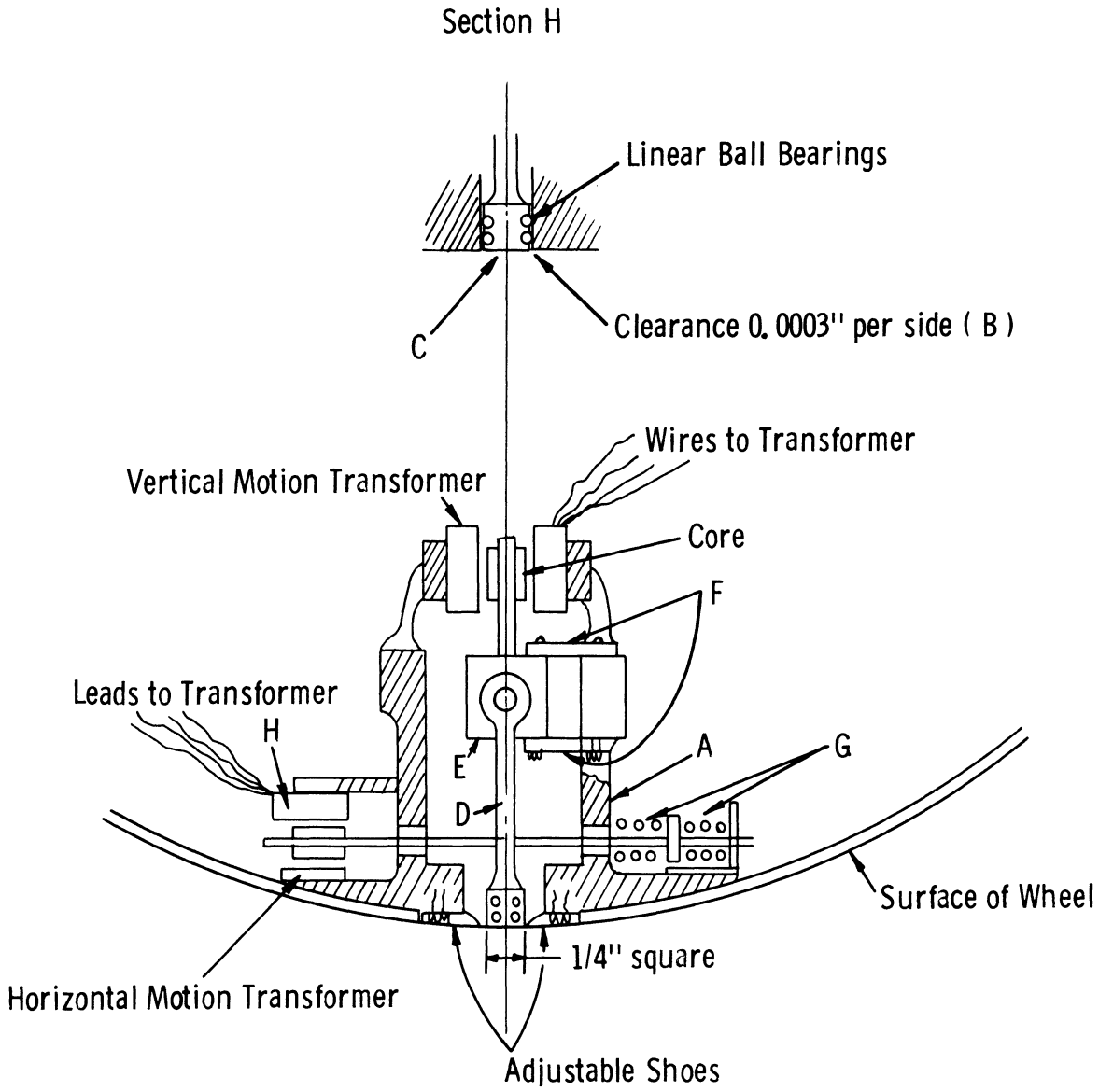

Fig. 95. Diagrammatic sketch of radial and tangential force transducer.

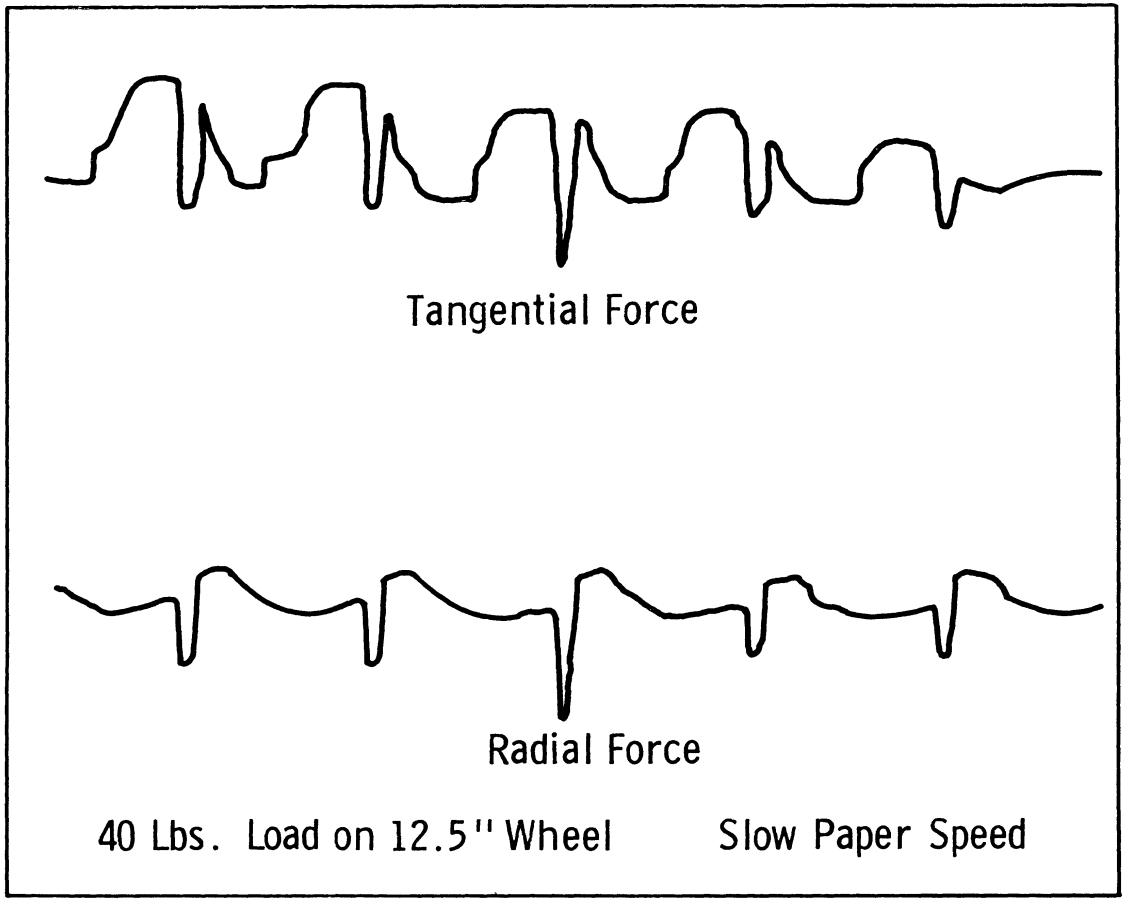

Fig. 96. First record of forces under load of 40 lb on 12.5-in. dia wheel.

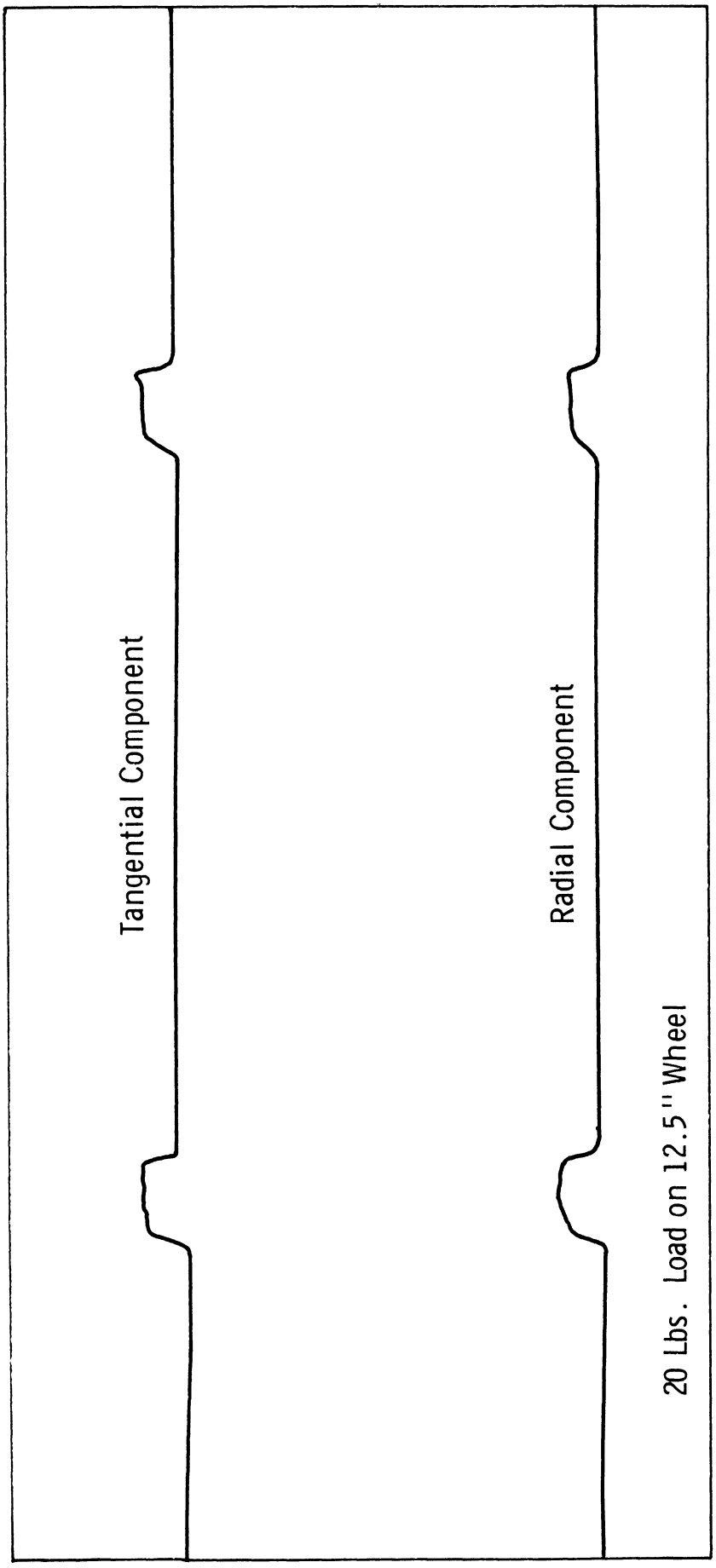

Fig. 97. Record of 20-lb load.

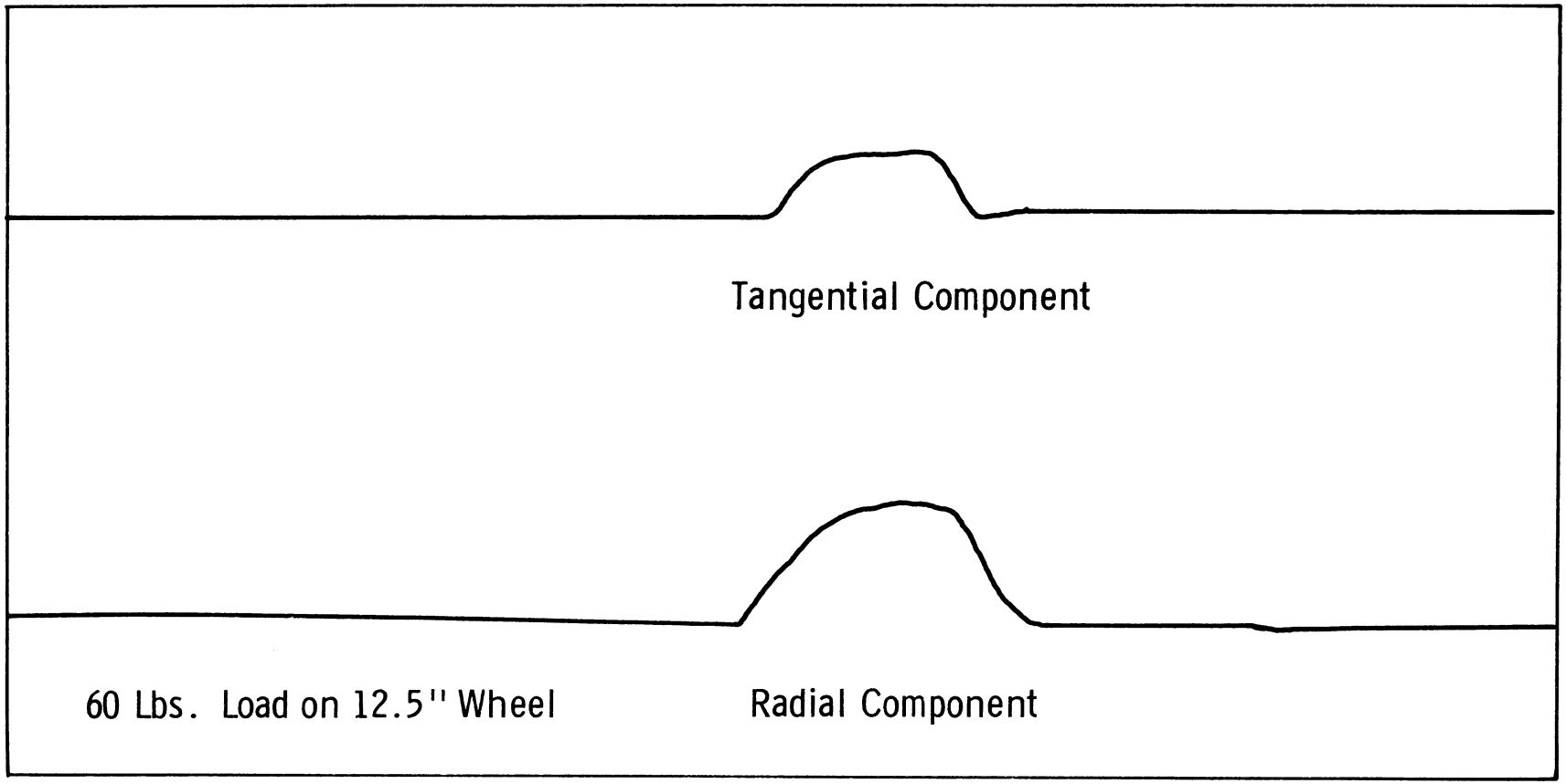

Fig. 98. Radial and shear loads under 60-lb load.